A HEURISTIC MODEL FOR MULTI-PARTICLE PRODUCTION IN π^-p INTERACTIONS

A DISSERTATION SUBMITTED TO THE GRADUATE DIVISION OF THE UNIVERSITY OF HAWAII IN PARTIAL FULFILLMENT OF THE REQUIREMENTS FOR THE DEGREE OF

DOCTOR OF PHILOSOPHY

IN PHYSICS

MAY 1972

By

Alfred David Johnson

Dissertation Committee:

V. J. Stenger
V. Z. Peterson
P. N. Dobson
W. R. Steiger
W. W. Peterson

ABSTRACT

Models based upon pion-exchange and diffraction dissociation have been fitted to data from reactions of the type

$$\pi^- p \rightarrow \text{Nucleon} + k\pi,\ 2 < k < 7$$

at 3.9 and 11.9 GeV/c incident momentum. These models, which include resonance production, give approximately correct mass- and t-distributions, as well as transverse and longitudinal components of momentum. Partial cross-sections for dominant channels have been estimated, and relations between cross-sections compared with theoretical predictions.

TABLE OF CONTENTS

LIST OF TABLES

LIST OF FIGURES

LIST OF FIGURES (continued)

1.0 INTRODUCTION

Much detailed study has been devoted in recent years to $\pi^- p$ interactions at energies up to 25 GeV/c,[1] from which a considerable spectrum of short-lived resonant states has been deduced. A majority of experiments to date have been limited to examination of a single final state at one energy. This final state is usually found to be composed of a mixture of resonant and nonresonant substates. In estimating partial cross-sections for resonance production, it is frequently necessary to approximate a background above which the resonance rises in a mass-plot. At low energies the assumption of phase-space background is usually sufficient to describe the background. At higher energies the resemblance of the background under the resonances to phase-space disappears. In addition, four-momentum transfer-squared, t, to the nucleon or to a cluster of particles deviate markedly from the statistically expected distributions even at fairly low beam momenta ~ 1 GeV/c.

Models, based upon phenomenology and an incomplete theory of strong interactions, have been developed to simulate what has come to be called "peripheral" behavior. For final-states consisting of up to 4 particles, these models are adequate to explain the observed phenomena and to demonstrate the effects of one production process upon the background for other processes.[2] Aside from computational complexities, there is no special difficulty in applying these same methods to more complex events. This is one major purpose of this work: to see whether the same types of amplitudes which simulate 4-body events are successful in reproducing the major kinematic features

of 5, 6, and 7-body final states, including background.

We attempt to fit related and internally consistent models to the following 6 final states.

Reaction 1	$\pi^- p \to p\pi^+\pi^-\pi^-$	4-body proton	EQN. 1.1
2	$\pi^- p \to p\pi^+\pi^-\pi^-\pi^0$	5-body proton (or 5-body π^0)	
3	$\pi^- p \to n\pi^+\pi^+\pi^-\pi^-$	5-body neutron	
4	$\pi^- p \to p\pi^+\pi^+\pi^-\pi^-\pi^-$	6-body proton	
5	$\pi^- p \to p\pi^+\pi^+\pi^-\pi^-\pi^-\pi^0$	7-body proton (or 7-body π^0)	
6	$\pi^- p \to n\pi^+\pi^+\pi^+\pi^-\pi^-\pi^-$	7-body neutron	

Each final state may comprise several distinct processes. We depict each process as a two-point Feynman graph having meson and baryon vertices. The number of pions outgoing from the meson vertex, or "vertex multiplicity," distinguishes a particular process from all others, and the presence of resonant groups among outgoing particles at either vertex further refines this distinction.

Each process takes place by an underlying reaction mechanism which we take to be either meson-exchange or diffraction dissociation, with possibly some phase-space-distributed background. Simplified amplitudes for these reaction mechanisms have been developed which reproduce the principal features of the data when several processes are taken in combination, and the relative contribution of each process is sought by a maximum-likelihood fit to the data. Fits to all 6 final states constitute a model for the experiment.

Since data are available at two energies (incident momentum 3.9 and 11.9 GeV/c) it is possible to inspect the energy dependence of cross-sections for the interaction mechanisms assumed in the model. This dependence is expected to differ for various mechanisms.

Finally, the Regge theory for the Pomeranchuk pole, which is thought to be related to the diffraction dissociation mechanism, assumes that it is factorizable.[3] This assumption has been tested in a limited set of cases, two-body or quasi-two-body, in which the final state contains resonances.[4] Factorization predicts relationships between partial cross-sections for different multiplicities at the same energy, given a model which determines these partial cross-sections and in which the final state is assumed to be quasi-two-body. In this sense we attempt to further test the factorization hypothesis.

For reasons of simplicity, the processes used here are all conceived as 2-vertex Feynman amplitudes; multiperipheral effects have not been included, although these effects may be approximated in the duality sense.

For practical reasons, the study has also been limited to non-strange-particle events. The cross-sections for strange-particle production are less by at least an order of magnitude than the non-strange-particle production.

Earlier work included the effects of quantum-mechanical angular correlations.[2] These have been dropped in the current study because they are difficult to apply to more complicated events and because some of the final-states studied are lacking sufficient statistics to demonstrate the angular correlations.

It is not generally feasible to predict a priori which processes (such as Δ or ρ production with a particular particle configuration) are present in significant amounts, so it has been necessary to try fitting with many combinations of processes which are not reported herein. Discussion is here limited to those processes which have

survived a sort of "distillation" which has taken roughly the following route.

First, for a given final state, histograms of the real data were inspected for evidence of low momentum transfer, leading-π effects, and noticeable mass shifts. Many cuts on the data were made, including subtraction of background near peaks such as in the $(p\pi^+)$ mass. From this, an initial guess was made as to which processes were significant, and these were then tried as a model. Processes which gave contributions less than .05 were then generally omitted in further model development. Comparison with a Monte-Carlo simulation next was used to determine what regions in phase-space were too densely populated (or too sparsely populated), and other processes were added to correct the deficiencies. This iteration--dropping processes which did not fit with significant amounts and selectively adding new ones a few at a time--was continued until a reasonable fit was obtained. In cases where it is herein reported that the cross-section for a particular process is small, this was determined by fitting again with a model which gives a reasonably good simulation of the real data with the "small" processes added. Thus the determination of cross-sections for a few strongly-contributing processes includes, in most cases, a determination of upper limits of cross-sections for a larger number of weakly-contributing processes. The cut-off taken was roughly at the 5% level. Processes contributing less than 5% in a fit were ignored in the final result.

2.0 EVOLUTION OF THE PERIPHERAL MODEL

Application of the maximum likelihood fitting technique to bubble-chamber data is due to J. Friedman (LRL)[5] and has been since extensively employed by other researchers. Originally the method utilized Breit-Wigner forms to simulate resonances, and a background distributed according to phase-space. This method has been used to study 4, 5, and 6-body final states at 3.9 GeV/c,[6] and is adequate for estimating cross-sections for resonance production but yields t-distributions which are not sufficiently peripheral even at moderate energies. To overcome this deficiency, we have incorporated factors in the amplitude which enhance low-t.

The course of this experiment has shown that two distinct types of low-t-enhancement factors are necessary, and are sufficient to produce a reasonable simulation of the real data. These are a pole in t to represent π-exchange, $\frac{1}{(1 - t/M_\pi{}^2)^2}$, and an exponential to represent diffraction dissociation, e^{bt}.

In an event pictured as a 2-vertex Feynman graph, the number of outgoing pions at the meson vertex may be odd or even. Only the even-pion case is suitably represented by the π-exchange pole term from G-parity considerations, and the t-dependence of a fraction of the events studied is described by such a pole term. Now the crux of the experimental situation is that there are events which do not fit the π-exchange description but which can be described by a diffraction dissociation amplitude. The π-exchange form has a very sharp t to even number of π's, while the diffractive component is less sharply peaked in t, and the experimental evidence distinguishes between them. This

experiment is an attempt to see how well these two amplitudes, in combination, suffice to explain the experimental results.

Various amplitudes for π exchange have been proposed[7] based upon a phenomenonological understanding of the strong interaction as resulting from the exchange of particles, particularly pions. This mechanism is expected to introduce a pole in t at the mass of the exchanged particle plus t-dependent vertex factors. We have found no particular need to use any of the various vertex factors which have been employed elsewhere, limiting ourselves to the simple pole form with vertex factors independent of t. That is, we basically assume pole-dominance, the vertex factors being calculated at the pole. Our experience has shown us that, for the purpose of describing the main features of the data, no further complications are needed and, indeed, the data are not sensitive to the various forms proposed.

The general form of the amplitude we use to represent pion-exchange is, then,

$$A_{\text{exchange}} = \left[\begin{matrix}\pi\pi \\ \text{vertex} \\ \text{factor}\end{matrix}\right] \cdot \left[\begin{matrix}\text{pion} \\ \text{propagator}\end{matrix}\right] \cdot \left[\begin{matrix}\pi\text{-nucleon} \\ \text{vertex} \\ \text{factor}\end{matrix}\right] \qquad \text{EQN. 2.1}$$

The vertex factors are amplitudes for scattering of the exchanged (off-shell) pion and incident pion or proton. They are approximated by on-mass-shell scattering, in our model, as discussed above.

This on-shell scattering is further simplified by assuming Breit-Wigner functions for resonant systems and S-wave scattering for nonresonant systems of particles. With these considerations we write, for Δ^{++} production in the 4-body state:

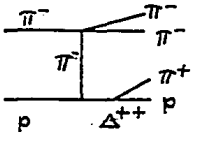

$$A_{\text{exchange}} = \left[M_{\pi\pi}\right]\left[\frac{1}{1 - t/M_{\pi}^{2}}\right] \cdot \left[BW(\Delta)\right] \qquad \text{EQN. 2.2}$$

where $t = t(p, p\pi^+) = t(\pi, \pi\pi)$

$$BW(\Delta) = \frac{M_\Delta \Gamma_\Delta / 2}{(M_{p\pi^+}^2 - M_\Delta^2) - iM_\Delta \Gamma_\Delta / 2}$$

Simultaneous production of ρ^0 and Δ^0 is similarly represented by

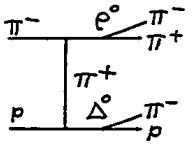

$$A_{exchange} = \left[BW(\rho^0)\right]\left[\frac{1}{1 - t/M_\pi^2}\right]\left[BW(\Delta^0)\right] \quad \text{EQN. 2.3}$$

M_Δ, Γ_Δ are the mass and width of the $\Delta(1236)$ as taken from the literature. These have not been allowed to vary in the fits, although it is of course feasible to do so. $M_{\pi\pi}$ and $M_{p\pi}$ stand for the invariant mass of the $\pi^-\pi^-$ and $p\pi^+$ combinations respectively.

Another example of π-exchange is 5-body production with or without resonances. Here, the vertex factor at the proton vertex can only depend on t which we, again, neglect.

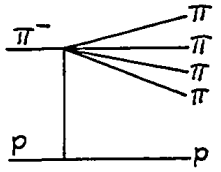

$$A_{exchange} = \left[1\right] \cdot \left[\frac{1}{1 - t/M_\pi^2}\right] \cdot \left[BW\right] \quad \text{EQN. 2.4}$$

$$t = t(p, p) = t(\pi, 4\pi)$$

In the case of ω production,

$$\left[BW\right] = \frac{M_\omega \Gamma_\omega / 2}{(M_{3\pi}^2 - M_\omega^2) - iM_\omega \Gamma_\omega / 2}$$

For cascade decay of $A \rightarrow \rho\pi$, this would involve two Breit-Wigner factors:

$$\left[BW\right] = \frac{M_A \Gamma_A / 2}{(M_{3\pi}^2 - M_A^2) - iM_A \Gamma_A / 2} \cdot \frac{M_\rho \Gamma_\rho / 2}{(M_{2\pi}^2 - M_\rho^2) - iM_\rho \Gamma_\rho / 2}$$

The extension of this form of interaction amplitude to higher multiplicities should now be obvious once the Feynman diagram for a process is drawn

Rho and omega exchanges, with t/M_π^2 replaced by t/M_ρ^2 or t/M_ω^2,

have also been used, for example, in A_2 production. Generally, it is found that these result in a t-dependence which closely resembles phase space. Peaks occur at values of t much larger than in the real data. Hence, phase space, which has been included in some places as a background, may be considered a substitute for exchange of mesons more massive than the pion.

Again, if the event is pictured as a 2-vertex Feynman graph, a process other than π-exchange is required to produce an odd number of pions at the meson vertex. Such events are characterized by an exponential t-dependence and small transverse 3-momentum, which is what one expects from a diffractive mechanism.[8] This mechanism we have simulated by a term with the general form, $\frac{1}{M^{*2}} e^{(b/2)t}$, where M^{*2} is a composite mass.

Such a model is suggested by Regge theory. Consider the diagram

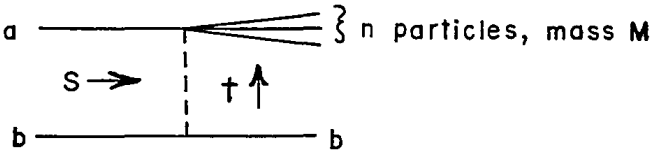

Regge theory connects the amplitude for $ab \to Mb$ with the cross channel process $b\bar{b} \to \bar{a}M$. . If a resonance of angular momentum ℓ denotes this latter process,

$$A(s, t, M) \sim P_\ell(\cos \theta_t) \qquad \text{EQN. 2.5}$$

where θ_t is the scattering angle in the cross channel and

$$\cos \theta_t = \frac{1}{4P_t P_t'} [s - u] \qquad \text{EQN. 2.6}$$

where u is the usual Mandelstam variable connected to s and t. P_t and P_t', the cross channel 3-momenta, are given by

$$P_t^2 = \frac{1}{4t}[t - (M_a + M)^2][t - (M_a - M)^2] \qquad \text{EQN. 2.7}$$

$$P_t'^2 = \frac{1}{4t}[t - 4M_b^2]\, t$$

In the usual Regge prescription, ℓ is replaced by a complex number $\alpha(t)$ which is interpreted as the Regge trajectory of the particles exchanged and the limit is taken as $s \to \infty$, $t \to 0$. Then,

$$A(s, t, M) \underset{s\to\infty}{\to} (\cos\theta_t)^{\alpha(t)} \sim \left(\frac{s}{M^2}\right)^{\alpha(t)} \qquad \text{EQN. 2.8}$$

Now, if we let $\alpha(t)$ be linear,

$$\alpha(t) = \alpha(0) + \alpha' t \qquad \text{EQN. 2.9}$$

then

$$A(s, t, M) \sim e^{\alpha' \ln(s/M^2)t} \left(\frac{s}{M^2}\right)^{\alpha(0)} \qquad \text{EQN. 2.10}$$

where $\alpha(0) = 1$ for the trajectory which is thought to be responsible for diffraction production.

The Regge residue factors contribute an unknown t-dependence and so the general form suggested is

$$A(s, t) \sim \exp\left(\frac{1}{2} b(s, M) t\right)\left(\frac{s}{M^2}\right) \qquad \text{EQN. 2.11}$$

where $b(s, M)$ is not given a priori by the theory, but might be expected to be of the order of that observed for elastic scattering (≈ 8 GeV^{-2}). We have chosen to use values of b which are reasonable by comparison with available data[10] and constant: b=5 for cases in which the diffraction appears to strip pions from the nucleus, b=8 for cases in which the incident pion appears as the dissociated particle. These values are not crucial to the results obtained. The experimental results are not sensitive enough to display a clear dependence on the specific

values chosen.

It has been shown by other investigators that πp interactions at high energy are characterized not only by low t (nucleon) but by small and nearly constant transverse component of 3-momentum, called $P_{\perp}$, for the outgoing particles.[11] This behavior has been shown to arise naturally in thermodynamic or "multiple-fireball" models. As will be seen below, our peripheral model also reproduces the effect.

The longitudinal component of 3-momentum, $P_{||}$, roughly resembles that predicted by phase space except for a "leading" pion, and a nucleon which is very backward in the CM for all multiplicities. A factor $\frac{1}{M^{*2} - M_{\pi}^{2}}$ (where M^* = mass of the outgoing pions) gives rise to a backward nucleon, and as such, simulates the diffractive process. Consider the general reaction

$$\pi_i + \text{Nucleon} \rightarrow M^* + \text{Nucleon} \qquad \text{EQN. 2.12}$$

Squaring the four-momenta in initial and final states, with a target nucleon N at rest, we obtain $M_i^2 + M_N^2 + 2E_iM_N$

$$= M_i^{*2} + M_N^2 + 2E_N'E_{M^*} - 2\overline{P}_N' \cdot \overline{P}_{M^*}$$

Now in the limit of low P and high energy, $E_iM_N \cong P_iM_T$,

$$2\overline{P}_N \cdot \overline{P}_{M^*} \cong 2|\overline{P}_{||}||\overline{P}_{M^*}|,\ E_N' \cong M_N,\ P_i \cong E_{M^*} \qquad \text{EQN. 2.13}$$

Then approximately

$$P = \frac{M^{*2} - M_i^2}{2P_i}$$

so we may write

$$\frac{1}{M^{*2} - M_i^2} = \frac{1}{2P_{||}P_i} \propto \frac{1}{P_{||}} \qquad \text{EQN. 2.14}$$

where $P_{||}$ is the component of momentum imparted to the nucleon, P_i = incident momentum, and M_i is mass of the incident particle. So the factor $\frac{1}{M^{*2} - M_i^2}$ may be looked upon as a form factor introduced to simulate the small $P_{||}$ which is seen as a backward nucleon.

These two factors, $\frac{1}{M^{*2}}$ from Regge theory and $\frac{1}{M^{*2} - M_\pi^2}$ from an analysis of the kinematics of peripheral interactions, are nearly equivalent since the pion mass is so small. The motivation for such a term really arises from the observation of a broad peak in 3π mass near 1.1 GeV/c^2 in, for example, the $p3\pi$ final state (that is, the much discussed A_1). In this same final state, as well as others, a broad enhancement in $M(p\pi\pi)$ is observed near 1.5 GeV/c^2; could this be a manifestation of diffraction dissociation of the nucleon system? Experimentally, it has been determined that a term of the form $\frac{1}{M^{*'2} - M_p^2}$ is effective in reproducing the low $M(p\pi\pi)$ enhancement and the leading-π effect, while a term $\frac{1}{M^{*'2}}$ is less successful. ($M^{*'2}$ is the mass of $pn\pi$ system, $n < 6$.) Therefore, a term of the form $\frac{1}{M^{*2} - M_i^2}$ has been incorporated in each diffractive amplitude, where by M^* we now mean the mass of particles emerging from a vertex with incident particle of mass M_i.

We may now write a general form for our model of diffractive processes:

$$A_{\text{Diffractive}} = \frac{1}{M^{*2} - M_\pi^2} e^{bt/2} \cdot \left[\begin{array}{c}\text{Breit-Wigner of function} \\ \text{for each resonance}\end{array}\right] \qquad \text{EQN. 2.15}$$

If the diffraction dissociation is pictured as taking place at the

meson vertex, b = 8. For example, in the 4-body case, the amplitude becomes

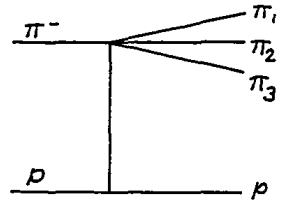

$$A_{\pi Diff} = \frac{1}{M_{3\pi}^2 - M_\pi^2}\, e^{8t/2}\, [BW] \qquad \text{EQN. 2.16}$$

$$t = t(p, p) = t(\pi, 4\pi)$$

If π_1 π_2 form a ρ,

$$[BW] = \frac{M_\rho \Gamma_\rho / 2}{(M_{\pi\pi}^2 - M_\rho^2) - i\Gamma_\rho M_\rho / 2}$$

Similarly, for diffraction dissociation of the baryon we write

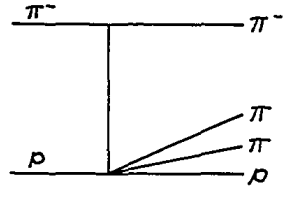

$$A_{pDiff} = \frac{1}{M_{p\pi\pi} - M_p^2}\, e^{5t/2}\, [BW] \qquad \text{EQN. 2.17}$$

$$t = t(p, p\pi\pi) = t(\pi, \pi)$$

[BW] = 1 if no resonance is assumed. A resonance in the $p\pi$ system is accomodated by replacing [BW] with $\frac{M_\Delta \Gamma_\Delta / 2}{(M_{p\pi}^2 - M_\Delta^2) - iM_\Delta \Gamma_\Delta / 2}$. A cascade decay of $N^* \to \Delta\pi$ would include one more Breit-Wigner factor for the N^*.

In the case of double diffraction dissociation, one might expect that two exponential factors and $\frac{1}{M^{*2}}$ factors should be included. Experimentally, it turns out that this gives too steep a t-dependence, and that better results are obtained with the following prescription:

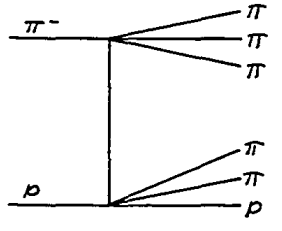

$$A_{\text{double-diff}} = \frac{1}{M_{3\pi}^2 - M_\pi^2}\, e^{8t/2}\, [BW] \qquad \text{EQN. 2.18}$$

$$t = t(p, p\pi\pi) = t(\pi, \pi\pi\pi)$$

That is, the meson vertex is treated as diffractive while the only t-dependence assumed at the baryon vertex is in the arrangement of the particles assumed in defining t. As usual, Breit-Wigner functions may

be included at either meson or baryon vertices, or both.

It is to be noted that the Regge arguments used to justify the diffraction form hold only for dissociation at one vertex. A singularity in cos θ_t at t = 0 occurs when the masses of particles at both vertices are different from the initial masses. Thus, the theory offers us no simple guideline to follow in this case and the above purely phenomenological form was used.

Diffraction dissociation is in one view actually "shadow scattering" rather than an exchange process.[8] The initial state consisting of a π and a nucleon is not in an eigenstate of G-parity, and, although parity and angular momentum conservation forbid creation of a 2π, nucleon final state, a final state consisting of a nucleon and $n\pi$'s, $n > 2$, are allowed.*

This has turned out to be an important feature of fits to our data at 12 GeV/c for it breaks down the distinction between what one would prefer to treat as Pomeron exchange, with an odd number of π's at the meson vertex, and π-exchange, with an even number. It turns out that the pole form of amplitude, used at our lower energy for π-exchange as discussed previously, does not give satisfactory fits at the higher energy. It appears, within the framework of the model used, that practically all of the π^-p interaction at 11.9 GeV/c is diffractive, including that which results in an even number of π's in the final state.

This view of diffraction dissociation differs from the picture in which a massless (and possibly fictitious) "vacuon" having zero quantum numbers is exchanged as in a 2-vertex diagram. We view the final state as a group of one or more mesons whose cm travels in very nearly the

*This fact is mentioned in Reference 8 in a note added in proof.

same direction as the original meson and a baryon, possibly with associated mesons, which travels nearly in the original baryon direction. The meson group has the same overall charge as the incident meson while the baryon with its associated mesons has the same overall charge as the incident baryon. Either system may contain any resonant sub-groups which are allowed by angular momentum and isotopic spin conservation.

We regard the exact nature of the interaction as unknown except for the kinematic effects which it produces: very forward mesons, backward nucleons, and an exponential t-dependence.

Now let us describe the actual fitting procedure. A model for a particular final state consisting of a nucleon and 3 to 6 pions is constructed by adding incoherently varying amounts of all processes which are found to contribute strongly in the interaction. A systematic search for the "best fit" is accomplished by a maximum-likelihood technique. For each event j, a frequency function is computed:

$$F_j = \sum_i \alpha_i \frac{\rho_{ij}}{N_i} \qquad \text{EQN. 2.19}$$

where

α_i = amount of the i^{th} process.

ρ_{ij} = (amplitude)^2, computed for j^{th} event.

$N_i = \int \rho_{ij} dR_n$ = normalization integral over available phase space for i^{th} process.

A likelihood function is computed for all events in the sample:

$$L = \Pi_j F_j$$

and the amounts α_i are varied, taking derivatives numerically, until L is maximized.

A Monte Carlo simulation of the experiment consists of events generated according to phase space but weighted according to F_j computed for the fake events just as for the real data. Projections from this non-uniform distribution are compared with the real data in the form of mass-plots, t-distributions, and angular distributions as seen in the following section.

3.0 APPLICATION OF THE PERIPHERAL MODEL TO MULTIPARTICLE FINAL STATES

The above model has been used as a heuristic tool for examining the class of events

$$\pi^- p \rightarrow \text{nucleon} + k\pi,\ 2 < k < 7 \qquad \text{EQN. 3.1}$$

at 3.9 and 11.9 GeV/c. The data comprise 12 distinct sets. Each of these has been modeled, and the results of the fits as well as the experimental details are presented in Figures 1 through 12. In the following text, data at 3.9 GeV/c are described in general; followed by a description of the salient features of data and model for each of the 6 final states at this energy. Then the data at 11.9 GeV/c are treated similarly.

Tables 1 through 12 present the results of maximum-likelihood fitting with major contributing processes. The cross-section for each final-state is taken from Table 13 (3.9 GeV data) or Table 14 (11.9 GeV data). "Vertex multiplicity" is the number of particles leaving that vertex. "Fraction fitted" is the result of the fit, and the process cross-section is this fraction multiplied by the final-state cross-section. Errors on partial cross-sections are root-mean-square combinations of statistical errors from the fit with errors on final-state cross-sections. To this has been added an estimated systematic error, designated SYS in the tables.

A selection of mass-distributions, t-distributions, and angular distributions is presented in Figures 1 through 12 to illustrate the results of the fitting process. Each figure is divided into two parts. The first is an "overview" in which the real data are depicted by histograms, and the distributions of Monte Carlo events simulated

according to the model are shown by asterisks (Part 1 of each figure). The second shows details of the fit. A row of connected numerals describes the contribution of the process whose numeral appears on the corresponding table of amounts (Part 2 of each figure).

The "overview" plots (Figures 1 through 12, Part 1) present the results of summing, for each event, the several process weights (calculated by the appropriate amplitude $A_{exchange}$ or A_{Diff}) multiplied by the phase-space weight for each Monte Carlo event. This yields an event weight, different for each event, which reflects how well that event is described by the model. The histograms plotted as asterisks are sums of these event weights. These histograms demonstrate the overall fit to the experimental data but fail to show how each individual process contributes to the resulting distribution. One may wish to know, for example, which specific processes yield the leading π^- effect.

In Figures 1 through 12, Part 2, selected overview plots have been broken down, process by process, to give a more detailed picture of how the individual processes contribute to each distribution.

Each curve on these plots has a number attached which is the process number in the corresponding table (Tables 1 through 12). The area under a given curve M represents the summed weights for all processes 1 through M, for all events. The uppermost curve represents the sum of all the processes, for all events, and thus corresponds to the row of asterisks in the overview plots. The prediction of the statistical model is presented as an unconnected curve of the letters PS. Hence one may compare the individual process contribution with the overall model, with the experimental data, and with phase-space.

Events weights vary by several orders of magnitude from event to event, and even with large samples of Monte Carlo events these distributions have considerable scatter from bin to bin. To ease the visual interpretation of these plots, the data have been smoothed somewhat. A polynomial of low order (generally 3) is fitted to several bins including the one to be smoothed, and the ordinate to be plotted is calculated from this polynomial. The polynomial slides over the bins by dropping one point behind and picking up a new one ahead as each bin is adjusted. Thus the plotted ordinates are influenced by points to right and left on the plot so as to reduce the scatter.

3.1 Experimental Results, $\pi^- p$ at 3.9 GeV/c

Data used in this study, consisting of about 32000 four-prongs and 2800 six-prongs events, were part of a large sample of film exposed to the Lawrence Radiation Laboratory 72-inch bubble chamber in 1963-64 and known as the π-63 experiment. These data, after being utilized at Berkeley, were loaned to us and became the first bubble-chamber film to be analyzed at the University of Hawaii. First they were scanned for all multiplicities. All 4-prong and 6-prong events were then measured with the Alvarez Scanning and Measuring Projector (SMP). Events satisfying the 4-, 5-, and 6-body hypotheses were processed using the PANAL, PACKAGE, WRING, EXAMINE sequence of programs. 7-body events were reduced with the programs TVGP, SQUAW, and ARROW. A chi-squared cutoff equivalent to a .02 confidence level was imposed for a one-constraint fits (1C, i.e., one neutral particle), a .0002 confidence level for four-constraint fits (4C, i.e., all momenta measured).

Events which fit both 1C and 4C hypotheses were treated as 4C. This selection left a small fraction of 4C events in which is was impossible, kinematically, to distinguish which positive particle was really the proton. These were resolved by arbitrarily choosing the hypothesis having the lower chi-squared. A partial scan of events for ionization density was made to ascertain that this procedure does not introduce a serious bias.

Events ambiguous between the hypotheses π^0-missing and neutron-missing were resolved by inspecting the complete sample of ambiguous events for ionization density. It is estimated that less than 3% remained unresolvable and may be misidentified.

Conspicuous features in these data are the production of Δ^{++}, ρ, and resonances, and a "leading" π^- which is frequently closely aligned with the incident π^-. The short lifetime of the ω results in a mass-width of 12 Mev, which is narrower than the experimentally-observed width. A maximum-likelihood fit to the ω with the width as a variable gives a best fit of 29 Mev, which is interpreted as an estimate of the limit of resolution of our measuring instrument (machines plus programs) at this energy.

Certain aspects of these data have been reported elsewhere.[2,6] The 4-, 5-, and 6-body events were first analyzed for resonance production with models which used a Breit-Wigner function. It was apparent then that this model did not produce the correct t-distributions. A later study of the 4-body events produced a good fit to both mass and t-distributions, and also angular distributions.[2] This was the prototype for the model used in this dissertation, and results obtained here are

virtually consistent with those of the earlier study. It should be emphasized that the present model employs no quantum-mechanical angular correlations. This springs from a desire to apply, as much as possible, the same model to all final-states, and there are insufficient numbers of 6- and 7-body events to justify incorporation of angular correlations per se.

It is considered a success of the model that it does reproduce the angular correlations between incident and outgoing π^- particles. In our model this is seen as a kinematical artifact of the peripheral nature of the interaction, that is, the kinematical requirement of low t between incident and outgoing particles at a vertex poses constraints on the "phase-space" available and distorts the longitudinal and transverse momentum distributions. Both $P_{||}$ and $P_{\perp}$ are well described by the model, as noted below.

Another noticeable feature of the data is a tendency toward low-mass groupings of $p\pi\pi$ and $\pi\pi\pi$. It is tempting to interpret these as resonances, $N^*(1470) \rightarrow p\pi\pi$ and $A_1(1070) \rightarrow \pi\pi\pi$, since the kinematical enhancements occur in the same mass regions as these resonances. However, the kinematical enhancements are broader than the resonances, and, while the peripheral model produces correct t-distributions and leading π^- effect, a model with pure N^* and A_1 resonance production does not. If one does not take account of the kinematics, one may overestimate the amount of resonance production in these regions.

We now look at the six individual final states. The results are summarized in Figures 1 through 6.

a. $\pi^- p \rightarrow p\pi^+\pi^-\pi^-$ at 3.9 GeV/c

Four-body events, in which all momenta are measured (4-constraint fits) present clearer evidence of resonance production and peripheral effects than the more complicated events. The leading $\pi^{\pm}$ effect is very pronounced; see Figure 1, Part 1(n) and (o). It has been shown in an earlier study that the $\pi^-\pi^-$ scattering is very forward peaked.[2] This would be expected for d-wave scattering, but not for s-wave scattering. The model, which assumes s-wave scattering, reproduces the effect. It appears as a kinematic artifact from events which have one π^- at the baryon vertex and one π^- at the meson vertex, which is thus a background to true $\pi^-\pi^-$ scattering.

The model assumed here is a simplification of the previous model in that no angular correlations have been assumed. The more complicated model achieved a somewhat better fit, but the two models yield practically the same amounts of Δ^{++}, Δ^{+}, Δ^{0}, and ρ^{0} resonances. (Figure 1, Part 1, (a), (b), and (d)).

This leading-π effect is elucidated by plotting the several contributing processes separately in Figure 1, Part 2(i) and (j). Here it is clear that, in our model, the peak at +1.0 in cos(π^- in, π^- out) is principally due to processes 4 and 1 (Table 1) which are Δ^{++} by diffraction and by π^- exchange, respectively. These processes also give the slight rise at -1.0, which is to be expected since one π^- is associated with the baryon vertex in this process.

b. $\pi^- p \rightarrow p\pi^+\pi^-\pi^-\pi^0$ at 3.9 GeV/c

In the 5-body events the peripheral nature of the interaction is not as dramatic as in the 4-body, but there is still a noticeable leading π^-

(Figure 2, Part 1(m)). There is considerable resonance production, mainly Δ^{++}, ρ, and ω. The amounts reported here (Table 2) differ somewhat from amounts found in an earlier study of the same data[6] and reported by other researchers.[13] However, earlier estimates of cross-sections for these resonances took no account of the peripheral nature of the reaction which does affect the background under, in particular, the Δ^{++} signal.

It is interesting to note that $M(4\pi)$ is spread out toward low mass more than is predicted from phase space (Figure 2, Part 1(j)) and that this broadening is, in our model, mostly due to ω production. (Figure 2, Part 2(b)). Note that no B(1220) production is assumed, the signal for it being barely perceptible. ω-production (Proc. 7, Table 2), which must be by π-exchange in a two-vertex model, also contributes to low mass $\pi^+\pi^-$ combinations (Figure 2, Part 2(f)). The same process contributes noticeably to low t (π) (Figure 2, Part 2(a)) as expected, and also to the forward π^- and π^+ (Figure 2, Parts 2(i) and (j)).

c. $\pi^-p \rightarrow n\pi^+\pi^+\pi^-\pi^-$ at 3.9 GeV/c

Very little has been written about the $n4\pi$ final state. At this energy, the distributions are not markedly different from phase-space predictions. Exceptions are ($M(n\pi^-)$, t(n), and $t(n\pi^+\pi^-)$, (Figure 3, Part 2(h), (c) and (a)). Amounts of the fitted processes are given in Table 3. The evidence for Δ^- production is clear, while ρ^0 production is swamped by having 3 "wrong" combinations plotted for every "right" combination. It is interesting that Δ^- production, process 2, reflects in a slight peak at high 4π mass (Figure 3, Part 2(d)). $t(n\pi^+\pi^-)$, or equivalently $t(\pi^+\pi^-)$, is shifted toward the low end of the spectrum by

ρ production (process 4) and also by Δ^- production (process 2).

t(neutron) has two separate peaks below .8 GeV, which appear to result from Δ^- production (process 2) and ρ^0 production (process 4) (Figure 3, Part 2(c)). It is seen that Δ^- production by one-pion-exchange also accounts for slight forward π^- and π^+ peaks (Figure 3, Parts 2(e) and (f)).

d. $\pi^-p \to p\pi^+\pi^+\pi^-\pi^-\pi^0$ at 3.9 GeV/c

This 6-body final state was formerly fitted by a resonance-production model with no peripheral effects.[6] A prominent feature of the data is an enhancement in $M(p\pi^+\pi^+)$ near 1400 which is associated with Δ^{++} and with a low $M(\pi^+\pi^+)$ (Figure 4, Parts 1(c), (a), and (e)). The present model gives slightly better fits to these distributions, but there still exists the possibility of something more interesting taking place such as production of an $I=\frac{5}{2}$ baryon resonance. One cannot, of course, rule out the possibility of a Bose-statistics effect for the identical π^+'s. This should also appear in $\pi^-\pi^-$. However, when the most forward of the three π^-'s is ignored, the $M(\pi^-\pi^-)$ plot is not distinguishable from the $\pi^+\pi^+$. We conclude that the low-mass $\pi\pi$ effect is a result of kinematics, and the difference between π^+ and π^- values is due to a leading π^- effect. Our model gives a quite adequate fit to t-distributions, (Figure 4, Parts 1(g), (h), (i)) which the former model did not.

The tendency to low t and a slightly forward π^- (Figure 4, Part 2(a), Figure 4, Part 1(q) both appear to be associated with Δ^{++} production (processes 2 and 3, Table 4)).

There are very few events in the sample so no strong statement may

be made about the low $M(p\pi^+)$, $M(p\pi^+\pi^+)$, and $M(\pi^+\pi^+)$; but similar effects have been observed on other experiments at nearby energies.

An asymmetry has been observed in the opening angles between like and unlike pions, unlike pions having on the average a greater opening angle.[15] These have been plotted in Figure 4, Part 1(r-u). There does appear to be a stronger peak near cos $\theta_{\pi\pi}$ (5π cm) for $\pi^+\pi^-$ than for $\pi^-\pi^-$, and the model nearly duplicates the effect. It is interesting to note the similarity between cos $\theta_{\pi^+\pi^+}$ and cos $\theta_{\pi^-\pi^-}$ when the most forward π^- is left out (Figure 4, Parts 1(s), (t)). This seems to indicate that, aside from a slight leading π^- effect, the pions all behave alike.

e. $\underline{\pi^-p \to p\pi^+\pi^+\pi^-\pi^-\pi^-\pi^0 \text{ at } 3.9 \text{ GeV/c}}$

The 7-body events are difficult to model, both at 3.9 and 11.9 GeV/c. This is due in part simply to the increased number of possible particle combinations which may be formed, aggravated by the redundancy of π^-'s and π^+'s. At this energy all experimental mass- and t-distributions resemble phase-space, so no strong case can be made for or against the peripheral model. Possible resonances are Δ^{++} and Δ^0; the data clearly rule out any significant ρ production (Figure 5, Part 1(c)).

The model which has been fit consists of processes which are not rejected by the fitting program; other processes have been tried, but the small number of events available preclude substantial results.

f. $\underline{\pi^-p \to n\pi^+\pi^+\pi^+\pi^-\pi^-\pi^-}$

What has been said for the 7-body proton events holds doubly true for the 7-body neutron events. Too few events, too many combinations, and very little clear evidence for resonance production make conclusions

very risky. It is reasonable to believe that some Δ^- production is present (Figure 6, Part 1(a)) and it is clear that this must take place with more than one pion at the meson vertex since there is no evidence for a leading π^- (Figure 6, Part 1(g)).

3.2 Experimental Results: π^-p at 11.9 GeV/c

The data described here are part of a 500,000 exposure sample taken at the SLAC 82-inch bubble chamber. The experiment was designed to study multi-particle boson resonances, and initial findings from this study have been reported elsewhere.[23] A search for decay modes of resonances reported from the CERN missing-mass spectrometer experiment[24] is also under way.[25]

Events found by scanning, mostly with Hawaii-built SP-5's, were measured with the SMP and reduced to four-vector form with a double-precision version of the TIPI-SQUAW-ARROW system on IBM-360 and IBM 7040 computers. The 6-prong sample comprises an essentially complete sample measured prior to June 1970, while the 4-prongs (approximately 10,000 events) were measured for this experiment. Fiducial volume cut-offs excluded the near and far ends of the chamber, and the same confidence levels for χ^2 were applied as for the 3.9 GeV/c sample.

For all events found, scanners recorded all "dark" tracks and this was used as an aid in reducing ambiguities. It is found that ionization information alone is sufficient to resolve events ambiguous between 4C and 1C in all but about 10 percent of the ambiguous events. Events ambiguous between $p4\pi$ and $n4\pi$ are more difficult to resolve; here application of ionization criteria leave more than 15 percent of the events still ambiguous, and a partial scan shows these events to be

unresolvable visually. This is due in part to difficulties in obtaining consistent illumination throughout the chamber.

There is clear evidence throughout the experiment for very backward peripherally-produced nucleons in the final state. It was deemed reasonable to assign the ambiguous events which are not resolved by ionization to the hypothesis which yielded the most backward nucleon. This method reduces, but does not eliminate, a bump in $M(4\pi)$ near 2100 Mev among $n4\pi$ events, which may otherwise be evidence for a 4π decay mode of a known resonance. It appears that considerably more data than are currently available would be needed to ascertain whether this method of resolution introduces biases which would lead to conclusions different from those inferred in this study.

As with the 3.9 GeV/c data, the 4-constraint events here present more distinct features than the 1-constraint fits. The model gives best results for 4-particle and 6-particle 4C events, not quite as good for 5-particle, and rather less conclusive results for 7-body events.

At increasing energy one expects to see an increased contribution from diffraction dissociation at the expense of π exchange. However, it is clear from the data that processes are operative which give very low t to groups of pions with an even number of particles.

Copious production of Δ and ρ resonances is clearly present, with some ω and undoubtedly lesser amounts of other resonances which would be evident in a larger sample of data.

The peripheral nature of the interaction is clear from t(nucleon) and cos(π^- in, π out) distributions.

These general features are next elaborated with reference to the

individual final states. The experimental data and fits for incident momentum 11.9 GeV/c are summarized in Figures 7 through 12.

a. $\pi^-p \to p\pi^+\pi^-\pi^-$ at 11.9 GeV/c

The 4-body events at this energy are characterized by Δ^{++} and ρ^o production (Figure 7, Parts 1(a) and (c)), very low t(p) and related forward π^+ and π^- (Figure 7, Part 1(i-k)). There is a distinct forward peak in the longitudinal momentum component of the π^- (Figure 7, Part 1(n)). From the detailed plots, Figure 7, Part 2, it is clear that the experimental data lack any resemblance to Lorentz invariant phase-space.

In this set of data one may clearly see the "reflections" of ρ and Δ production by diffraction onto other distributions. The ρ (process 3, Table 7) contributes to high $M(p\pi^+\pi^-)$ and low t(p) (Figure 7, Parts 2(d) and (a)); while Δ^{++} (process 4, Table 7) gives rise to low $M(p\pi^+\pi^-)$ and $t(p\pi^+\pi^-)$ (Figure 7, Parts 2(d) and (c)). The shape of the $\cos(\pi^-$ in, $\pi^\pm$ out) distributions (Figure 7, Parts 2(g) and (h)) are also a consequence of these resonances with some contribution from non-resonant diffraction production (process 2 and 5, Table 7).

The behavior of $P_{||}$ for π^- is dramatically different from that for π^+ (Figure 7, Parts 1(m) and (n)). The π^- is far more likely to retain the kinematic characteristics of the beam particle than to transfer these to the π^+. The model does not quite simulate either the very low-energy π^- (peaked near zero) or the very fast π^- (peaked near 2).

b. $\pi^-p \to p\pi^+\pi^-\pi^-\pi^o$ at 11.9 GeV/c

These events, with a missing neutral π, are 1C fits and are not as well-determined kinematically as the 4C events. This and the added

complexity due to the many possible additional intermediate states renders interpretation difficult. There is evidence for Δ^{++} production, some ρ, and a small amount of ω (which is not included in the model, Table 8) (Figure 8, Parts 1(a), (c), and (e)).

Distributions in $\cos(\pi^-$ in, $\pi^{\pm}$, π^-, π^0 out) show that the π^0 and π^- have much stronger forward peaks than the π^+ has. (Figure 8, Part 1(g-i) and Figure 8, Part 1(n-p)). The forward peaking in these plots as well as the low t(p) (Figure 8, Part 1(l)) are not as dramatic as in the 4-body case, and it is clear from $M(4\pi)$ and $P_{||}(p)$ (Figure 8, Parts 1(f) and (m)) that the model is not entirely satisfactory. Difficulties in modeling arise from ambiguities between this and other final states which have probably not been completely resolved and from the lack of a large enough data sample clearly to delineate all the features of this complicated system of particles.

c. $\underline{\pi^-p \to n\pi^+\pi^+\pi^-\pi^- \text{ at } 11.9 \text{ GeV/c}}$

Although there is evidence for Δ^- and ρ^0 production as well as very low t(n) (Figure 9, Parts 1(a), (d), (f), and (i)), this type of event also lacks sufficient statistics to make possible a good fit. There is strong evidence for forward π^+ and π^- (Figure 9, Parts 1(j), (k), (o), and (p)). The data differ markedly from the prediction of phase space (Figure 9, Part 2(a-h)) and Δ^- production (processes 3 and 4) is seen to exert a strong influence on the overall kinematics.

d. $\underline{\pi^-p \to p\pi^+\pi^+\pi^-\pi^-\pi^- \text{ at } 11.9 \text{ GeV/c}}$

This type of event yields a 4C fit and is more amenable to analysis and fitting than the 5-body systems. There is considerable Δ^{++}, and ρ^0

production (Figure 10, Parts 1(a), (c), and (f)). It is noteworthy that non-leading π^- produces far lower $M(\pi^+\pi^-)$ than does the leading π^-. Even with 6 particles in the final state, the deviations from phase space are quite drastic. (Figure 10, Part 2(a-i)).

As with 6-body events at 3.9 GeV/c, there is a marked tendency to low $M(\pi^+\pi^+)$, but here there is little low $M(p\pi^+\pi^+)$ (Figure 10, Parts 1(e) and (b)).

The proton is very backward in the cm (Figure 10, Part 1(s)). This effect and a tendency to low $t(p\pi^+\pi^-)$ as well as a forward π^+ are all attributed, in the model (see Table 10), to processes 4, 5, and 6 which produce ρ^0 in the final state (Figure 10, Parts 2(a), (d), and (h)). Δ production, on the other hand, is responsible for the leading π^- (processes 2 and 3) (Figure 10, Part 2(f)).

Again, as in the 3.9 GeV/c data, there appears to be some asymmetry in cos $\theta_{\pi^-\pi^-}$ and cos $\theta_{\pi^+\pi^-}$ (5π cm), and again it appears to be an artifact of the kinematics (Figure 10, Parts 1(w) and (x)).

e. $\underline{\pi^-p \rightarrow p\pi^+\pi^+\pi^-\pi^-\pi^-\pi^0 \text{ and } n\pi^+\pi^+\pi^+\pi^-\pi^-\pi^-}$

These 7-body events with one missing neutral particle (1C fits) are very complicated. Considerable effort was spent in trying to fit them without completely satisfactory results. The general features of low t(nucleon), leading π, and production of Δ^{++} and ρ resonances are visible (Figure 11 and Figure 12). However, the number of possible combinations of particles in the framework of the model is enormous. It seems likely that successful fits to these states could be achieved if one were willing (and had the computing power) to continue the necessary search for contributing processes. It is quite likely that multiple-π

resonances contribute also, and decay by cascade processes. Determination of the mode of decay of such complicated states (possibly with high spin) would be difficult to do methodically because of the high multiplicity of identical π's.

The fitted results reported in Tables 11 and 12 and displayed in Figures 11 and 12 should therefore be treated as very approximate. They have been included to allow comparison with the lower-multiplicity events.

3.3 Behavior of Longitudinal and Transverse Momentum Components

In addition to the distributions of mass combinations and four-momentum transfer, the longitudinal and transverse components of three-momentum show deviations from phase-space predictions and may be regarded as a test of the model. Distributions in these variables are displayed as the last set of plots in Figures 1-12, Part 1. While mass-plots are useful for detecting the presence of resonances, and t-distributions point out the peripheral nature of the interaction, it is not easy to construct a set of independent quantities in these variables for projecting the varying density in phase space. The components of three-momentum of each particle parallel to and perpendicular to the incoming particle direction ($P_{||}$, and $P_{\perp}$) are, at least, independent variables and give a different perspective on the complicated multi-dimensioned space.

$P_{\perp}$ is remarkably similar for all pions at both energies. This fact has been pointed out by others and is surely directly connected with the peripheral nature of the interaction. Here we have approximated peripherality by exponential and pole forms, and the results from Monte Carlo simulation show that the approximation is quite good. There is a

definite tendency, however, in the real data toward sharper, narrower peaks than the model yields.

The same is true of the longitudinal component, $P_{||}$. The experimental peaks near zero are narrower than the Monte Carlo distributions, while phase-space predicts generally broader, more symmetrical peaks.

In the 4-body case the leading π^- effect shows up as a shoulder in $P_{||}(\pi^-)$ at 3.9 GeV/c (Figure 1, Part (t)) which becomes a separate sharp peak at 11.9 GeV/c (Figure 7, Part 1(n)). It is also clear that this forward peak is not perfectly modeled. The distinction between "nonleading" and "leading" π^- is more pronounced in the real data than in the Monte Carlo simulation.

It is notable that, in the $p\pi^+\pi^-\pi^-\pi^0$ final state, the π^0 shows a tendency to be "leading" as well as the π^-, while there is less tendency toward a "leading" π^+. (See $\cos(\pi^-$ in, π^+, π^-, π^0 out) as well as P_{long}, Figure 8, Parts 1(g-1) and (n-p)). This we interpret to mean that the very forward π^- particles, and sometimes π^0, are diffractively produced. Diffractive production of a π^+ requires simultaneous production of a π^- to conserve charge, and hence is suppressed.

4.0 RELATIONS BETWEEN PARTIAL CROSS-SECTIONS

We have a model which approximately fits 4-, 5-, 6-, and 7-body final states for incident momenta 3.9 and 11.9 GeV/c, and relate this to available data for 2- and 3-body final states at these two energies.[16] Since 5- and 7-body states each may have either a π^0 or a neutron unmeasured (one-constraint fits), the model has been applied to 12 different final states. These are pictured as a mixture of diffraction dissociation and one pion exchange. The model-fitting attempts to measure the partial cross-sections for various channels, including resonance production. Our purpose is to make whatever consistency checks are possible between these 12 sets of partial cross-sections.

There are two independent types of comparisons which can be made. One may compare π-exchange or diffraction dissociation cross-sections at the two energies, and also ratios of cross-sections for specific final state diagrams which must be approximately equal if the Pomeron pole residue factorizes.

A difficulty exists in defining "π-exchange" and "diffraction dissociation" for this comparison because we now wish to visualize the interaction as quasi-two-body. The comparison of partial cross-sections at separate energies by Hansen, Kittel, and Morrison[17] is in terms of "Pomeron exchange" or scattering of the incident pion by a (virtual) Pomeron, and we take this to mean that the number of outgoing mesons from this vertex should be odd.

On the other hand, we have found it necessary to employ the diffractive amplitude $A_{diffractive}$ in fitting 5- and 7-body final states at 11.9 GeV/c for the final states with an even number of pions outgoing

from the meson vertex (see Tables 8, 9, 11, and 12). These are events which have been assigned to the 1C hypothesis, and, as has already been mentioned, the fits are inferior to those for 4C events. There is, however, evidence for low t(nucleon) in the 5-body events which is reasonably well fitted by the $e^{bt(\pi,n\pi)}$ amplitude and has not been successfully fitted without it.

The inconsistency in definition concerns only those processes which have 4 or 6 pions outgoing at the meson vertex; processes with 2 pions have been treated as π-exchange and the appropriate amplitude, $A_{exchange}$, employed. This is consistent with the definition of diffraction dissociation of Good and Walker.[8]

We arbitrarily treat the processes with 4 or 6 pions outgoing from the meson vertex (designated as EPD in the Tables) neither as pion-exchange nor as Pomeron-exchange but consider them as diffractive background to be added to our other background, e.g., phase-space and heavy-particle exchange. Our model depends upon the kinematic distinction between $e^{bt(\pi,n\pi)}$ with n even and n odd, and we assume that cross-sections for processes with n odd are approximately correct.

With these considerations, we show in Table 15 the cross-sections inferred for the various mechanisms in each reaction.

4.1 Variation of Cross-Sections with Energy

We choose to study the variation with energy of π-exchange and diffraction dissociation cross-sections as suggested by Hansen, Kittel, and Morrison.[17] They have shown that cross-sections for a wide variety of multibody final states at several energies are linked to the reaction mechanism and to 2-body interactions in a way which separates the

"physics" from phase-space considerations. For 2-body interactions, $\sigma = \text{const} \cdot P_{lab}^{-n}$ is a good approximation, where n depends on the reaction mechanism. For multibody events, they show that one may take

$$\sigma = (\text{const}) \cdot (\text{phase-space volume}) \cdot P_{lab}^{-(n_a+K)+2}$$

where $n_a = 2$ for π-exchange and $n_a = 0.2$ for Pomeron exchange, and K is the number of particles in the final state.

The value of n_a is approximately what would be expected from Regge ideas where

$$\sigma(s) \sim \left(\frac{s}{s_o}\right)^{2\alpha(0)-2}$$

For the pion trajectory, $\alpha(0) \approx 0$, while for the Pomeron, $\alpha(0) \approx 0.9$

This predicts ratios of partial cross-sections for each individual process at our two energies:

$$\pi\text{-exchange:} \quad \frac{\sigma(3.9)}{\sigma(11.9)} = \frac{\text{P.S.Vol.}(3.9)}{\text{P.S.Vol.}(11.9)} \cdot \left(\frac{3.9}{11.9}\right)^{-K} \qquad \text{EQN. 4.1}$$

$$\text{Pomeron exchange:} \quad \frac{\sigma(3.9)}{\sigma(11.9)} = \frac{\text{P.S.Vol.}(3.9)}{\text{P.S.Vol.}(11.9)} \cdot \left(\frac{3.9}{11.9}\right)^{+1.8-K} \qquad \text{EQN. 4.2}$$

In reality, our knowledge of the cross-section for any individual process is insufficient, due to lack of statistics, to carry out a detailed comparison. However, it is worthwhile to compare, at least, the summed cross-sections for π and Pomeron exchange for the four-constraint events.

We take the results of fits presented in Tables 1, 4, 7, and 10 and use these in the above formulas. Results of this calculation for 4, 5, and 6-body final states are summarized in Figure 13. In this figure, $\log \sigma_{3.9}^{(p)}$ is plotted versus $\log \left(\sigma_{11.9}^{(p)} \cdot \frac{\text{P.S.Vol.}(3.9)}{\text{P.S.Vol.}(11.9)} \cdot \left(\frac{3.9}{11.9}\right)^{M}\right)$ where

M = multiplicity (in case of π-exchange)

M = 1.8 - multiplicity (in case of Pomeron exchange)

$\sigma^{(p)}_{3.9}$ represents the partial cross-section for a process at 3.9 GeV/c, and $\sigma^{(p)}_{11.9}$ for the partial cross-section for the same process at 11.9 GeV/c. If the model of Hansen, et al., is to be verified, all points on the graph should lie on a line of unit slope. On the figure, circles represent π-exchange cross-sections and squares are used for Pomeron-exchange. The numbers inside these symbols represent multiplicity K, with subscripts to distinguish whether the nucleon is proton or neutron.

The point which appears to be in the most serious disagreement with the others is the 5-body final state (neutron, 4π) Pomeron-exchange process. This final state is well-described by a model which has almost pure π-exchange with a large phase-space background. (See Table 3 and Figure 3.) It is possible that this background obscures a 5 to 10 percent Pomeron-exchange contribution which is needed to make this point consistent with the others. It seems even more likely that the Pomeron-exchange component at 11.9 GeV/c is over-estimated, and this cannot be determined with present statistics.

In general, it appears that the one-constraint events (5-body) give less consistent results than the four-constraint fitted events (4- and 6-body), but the statement can be made that the results show the dependence on beam momentum expected for the mechanism of pion and Pomeron exchange and phenomenologically in agreement with that for any other reactions.

4.2 Connections Between Cross-Sections at One Energy

One of the goals of this study was to test, if possible, the factorization hypothesis for the Regge residue of the Pomeranchuk singularity. This hypothesis predicts ratios between cross-sections for specific 2-body final states. Since what we have assumed for a model is a quasi-two-body final state, and the fitting of the model measured cross-sections for a variety of such quasi-two-body final states, it seems natural to apply the factorization principal to these states and see whether any detectable violations appear.

As energy increases, diffraction dissociation emerges as the most important process. We here treat only those quasi-two-body final states which may be viewed as due to Pomeron exchange. The nature of this exchange must finally be determined by experiment. It is a necessary but not sufficient condition that, if the Pomeranchuk singularity is a pole, its Regge residue must factorize.[18]

We shall adopt the notation of L. van Hove.[19] Consider the general hadronic reaction

$$A + B \longrightarrow A' + B' \qquad \text{EQN. 4.3}$$

where A' = A or is a resonant or non-resonant system of hadrons produced by diffraction dissociation of A, and similarly for B and B'.

There are four possible cases:

$$\begin{aligned} &A' = A \text{ and } B' = B \quad \text{(elastic scattering)} \\ &A' \neq A \text{ and } B' = B \quad \text{(single dissociation of A)} \\ &A' = A \text{ and } B' \neq B \quad \text{(single dissociation of B)} \\ &A' \neq A \text{ and } B' \neq B \quad \text{(double dissociation)} \end{aligned} \qquad \text{EQN. 4.4}$$

The conventional definition of factorization in the t-channel is to write the invariant collision probability thus:

$$|T|^2 = |f(s,t)\ \gamma(t,X_A,X_{A'})\ \gamma(t,X_B,X_{B'})|^2 \qquad \text{EQN. 4.5}$$

where

$$t = (P_A - P_{A'})^2 = (P_B - P_{B'})^2$$

$$s = (P_A + P_B)^2$$

as usual and $(X_A,X_{A'})$, $(X_B,X_{B'})$ define the helicity of A and full state of A', in a reference frame defined in terms of A, A', and for B, B' respectively. This equation for T expresses that in the absence of degeneracy the residue factorizes, and then

$$f(s,t) = -\exp(-i\,\tfrac{\pi}{2}\,\alpha(t))\ s^{\alpha(t)} \qquad \text{EQN. 4.6}$$

where $\alpha(t) \cong 1$ for small t, the Pomeranchuk trajectory.

The usual illustration of factorization[20] relates the $\pi\pi$ scattering cross-section to the measurable πN and NN scattering cross-sections:

$$\begin{aligned} \sigma_{\pi N} &\propto |T_{\pi N}|^2 = |f_{\pi N}\ \gamma_{\pi\pi}\ \gamma_{NN}|^2 \\ \sigma_{NN} &\propto |T_{NN}|^2 = |f_{NN}\ \gamma_{NN}\ \gamma_{NN}|^2 \\ \sigma_{\pi\pi} &\propto |T_{\pi\pi}|^2 = |f_{\pi\pi}\ \gamma_{\pi\pi}\ \gamma_{\pi\pi}|^2 \end{aligned} \qquad \text{EQN. 4.7}$$

Assuming large s and Pomeron exchange, one obtains easily $\sigma_{\pi N}{}^2 = \sigma_{\pi\pi}\ \sigma_{NN}$. Unfortunately, this cannot be used as a direct test of factorization because $\sigma_{\pi\pi}$ can only be measured indirectly.[21]

As a parameterization, one may take $\gamma(t,X_A,X_{A'}) = \gamma_o e^{bt}$. Our information about γ_o and b is very incomplete. It has been demonstrated

that b decreases with increasing m_A'. This is natural if we take the Pomeron mass to be $(t)^{1/2}$. Then the virtual process $P + A \dashrightarrow A'$ has decreasing dependence upon t as m_A', the energy of $P + A \dashrightarrow A'$ in its own rest frame, increases.[22]

In this study we have assumed approximately constant values of b and have determined γ_0 experimentally for several final states. (Given sufficiently good data one could in principle also determine b for each process by allowing it to be a variable parameter in the fitting process.)

To the degree that the assumption of constant b is justified, one obtains from the equation for T

$$\frac{d\sigma}{dt} = s^{-2}|f\gamma_{AA'}(t)\gamma_{BB'}(t)|^2 \qquad \text{EQN. 4.8}$$

where $\gamma_{AA'}$, $\gamma_{BB'}$ stand for measured quantities in which sums have been made over most of the (X,X') variables. One then obtains ratios in which the t-dependence cancels.

$$\frac{\frac{d\sigma}{dt}(BB \to BB)}{\frac{d\sigma}{dt}(AB \to AB)} = \frac{\frac{d\sigma}{dt}(BB \to BB')}{\frac{d\sigma}{dt}(AB \to AB')} = \frac{\frac{d\sigma}{dt}(BB \to BB'')}{\frac{d\sigma}{dt}(AB \to AB'')} \qquad \text{EQN. 4.9}$$

The case analyzed by Freund[18] is precisely this, with B = proton, $A = \pi$, $B' = N^*(1400)$, and $B'' = N^*(1688)$. The experimental results are consistent with the validity of factorization. We note that, as pointed out by Freund, if this equation holds at $t = 0$, it will hold at all t.

The factorization property is not limited to 2-body final states. A' and B' may just as well be composites of particles which may or may not contain resonances. For nonresonant final states with n pions, m

of which are at the meson vertex,

$$\frac{\frac{d\sigma}{dt}[\pi p \to (p\pi \cdots \pi_{n-m})(\pi_{n-m+1} \cdots \pi_n)]}{\frac{d\sigma}{dt}[\pi p \to (p\pi \cdots \pi_{n-1})(\pi_n)]} \quad \frac{\frac{d\sigma}{dt}[\pi p \to (p)(\pi_1 \cdots \pi_n)]}{\frac{d}{dt}[\pi p \to (p)(\pi)]} \qquad \text{EQN. 4.10}$$

where $(p\pi \cdots \pi)$, $(\pi_1 \cdots \pi)$ represent clusters of particles at baryon and meson vertices respectively.

It is now possible to write down a large number of such ratios which must be approximately satisfied. Figure 14a displays the non-resonant channels possible with 2 to 7 particles in the final state. There are also a limited number of resonant states where factorization imposes restrictions and where the data are good enough to allow comparisons. We limit the comparison to $I_3 = 3/2$ $\Delta(1236)$ production, since the $I_3 = 1/2$ substates are less pronounced (being suppressed by Clebsch-Gordan coefficients), and selected examples where ρ production is prominent. Diagrams for these final states are presented in Figure 14b.

The many ratios which one may write fall into three classes which are designated A, B, and C in Figure 14c. The number of π's at a vertex (j, k, l, or m in the figure) must be the same in numerator as denominator in order that γ cancel. Cross-sections for resonances in final states are considered separately from nonresonant cross-sections; here again, the resonance must appear in a γ in such a way that it cancels in the ratio equation. Capital N stands for nucleon, either proton or neutron; it must also be the same in order for γ to cancel in an equation (as in Class B).

The ratios for which some information is obtained from the experiment

are now to be tested. These are listed by class in the form of ratio equations.

Class A: $\frac{\gamma_{p,m\pi p}}{\gamma_{p,m\pi n}}$ ($= \frac{1}{2}$ for pure $I = \frac{1}{2}$)

$$\left(\frac{\sigma_1}{\sigma_2}\right)_{m=1} = \underset{(1)}{\frac{\gamma_{\pi,\pi\gamma p,\pi p}}{\gamma_{\pi,\pi\gamma p,\pi n}}} = \underset{(2)}{\frac{\gamma_{\pi,3\pi\gamma p,\pi p}}{\gamma_{\pi,3\pi\gamma p,\pi n}}} = \underset{(3)}{\frac{\gamma_{\pi,5\pi\gamma p,\pi p}}{\gamma_{\pi,5\pi\gamma p,\pi n}}} = \underset{(4)}{\frac{\gamma_{\pi,\rho\pi\gamma p,\pi p}}{\gamma_{\pi,\rho\pi\gamma p,\pi n}}} \qquad \text{EQN. 4.10}$$

$$\left(\frac{\sigma_1}{\sigma_2}\right)_{m=3} = \underset{(5)}{\frac{\gamma_{\pi,\pi\gamma p,3\pi p}}{\gamma_{\pi,\pi\gamma p,3\pi n}}} = \underset{(6)}{\frac{\gamma_{\pi,\rho\pi\gamma p,3\pi p}}{\gamma_{\pi,\rho\pi\gamma p,3\pi n}}} \qquad \text{EQN. 4.11}$$

Class B: $\frac{\gamma_{\pi,\ell\pi}}{\gamma_{\pi,j\pi}}$

$$\left(\frac{\sigma_1}{\sigma_2}\right)_{\substack{\ell=1\\ j=3}} = \underset{(1)}{\frac{\gamma_{\pi,\pi\gamma p,\pi p}}{\gamma_{\pi,3\pi\gamma p,\pi p}}} = \underset{(2)}{\frac{\gamma_{\pi,\pi\gamma p,\pi n}}{\gamma_{\pi,3\pi\gamma p,\pi n}}} = \underset{(3)}{\frac{\gamma_{\pi,\pi\gamma p,2\pi p}}{\gamma_{\pi,3\pi\gamma p,2\pi p}}} = \underset{(4)}{\frac{\gamma_{\pi,\pi\gamma p,3\pi n}}{\gamma_{\pi,3\pi\gamma p,3\pi n}}} \qquad \text{EQN. 4.12}$$

$$= \underset{(5)}{\frac{\gamma_{\pi,\pi\gamma p,3\pi p}}{\gamma_{\pi,3\pi\gamma p,3\pi p}}} = \underset{(6)}{\frac{\gamma_{\pi,\pi\gamma p,\pi\Delta^{++}}}{\gamma_{\pi,3\pi\gamma p,\pi\Delta^{++}}}} = \underset{(7)}{\frac{\gamma_{\pi,\pi\gamma p,2\pi\Delta^{++}}}{\gamma_{\pi,3\pi\gamma p,2\pi\Delta^{++}}}} \qquad \text{EQN. 4.13}$$

Class C: $\frac{\gamma_{p,m\pi N}}{\gamma_{p,k\pi N}}$

$$\left(\frac{\sigma_1}{\sigma_2}\right)_{\substack{m=0\\ k=2}} = \underset{(1)}{\frac{\gamma_{\pi,\pi\gamma p,p}}{\gamma_{\pi,\pi\gamma p,\pi p}}} = \underset{(2)}{\frac{\gamma_{\pi,3\pi\gamma p,p}}{\gamma_{\pi,3\pi\gamma p,\pi p}}} = \underset{(3)}{\frac{\gamma_{\pi,5\pi\gamma p,p}}{\gamma_{\pi,5\pi\gamma p,\pi p}}} \qquad \text{EQN. 4.14}$$

nonresonant

$$= \underset{(4)}{\frac{\gamma_{\pi,\rho\pi\gamma p,p}}{\gamma_{\pi,\rho\pi\gamma p,\pi p}}} = \underset{(5)}{\frac{\gamma_{\pi,\rho3\pi\gamma p,p}}{\gamma_{\pi,\rho3\pi\gamma p,\pi p}}}$$

$$\frac{\sigma_1}{\sigma_2}_{\substack{m=0\\k=2\\\text{nonresonant}}} = \frac{\gamma_{\pi,\pi}\gamma_{p,p}}{\gamma_{\pi,\pi}\gamma_{p,2\pi p}} = \frac{\gamma_{\pi,3\pi}\gamma_{p,p}}{\gamma_{\pi,3\pi}\gamma_{p,2\pi p}} \qquad \text{EQN. 4.15}$$

(6) (7)

$$\frac{\sigma_1}{\sigma_2}_{\substack{m=0\\k=2\\\text{resonant}}} = \frac{\gamma_{\pi,\pi}\gamma_{p,p}}{\gamma_{\pi,\pi}\gamma_{p,\pi\Delta^{++}}} = \frac{\gamma_{\pi,\rho\pi}\gamma_{p,p}}{\gamma_{\pi,\rho\pi}\gamma_{p,\pi\Delta^{++}}} \qquad \text{EQN. 4.16}$$

(8) (9)

$$\frac{\sigma_1}{\sigma_2}_{\substack{m=0\\k=1\\\text{resonant}}} = \frac{\gamma_{\pi,\pi}\gamma_{p,p}}{\gamma_{\pi,\pi}\gamma_{p,\pi n}} = \frac{\gamma_{\pi,3\pi}\gamma_{p,p}}{\gamma_{\pi,3\pi}\gamma_{p,\pi n}} = \frac{\gamma_{\pi,5\pi}\gamma_{p,p}}{\gamma_{\pi,5\pi}\gamma_{p,\pi n}} \qquad \text{EQN. 4.17}$$

(10) (11) (12)

$$= \frac{\gamma_{\pi,\rho\pi}\gamma_{p,p}}{\gamma_{\pi,\rho\pi}\gamma_{p,\pi n}} = \frac{\gamma_{\pi,\rho 3\pi}\gamma_{p,p}}{\gamma_{\pi,\rho 3\pi}\gamma_{p,\pi n}}$$

(13) (14)

These three classes of ratios are plotted in Figure 15, with σ_1 (numerators) plotted as ordinates and σ_2 (denominators) plotted as abscissae. Data for 3.9 and 11.9 GeV/c are plotted separately, to left and right respectively. Numbers beside the data points correspond to terms in Equations 4.10 to 4.17.

In Figure 15(a), which presents ratios of Class A, term (1) at each energy has non-zero cross-sections. These are total cross-sections taken from Tables 13 and 14 literature (not determined in this experiment). All other experimentally-determined cross-sections for Class A are consistent with zero, and therefore the corresponding terms are near the origin. We see that these three points indeed lie on a straight line. The line, however, is not that predicted for I = 1/2,

which is also shown in the figure. We explain this by noting that the points taken from the literature (unlike those determined in this work) are not the result of model fits and thus contain contributions from processes other than Pomeron exchange.

Figure 15(b) presents ratios of Class B. Points not appearing on the plot are clustered at the origin. In this set of ratios, cross-sections for lower multiplicities appear in the numerator and for higher multiplicities in the denominator, so it is not surprising that all points group along the vertical axis. There is no noticeable exception to the rule that the partial cross-section decreases with increasing multiplicity, even at 11.9 GeV/c where there is ample energy to create pions.

Figure 15(c) presents ratios of Class C. The ratios containing cross-sections for elastic scattering cannot be plotted to the same scale as the others, since $\sigma_{elastic} \sim 6$ mb. Therefore, these terms (1, 6, 8, and 10 in the ratio equations) have been plotted above the other ratios in Figure 15(c) with different scaling.

Class C actually consists of 4 independent ratio equations: m=0, k=1, resonant and nonresonant; m=0, k=2, resonant and nonresonant. Terms without numbers appearing on the 4 graphs (which represent these 4 equations) have $\sigma_1 = \sigma_2 = 0$, i.e., they again cluster at the origin.

The paucity of well-determined data points in the graphs of Figure 15 is due in part to limited data. This is especially true of 6- and 7-body events at the lower energy, and of 5-body events at the higher energy. This increases the tendency of points to cluster at the origin: cross-sections for processes not included in our model are taken as zero.

Since the model-fitting procedure measures the partial cross-sections for the major processes, the cross-sections not measured must be small, and the clustering of points near the origin is then presumably real. Although we are unable to determine accurate slopes for the lines connecting terms in the ratio equations, we have shown that these lines pass through the origin.

The factorization principle implies a correlation between partial cross-sections. Thus, even in the case when both cross-sections are zero, we have a corroboration of the principle. If one cross-section is zero, the other must be also.

Ratios in Class C with k=1 relate 4-constraint fits (with all variables measured) to 1-constraint fits (having one missing neutral particle). Results, shown in Figure 15(c), indicate that the numerator in each ratio of Equation 4.14 is much larger than the corresponding denominator. Also, the ratios of total cross-sections

$$\frac{\sigma(\pi^- p \to \pi^- p)}{\sigma(\pi^- p \to \pi^- \pi^0 p)} \; , \; \frac{\sigma(\pi^- p \to \pi^- p)}{\sigma(\pi^- p \to \pi^- \pi^+ n)}$$

are much greater than 1 at both energies; one would expect ratios nearer 1 from an intuitive viewpoint, since there is ample excess energy for the creation of the additional pion. Schilling[16] has demonstrated that Pomeron exchange is important in the production of the 3-body states $\pi^-\pi^0 p$ and $\pi^-\pi^+ n$, but does not entirely dominate the reaction.

If these states are produced by Pomeron exchange, they must have $\pi^0 p$ or $\pi^+ n$ at the baryon vertex. Apparently this configuration is suppressed. Factorization then predicts the suppression of <u>all</u> states with $\pi^0 p$ or $\pi^+ n$ at the baryon vertex and an odd number of pions at the

meson vertex, and this is exactly what is observed in Figure 15(c).

In other words, if Pomeron exchange does not dominate the 3-body final state, factorization suggests that it will not dominate in 5-body and 7-body final states either. It has been observed in this experiment and others that the ratios

$$\frac{\sigma(\pi^- p \to p\pi^+\pi^-\pi^-\pi^0)}{\sigma(\pi^- p \to n\pi^+\pi^+\pi^-\pi^-)} \; , \; \frac{\sigma(\pi^- p \to p\pi^+\pi^+\pi^-\pi^-\pi^-\pi^0)}{\sigma(\pi^- p \to n\pi^+\pi^+\pi^+\pi^-\pi^-\pi^-)}$$

are significantly greater than 1, and should be 1/2 for pure Pomeron exchange (I = 1/2). Thus, the clustering of all high-multiplicity points in Figure 15(a) (see Equations 4.10 and 4.11) seems to imply that a production mechanism other than Pomeron exchange is operative for producing final states with an even number of pions. In the models presented here, this has been approximated with a diffractive (exponential) dependence on t, called EPD in Tables 8, 9, 11, and 12. Although the results are not conclusive, it appears that the importance of this "even-pion diffraction" increases with multiplicity.

5.0 SUMMARY AND CONCLUSIONS

This study concerns the kinematic behavior of final-state particles in the generic reaction

$$\pi^- + p \rightarrow \text{nucleon} + k\pi,\ 2 < k < 7$$

A mathematical model has been constructed heuristically by testing various types of matrix elements to see which yield kinematic features which simulate the real data. It has been found that a combination of processes, designated as π-exchange and diffraction dissociation, rather closely imitates the experimental data on each of the six final states studied.

The interaction amplitudes representing each of these processes contain factors which cause enhancement at low four-momentum-transfer to particular combinations of particles. These consist of a pole in t for π-exchange, an exponential for diffraction. Each also has factors which represent the formation of resonances in final state particles where applicable, notably ρ, Δ, and ω. Each process is visualized as a two-vertex Feynman diagram; no multiperipheral factors are introduced, and the exchanged pion is treated as being on its mass-shell.

Fits to data yield estimates of the relative strengths of final-state channels, which are translated into cross-sections. The experiment therefore measures cross-sections for a fairly large number of substates, notably ρ and Δ production, in specific configurations. This is itself new information, but of greater interest is a comparison of these experimentally-determined cross-sections with theoretical predictions. For example, the cross-section for π-exchange is expected to decrease

with incident momentum as $\frac{1}{p^2}$. Hence, a fairly substantial π-exchange signal at 3.9 GeV/c will be reduced to an inconsequential amount at 11.9 GeV/c. This prediction seems to be borne out by the data: 5-body data which are fitted well by a model which is chiefly π-exchange at 3.9 GeV/c have little or no π-exchange signal at 11.9 GeV/c. Instead, these events appear to have been produced by diffractive processes and are best described by an exponential t-dependence.

Existence of a strongly-contributing diffractive process should make possible detailed tests of the factorization hypothesis. This relates ratios of cross-sections for different multiplicities at a fixed energy. Several of these ratios have been tested. The results, unfortunately, are not very conclusive. Difficulties arise from a lack of sufficient statistics in most channels of interest, so that the ratios are indeterminate. Each final-state is composed of several contributing processes, no one of which dominates the reaction. Even those processes which have appreciable cross-sections appear in the ratios with other processes of low cross-section so that the ratio is not well defined.

Despite these difficulties, there are at least two points which deserve mention. First, the amounts of non-resonant diffraction dissociation appear to be small. Even at the higher energy, there is strong evidence for resonance production. Second, no strong violation of factorization is evident. Had there been one process dominating in a certain final state such that factorization is really violated, this should be visible in the ratios. Since no constraint was placed on the amount of any given process which may be fitted in a model, and 12 fits

have been developed, each consisting of several processes, it seems unlikely that the ratios computed would accidentally be consistent with the factorization hypothesis. If one assumes that factorization is correct, then the argument may be turned around to infer that the models constructed appear plausible.

The ratio of elastic (2-body) to inelastic (3-body) 2-prong cross-sections predicts that all non-resonant final-state configurations with an odd number of pions at the meson vertex and one pion at the baryon vertex will be suppressed. This has been amply verified in the experiment. One may also observe that the production of 2 additional pions at the meson vertex is accompanied with a reduction in cross-section of about a factor of 10. It appears that a similar principle is operative with regard to multiplicity of pions at the baryon vertex. It appears as a result that all non-resonant processes with an odd number of pions at the meson vertex have very small cross-sections.

Based on intuitive arguments, one might expect that the transition from 4-body to 5-body events (or from 6-body to 7-body) would be accomplished by formation of an extra pion at the baryon vertex. That this does not take place has been noted by other experimenters and is verified in this experiment. Now in the light of the prediction of factorization from the ratio of 2- to 3-body events, this effect is no longer surprising.

The factorization tests relate different multiplicities at one energy. Since we have measured a set of cross-sections at each of two energies, it is interesting to see how various partial cross-sections behave as a function of energy. This is directly related to the

observations of Hansen, Kittel, and Morrison[17] who have studied reactions which are "pure" π and Pomeron exchange. We have estimated cross-sections for each of these processes and computed ratios using their formulas. The results are generally consistent within the precision to which the parameters are known and the various cross-sections are determined.

ACKNOWLEDGEMENTS

The film at 3.9 GeV/c was taken at the Lawrence Radiation Laboratory using the 72-inch bubble chamber and was loaned by the Powell-Birge and Trilling-Goldhaber groups. Data at 11.9 GeV/c were taken at the Stanford Linear Accelerator Center, and we wish to express appreciation for the careful work of the 82-inch bubble-chamber crew.

The experiment could not have been successful without the excellent cooperation of our scanning and measuring staff, and especially William Roseman who did a multitude of programming tasks in addition to his other responsibilities.

Discussion with a number of physicists led to the ideas developed here. Among those who offered substantial help were: Dr. Gerson Goldhaber of LRL; Dr. Leon van Hove of CERN; and Dr. Vernon Barger of the University of Wisconsin. It is a particular pleasure to remember many useful and stimulating discussions with my friend and colleague Peter Wohlmut.

This work was done under the auspices of the U.S. Atomic Energy Commission.

REFERENCES

1. Saclay-Orsay-Bari-Bologna Collaboration, Nuovo Cimento 29 (1963) 515;
C. Allf-Steinberger et al., Phys. Rev. 145 (1966) 1072;
Aachen-Berlin-Birmingham-Bonn-Hamburg-London (I.C.)-München Collaboration, Phys. Rev. 138 (1965) B897;
R. Christian et al., Phys. Rev. 143 (1966) 1105;
D. D. Carmony, F. Grard, R. T. Van de Walle, and N. H. Xuong, in Proceedings of the 1962 Annual International Conference on High-Energy Nuclear Physics at CERN, edited by J. Prentki (CERN, Geneva, 1962) p. 44;
P. R. Klein et al., Phys. Rev. 150 (1966) 1123;
J. Alitti et al., Nuovo Cimento 35 (1965) 1;
A. W. Key et al., Phys. Rev. 166 (1968) 1430;
S. U. Chung et al., Phys. Rev. 165 (1968) 1491;
Y. Y. Lee et al., Phys. Rev. 159 (1967) 1156;
V. Hagopian, Ph.D. thesis, University of Pennsylvania, 1964 (unpublished);
B. C. Shen et al., Phys. Rev. Letters 15 (1965) 731;
T. G. Schumann, Ph.D. thesis, University of California, Berkeley, UCLRL-11942, 1965 (unpublished);
R. B. Willman et al., Phys. Rev. Letters 24 (1970) 1260;
K. F. Shen et al., Phys. Rev. D1 (1970) 54;
E. W. Anderson et al., Phys. Rev. Letters 25 (1970) 699;
E. West et al., Phys. Rev. 149 (1968) 1089;
N. Angelov et al., Resonance Production in 4-Prong at 2.34 GeV/c, Communications of the Joint Institute for Nuclear Research, Dubna (1969);

N. M. Cason et al., Phys. Rev. D1 (1971) 851;

G. W. Brandenburg et al., Nucl. Phys. B16 (1970) 287.

2. K. Abe et al., Phys. Rev. Letters 22 (1969) 251;

P. G. Wohlmut et al., Nucl. Phys. B18 (1970) 505.

3. L. Van Hove, Nucl. Phys. B9 (1969) 331.

4. P. G. O. Freund, Phys. Rev. Letters 21 (1968) 1375;

E. W. Anderson et al., Phys. Rev. Letters 25 (1970) 699.

5. J. Friedman, R. Ross, Alvarez Group Memo P-102, Lawrence Radiation Lab. (unpublished);

J. Friedman, Alvarez Group Memo P-156, Lawrence Radiation Lab. (unpublished).

6. P. G. Wohlmut, M.S. Thesis, University of Hawaii (1968) UH-511-18-68 (unpublished);

A. D. Johnson, M.S. Thesis, University of Hawaii (1968) UH-511-17-68 (unpublished);

K. Abe et al., Phys. Rev. D1 (1970) 91.

7. E. Ferrari, F. Selleri, Nuovo Cimento 21 (1961) 1028;

J. D. Jackson, Rev. Mod. Phys. 37 (1965) 484;

H. P. Dürr, H. Pilkuhn, Nuovo Cimento 40 (1965) 899.

8. M. L. Good, W. D. Walker, Phys. Rev. 120 (1960) 1857.

9. B. Y. Oh, W. D. Walker, Phys. Letters 28B (1969) 564;

G. Alexander et al., Phys. Rev. 177 (1969) 2092;

E. W. Anderson et al., Phys. Rev. Letters 16 (1966) 855;

W. D. Walker et al., Phys. Rev. Letters 20 (1968) 133.

10. J. A. Gaidos et al., Phys. Rev. D2 (1970) 1226.

11. L. Van Hove, Nucl. Phys. B9 (1969) 331;

A. Bialas et al., Nuc. Phys. B11 (1969) 479.

12. G. W. Brandenburg et al., Nucl. Phys. B16 (1970) 369.
13. S. U. Chung et al., Phys. Rev. 165 (1968) 1491;
    B. C. Shen, UCRL-16170 (Thesis)(1965).
14. E. Hegedue et al., Z. Physik 225 (1969) 121.
15. S. Goldhaber et al., Phys. Rev. Letters 3 (1959) 181 (see also 1969 Lund Conference Notes, p. 161).
16. P. Shilling, DESY R1-70/3 (Thesis)(1970).
17. J. D. Hansen et al., CERN D. PH.II, 7-32, 12, 18 (1970) (submitted to Nucl. Phys. B).
18. P. G. O. Freund, Phys. Rev. Letters 21 (1968) 1375 (see also 1969 Lund Conference Notes, p. 172, for further tests of factorization).
19. L. Van Hove, CERN TH. 1209 (1970).
20. M. Gell-Mann, Phys. Rev. Letters 8 (1962) 263.
21. E. Colton et al., UCRL-20053.
22. H. Satz, Phys. Letters 29B (1969) 38.
23. M. Peters et al., paper submitted to Kiev Conference on High-Energy Physics (1970).
24. M. N. Focacci et al., Phys. Rev. Letters 17 (1966) 890.
25. P. G. Wohlmut, University of Hawaii, Ph.D. Thesis (unpublished).
26. L. D. Jacobs, Ph.D. Thesis, University of California.

TABLE 1

Model fit to $\pi^- p \to p\pi^+\pi^-\pi^-$ at 3.9 GeV/c. Reaction 1, abbreviated P4(3.9). SYS is an estimate of systematic error in the fitting procedure. Vertex Multiplicity gives the number of particles taken to be outgoing from the meson and baryon vertices of a 2-vertex Feynman graph. OPE stands for one-pion-exchange, which is assumed to be dominated by a pole at the pion mass. DIFF means that an exponential t-dependence has been assumed, with an odd number of mesons at the meson vertex. EPD, for even-pion diffraction, is a process having an exponential t-dependence but an even number of pions at the meson vertex. (The above remarks apply to Tables 1 - 12.)

TABLE 1

PI-P AT 4 GEV/C, PROTON,3PI

REACTION 1 P INCIDENT = 3.90 7980 EVENTS CROSS-SECTION = 1.92 MB. SYS = .01

	PROCESS	VERTEX MULTIPLICITY MESON	BARYON	MECHANISM	FRACTION FITTED	CROSS SECTION(MB)	EXPTL. ERROR(MB)
1.	DEL++	2	2	OPE	0.130	0.25	0.034
2.	DELO,RHO	2	2	OPE	0.120	0.23	0.038
3.	RHOO	3	1	DIFF.	0.133	0.26	0.041
4.	DEL++	1	3	DIFF.	0.203	0.39	0.044
5.	AZ-,RHO	3	1	RHO-EXCH	0.093	0.18	0.040
6.	PHASESPACE				0.322	0.62	0.039

TABLE 2

Model fit to $\pi^- p \to p\pi^+\pi^-\pi^-\pi^0$ at 3.9 GeV/c. Reaction 2, abbreviated P5(3.9).

TABLE 2

PI-P AT 4 GEV/C, PROTON,4PI

REACTION 2 P INCIDENT = 3.90 6870 EVENTS CROSS-SECTION = 2.08 MB. SYS = .02

	PROCESS	VERTEX MULTIPLICITY MESON	BARYON	MECHANISM	FRACTION FITTED	CROSS SECTION(MB)	EXPTL. ERROR(MB)
1.	DEL++	1	4	DIFF.	0.103	0.21	0.062
2.	DEL++	2	3	OPE	0.099	0.21	0.067
3.	DELO	2	3	OPE	0.068	0.14	0.067
4.	NONRES.	4	1	OPE	0.071	0.15	0.062
5.	RHOO	4	1	OPE	0.076	0.16	0.081
6.	RHO-	4	1	OPE	0.101	0.21	0.081
7.	OMEGA	4	1	OPE	0.152	0.32	0.067
8.	PHASESPACE				0.330	0.69	0.084

TABLE 3

Model fit to $\pi^- p \to N\pi^+\pi^+\pi^-\pi^-$ at 3.9 GeV/c. Reaction 3, abbreviated N5(3.9).

TABLE 3

PI-P AT 4 GEV/C, NEUTRON,4PI

REACTION 3 P INCIDENT = 3.90 3560 EVENTS CROSS-SECTION = 1.08 MB. SYS = .02

	PROCESS	VERTEX MULTIPLICITY MESON	BARYON	MECHANISM	FRACTION FITTED	CROSS SECTION(MB)	EXPTL. ERROR(MB)
1.	DEL-	1	4	DIFF.	0.010	0.01	0.039
2.	DEL-	2	3	OPE	0.250	0.27	0.046
3.	RHOO	2	3	OPE	0.082	0.09	0.047
4.	RHOO	4	1	OPE	0.165	0.18	0.052
5.	NONRES.	4	1	OPE	0.124	0.13	0.051
6.	PHASESPACE				0.370	0.40	0.054

TABLE 4

Model fit to $\pi^- p \rightarrow p\pi^+\pi^+\pi^-\pi^-\pi^-$ at 3.9 GeV/c. Reaction 4, abbreviated P6(3.9).

TABLE 4

PI-P AT 4 GEV/C, PROTON,5PI

REACTION 4 P INCIDENT = 3.90 456 EVENTS CROSS-SECTION = 0.12 MB. SYS = .03

	PROCESS	VERTEX MULTIPLICITY MESON	BARYON	MECHANISM	FRACTION FITTED	CROSS SECTION(MB)	EXPTL. ERROR(MB)
1.	RHOO	2	4	OPE	0.199	0.02	0.009
2.	DEL++	4	2	OPE	0.249	0.03	0.009
3.	DEL++	1	5	DIFF.	0.139	0.02	0.008
4.	PHASESPACE				0.414	0.05	0.011

TABLE 5

Model fit to $\pi^- p \rightarrow p\pi^+\pi^+\pi^-\pi^-\pi^-\pi^0$ at 3.9 GeV/c. Reaction 5, abbreviated P7(3.9).

TABLE 5

PI-P AT 4 GEV/C, PROTON,6PI

REACTION 5 P INCIDENT = 3.90 603 EVENTS CROSS-SECTION = 0.13 MB. SYS = .1

	PROCESS	VERTEX MULTIPLICITY MESON,BARYON		MECHANISM	FRACTION FITTED	CROSS SECTION(MB)	EXPTL. ERROR(MB)
1.	DEL++	1	6	DIFF.	0.278	0.04	0.027
2.	DEL++	3	4	DIFF.	0.071	0.01	0.017
3.	OMEGA	4	3	OPE	0.345	0.04	0.014
4.	PHASESPACE				0.306	0.04	0.026

TABLE 6

Model fit to $\pi^- p \to N\pi^+\pi^+\pi^+\pi^-\pi^-\pi^-$ at 3.9 GeV/c. Reaction 6, abbreviated N7(3.9).

TABLE 6

PI-P AT 4 GEV/C, NEUTRON,6PI

REACTION 6 P INCIDENT = 3.90 292 EVENTS CROSS-SECTION = 0.06 MB. SYS = .1

	PROCESS	VERTEX MULTIPLICITY MESON	BARYON	MECHANISM	FRACTION FITTED	CROSS SECTION(MB)	EXPTL. ERROR(MB)
1.	DEL-	4	3	OPE	0.300	0.02	0.012
2.	DEL+OR-	3	4	DIFF.	0.200	0.01	0.012
3.	PHASESPACE				0.500	0.03	0.012

TABLE 7

Model fit to $\pi^- p \to p\pi^+\pi^-\pi^-$ at 11.9 GeV/c. Reaction 1, abbreviated P4(12).

TABLE 7

PI-P AT 12 GEV/C, PROTON,3PI

REACTION 1 P INCIDENT = 11.90 931 EVENTS CROSS-SECTION = 0.84 MB. SYS = .02

	PROCESS	VERTEX MULTIPLICITY MESON	BARYON	MECHANISM	FRACTION FITTED	CROSS SECTION(MB)	EXPTL. ERROR(MB)
1.	RHOO,DELO	2	2	OPE	0.072	0.06	0.025
2.	NONRES.	3	1	DIFF.	0.203	0.17	0.067
3.	RHOO	3	1	DIFF.	0.338	0.28	0.040
4.	DEL++	1	3	DIFF.	0.261	0.22	0.032
5.	NONRES.	1	3	DIFF.	0.090	0.08	0.029
6.	PHASESPACE				0.036	0.03	0.042

TABLE 8

Model fit to $\pi^- p \rightarrow p\pi^+\pi^-\pi^-\pi^0$ at 11.9 GeV/c. Reaction 2, abbreviated P5(12).

TABLE 8

PI-P AT 12 GEV/C, PROTON,4PI

REACTION 2 P INCIDENT = 11.90 1519 EVENTS CROSS-SECTION = 1.36 MB. SYS = .03

	PROCESS	VERTEX MULTIPLICITY MESON	BARYON	MECHANISM	FRACTION FITTED	CROSS SECTION(MB)	EXPTL. ERROR(MB)
1.	DEL++	1	4	DIFF.	0.080	0.11	0.050
2.	NONRES.	1	4	DIFF.	0.083	0.11	0.057
3.	NONRES.	4	1	EPD	0.379	0.52	0.071
4.	RHO-	2	3	OPE	0.218	0.30	0.059
5.	RHOO	2	3	OPE	0.113	0.15	0.055
6.	PHASESPACE				0.127	0.17	0.095

TABLE 9

Model fit to $\pi^- p \to N\pi^+\pi^+\pi^-\pi^-$ at 11.9 GeV/c. Reaction 3, abbreviated N5(12).

TABLE 9

PI-P AT 12 GEV/C, NEUTRON,4PI

REACTION 3 P INCIDENT = 11.90 1076 EVENTS CROSS-SECTION = 0.97 MB. SYS = .05

	PROCESS	VERTEX MULTIPLICITY MESON	BARYON	MECHANISM	FRACTION FITTED	CROSS SECTION(MB)	EXPTL. ERROR(MB)
1.	NONRES.	4	1	EPD	0.210	0.20	0.088
2.	A2,RHO	4	1	EPD	0.090	0.09	0.087
3.	DEL-	2	3	OPE	0.180	0.17	0.087
4.	DEL-	1	4	DIFF.	0.090	0.09	0.068
5.	DEL+	1	4	DIFF.	0.110	0.11	0.078
6.	RHOO	3	2	DIFF.	0.180	0.17	0.087
7.	NONRES.	3	2	DIFF.	0.070	0.07	0.068
8.	PHASESPACE				0.070	0.07	0.097

TABLE 10

Model fit to $\pi^- p \rightarrow p\pi^+\pi^+\pi^-\pi^-\pi^-$ at 11.9 GeV/c. Reaction 4, abbreviated P6(12).

TABLE 10

PI-P AT 12 GEV/C, PROTON,5PI

REACTION 4 P INCIDENT = 11.90 1350 EVENTS CROSS-SECTION = 0.19 MB. SYS = .02

	PROCESS	VERTEX MULTIPLICITY MESON	BARYON	MECHANISM	FRACTION FITTED	CROSS SECTION(MB)	EXPTL. ERROR(MB)
1.	RHOO	2	4	OPE	0.177	0.03	0.007
2.	DEL++	1	5	DIFF.	0.141	0.03	0.007
3.	DELO	1	5	DIFF.	0.145	0.03	0.007
4.	DELO,RHO	3	3	DIFF.	0.223	0.04	0.007
5.	A1,RHO	5	1	DIFF.	0.111	0.02	0.007
6.	A2,RHO	5	1	DIFF.	0.154	0.03	0.007
7.	PHASESPACE				0.050	0.01	0.008

TABLE 11

Model fit to $\pi^- p \rightarrow p\pi^+\pi^+\pi^-\pi^-\pi^-\pi^0$ at 11.9 GeV/c. Reaction 5, abbreviated P7(12).

TABLE 11

PI-P AT 12 GEV/C, PROTON,6PI

REACTION 5 P INCIDENT = 11.90 2000 EVENTS CROSS-SECTION = 0.81 MB. SYS = .04

	PROCESS	VERTEX MULTIPLICITY MESON	BARYON	MECHANISM	FRACTION FITTED	CROSS SECTION(MB)	EXPTL. ERROR(MB)
1.	DEL++	3	4	DIFF.	0.082	0.07	0.065
2.	RHOO	4	3	EPD	0.166	0.13	0.055
3.	DEL++	1	6	DIFF.	0.216	0.17	0.065
4.	NONRES.	6	1	EPD	0.136	0.11	0.049
5.	RHOO OR-	6	1	EPD	0.096	0.08	0.049
6.	PHASESPACE				0.304	0.25	0.065

TABLE 12

Model fit to $\pi^- p \to N\pi^+\pi^+\pi^+\pi^-\pi^-\pi^-$ at 11.9 GeV/c. Reaction 6, abbreviated N7(12).

TABLE 12

PI-P AT 12 GEV/C, NEUTRON,6PI

REACTION 6 P INCIDENT = 11.90 1500 EVENTS CROSS-SECTION = 0.27 MB. SYS = .08

	PROCESS	VERTEX MULTIPLICITY MESON	BARYON	MECHANISM	FRACTION FITTED	CROSS SECTION(MB)	EXPTL. ERROR(MB)
1.	DEL+OR-	4	3	EPD	0.200	0.05	0.038
2.	RHOO	4	3	EPD	0.300	0.08	0.038
3.	RHOO	5	2	DIFF.	0.150	0.04	0.038
4.	NONRES.	6	1	EPD	0.150	0.04	0.038
5.	PHASESPACE				0.200	0.05	0.049

TABLE 13

Partial cross-sections by multiplicity for $\pi^- p$ at 3.9 GeV/c. Constraint class is 4C for all momenta measured, 1C for events with one neutral particle whose momentum is unmeasured. Number of events used in determining cross-sections is not the same, generally, as was used in the fitting procedure. Events which have more than one missing neutral have been excluded (missing-mass events).

TABLE 13. INTERACTION CROSS-SECTIONS BY MULTIPLICITY: π^-p AT 3.9 GeV/c

Abbr.	Final State	Constant Class	No. of Events	Cross-Section (mb)	Source
P239	$\pi^-p \rightarrow \pi^-p$	4C	12000	6.6 ± .03	L. D. Jacobs (26)
P339	$\pi^-\pi^0p$	1C	6000	2.3 ± 0.1	L. D. Jacobs (26)
N339	$\pi^-\pi^+n$	1C	7700	1.8 ± 0.1	L. D. Jacobs (26)
P439	$2\pi^-\pi^+p$	4C	7900	1.92 ± 0.1	S. U. Chung (13)
P539	$2\pi^-\pi^+\pi^0p$	1C	6800	2.08 ± 0.1	S. U. Chung (13)
N539	$2\pi^-2\pi^+n$	1C	3700	1.08 ± 0.1	S. U. Chung (13)
P639	$3\pi^-2\pi^+p$	4C	450	.115 ± .02	K. Abe (2)
P739	$3\pi^-2\pi^+\pi^0p$	1C	608	.13 ± .03	This Experiment
N739	$3\pi^-3\pi^+n$	1C	292	.06 ± .02	This Experiment
	All 2-prongs			8.9	
	All 4-prongs			5.08	
	All 6-prongs			.31	
	All 8-prongs			.02	
	Total (inelastic)			14.31	
	Total (inelastic and elastic)			30.9	

TABLE 14

Partial cross-sections by multiplicity for π^-p at 11.9 GeV/c. Same comments apply as for Table 13.

TABLE 14. CROSS-SECTIONS BY MULTIPLICITY IN FINAL STATE: $\pi^- p$ AT 12 GeV/c

Abbr.	Reaction	Constraint Class	No. of Events	Cross-Section (mb)	Source
P212	$\pi^- p \rightarrow \pi^- p$	4C		4.86 ± .21	Schilling (16)
N312	$\pi^- p \rightarrow n\pi^+\pi^-$	1C		.80 ± .08	Schilling (16)
P312	$\pi^- p \rightarrow p\pi^-\pi^0$	1C		.66 ± .08	Schilling (16)
P412	$\pi^- p \rightarrow p\pi^+\pi^-\pi^-$	4C	931	.84 ± .05	This Experiment
P512	$p\pi^+\pi^-\pi^-\pi^0$	1C	1519	1.36 ± .04	This Experiment
N512	$n\pi^+\pi^+\pi^-\pi^-$	1C	1078	.97 ± .06	This Experiment
P612	$p\pi^+\pi^+\pi^-\pi^-\pi^-$	4C	1378	.19 ± .02	A. Yee (this experiment)
P712	$p\pi^+\pi^+\pi^-\pi^-\pi^-\pi^0$	1C	6048	.81 ± .08	A. Yee (this experiment)
N712	$n\pi^+\pi^+\pi^+\pi^-\pi^-\pi^-$	1C	2063	.27 ± .03	A. Yee (this experiment)
	All 2-prongs		(~130000)	6.32	
	All 4-prongs		4698	3.18	
	All 6-prongs		25688	1.27	
	All 8-prongs		250	.3	
	Total (inelastic)			21.5	
	Total (inelastic and elastic)			26.2	

TABLE 15

Summary of partial cross-sections for π-exchange, Pomeron exchange, and background. Cross-sections for individual processes have been summed, from Tables 1-12, to estimate cross-sections for π-exchange, P-exchange (with an odd number of pions at the meson vertex), and background due to phasespace, exchange of heavy mesons, and diffraction dissociation with an even number of pions. Errors are estimated by RMS sums of relative errors in the individual cross-sections.

TABLE 15

SUMMARY OF PARTIAL CROSS-SECTIONS FOR π-EXCHANGE, P-EXCHANGE, AND BACKGROUND (MILLIBARNS)

Reaction	$\sigma_{\pi\text{-exchange}}$	$\sigma_{\text{P-exchange}}$	$\sigma_{\text{background}}$
$P_{incident}$ = 3.9 GeV/c			
1. $\pi^-p \rightarrow p\pi^+2\pi^-$	.48 ± .05	.65 ± .06	.80 ± .056
2. $\rightarrow p\pi^+2\pi^-\pi^o$	1.19 ± .17	.21 ± .062	.69 ± .084
3. $\rightarrow n2\pi^+2\pi^-$	.67 ± .098	.01 ± .039	.4 ± .054
4. $\rightarrow p2\pi^+3\pi^-$	.05 ± .013	.02 ± .008	.05 ± .011
5. $\rightarrow p2\pi^+3\pi^-\pi^o$	.04 ± .014	.05 ± .032	.04 ± .026
6. $\rightarrow n3\pi^+3\pi^-$	.02 ± .012	.01 ± .012	.03 ± .012
$P_{incident}$ = 11.9 GeV/c			
1. $\pi^-p \rightarrow p\pi^+2\pi^-$	.06 ± .025	.75 ± .089	.03 ± .042
2. $\rightarrow p\pi^+2\pi^-\pi^o$	.45 ± .081	.22 ± .076	.69 ± .12
3. $\rightarrow n2\pi^+2\pi^-$	.17 ± .088	.44 ± .15	.36 ± .16
4. $\rightarrow p2\pi^+3\pi^-$	.03 ± .007	.15 ± .016	.01 ± .008
5. $\rightarrow p2\pi^+3\pi^-\pi^o$	.05 ± .05	.24 ± .092	.57 ± .11
6. $\rightarrow n3\pi^+3\pi^-$	< .02 ± .02	.04 ± .038	.22 ± .082

FIGURE 1

Part 1: Overview $\pi^- p \rightarrow p\pi^+\pi^-\pi^-$ at 3.9 GeV/c. Solid lines represent real data, square data Monte Carlo simulation. See Section 3.0 for description of Figures 1-12. a-f, masses of selected particle combinations; events/40 mev. g-m, momentum-transfer-squared (t) to selected particle groups; events/40 mev^2. n-o, cos(π^- incident, $\pi^{\pm}$ outgoing) in cm; events/.04. p-u, longitudinal and transverse components of momentum for each particle in laboratory system; events/50 mev/c for $P_{||}$, events/40 mev/c for $P_{\perp}$.

Part 2: Details. Solid straight lines represent real data, curves represent processes in the Monte Carlo model. See Section 3.0 for description of Figures 1-12. a and e, momentum-transfer-squared to proton and $p\pi^+\pi^-$ combination; events/50 mev^2. b-d and f-h, masses of selected particle combinations; events/40 mev. i, j, cos(π^- incident, $\pi^{\pm}$ outgoing) in cm; events/.05.

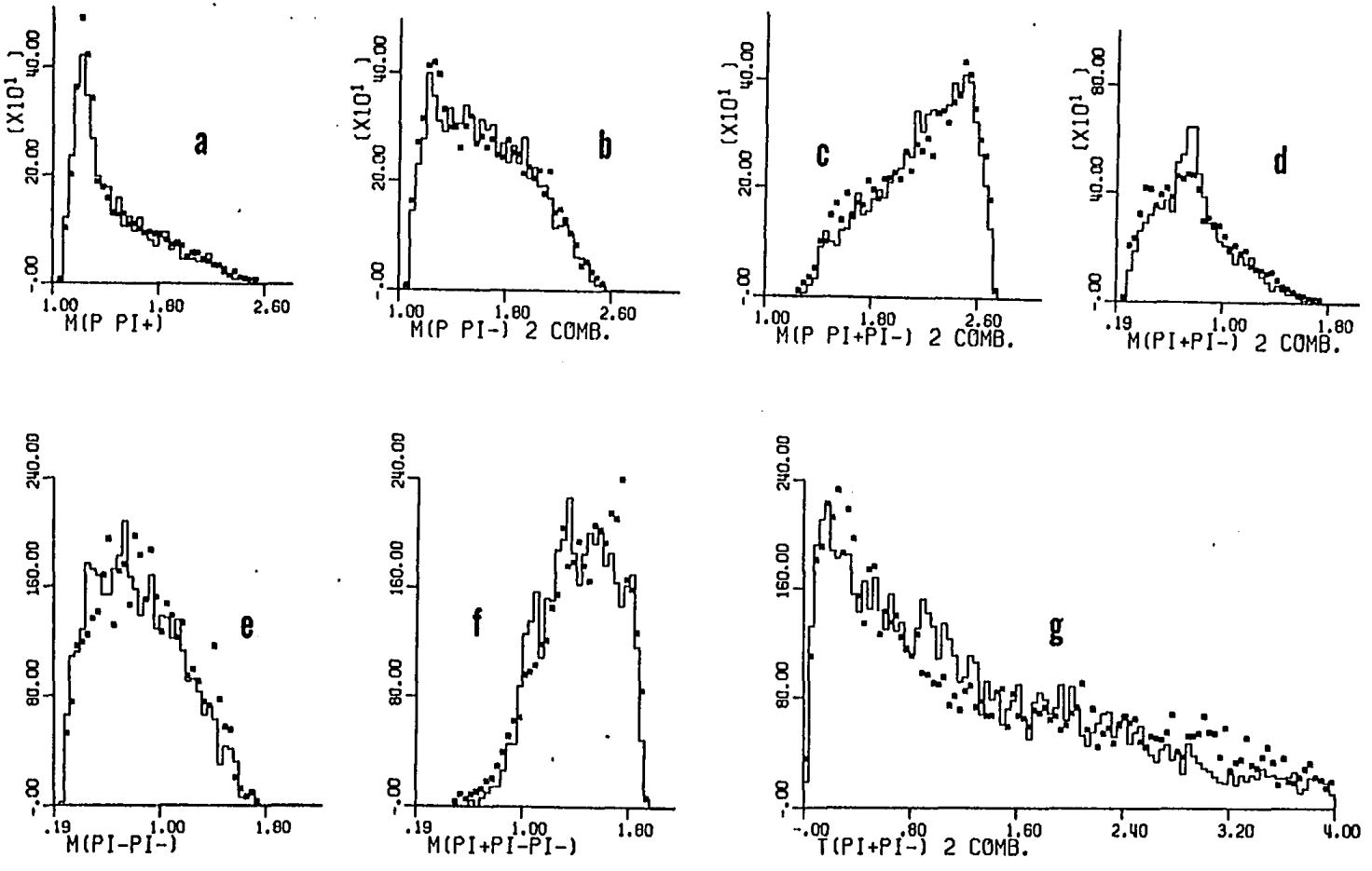

FIG. 1, PART 1 PROTON,3 PI (3.9 GEV/C)

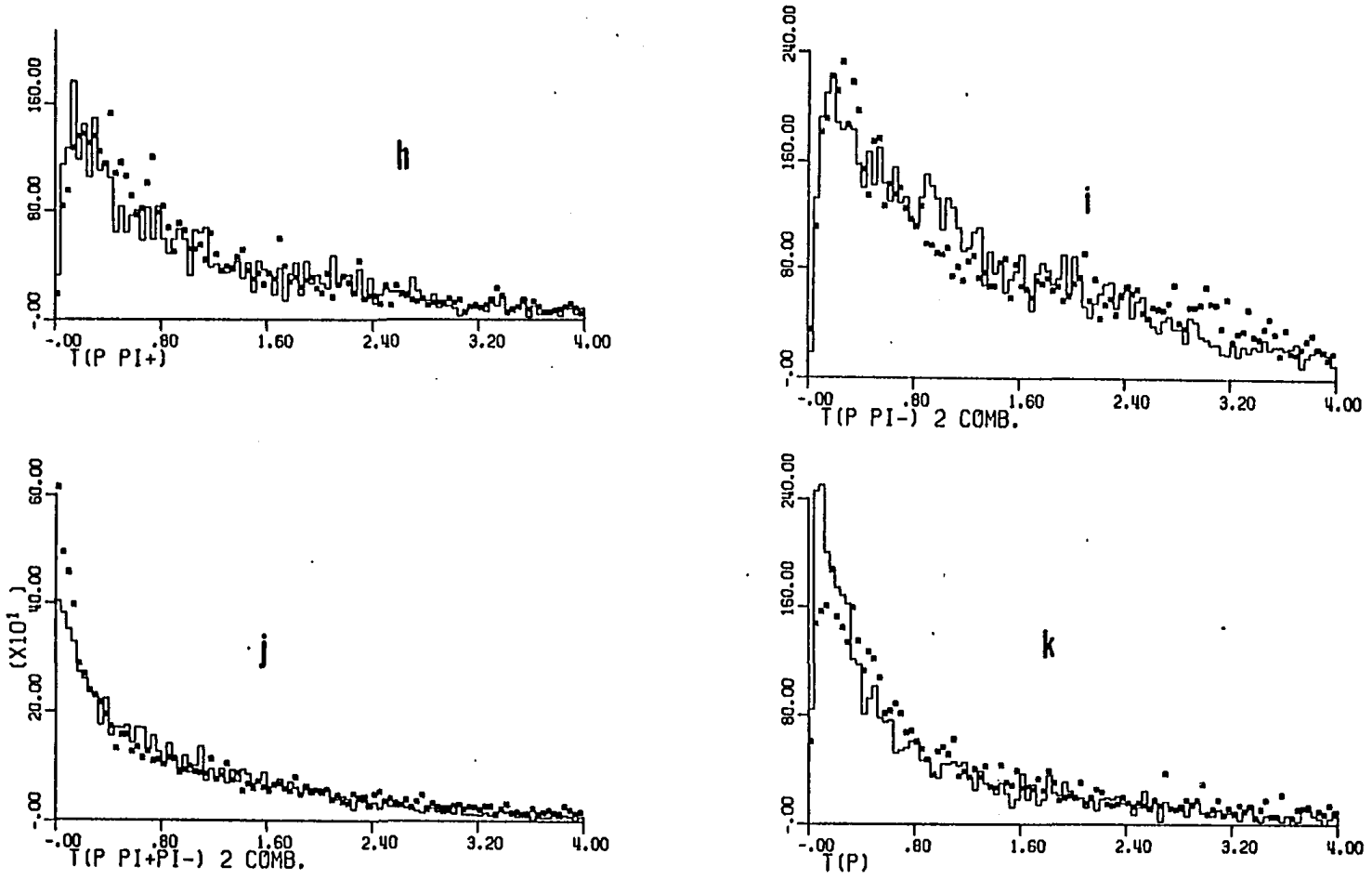

FIG. 1, PART 1 PROTON,3 PI (3.9 GEV/C)

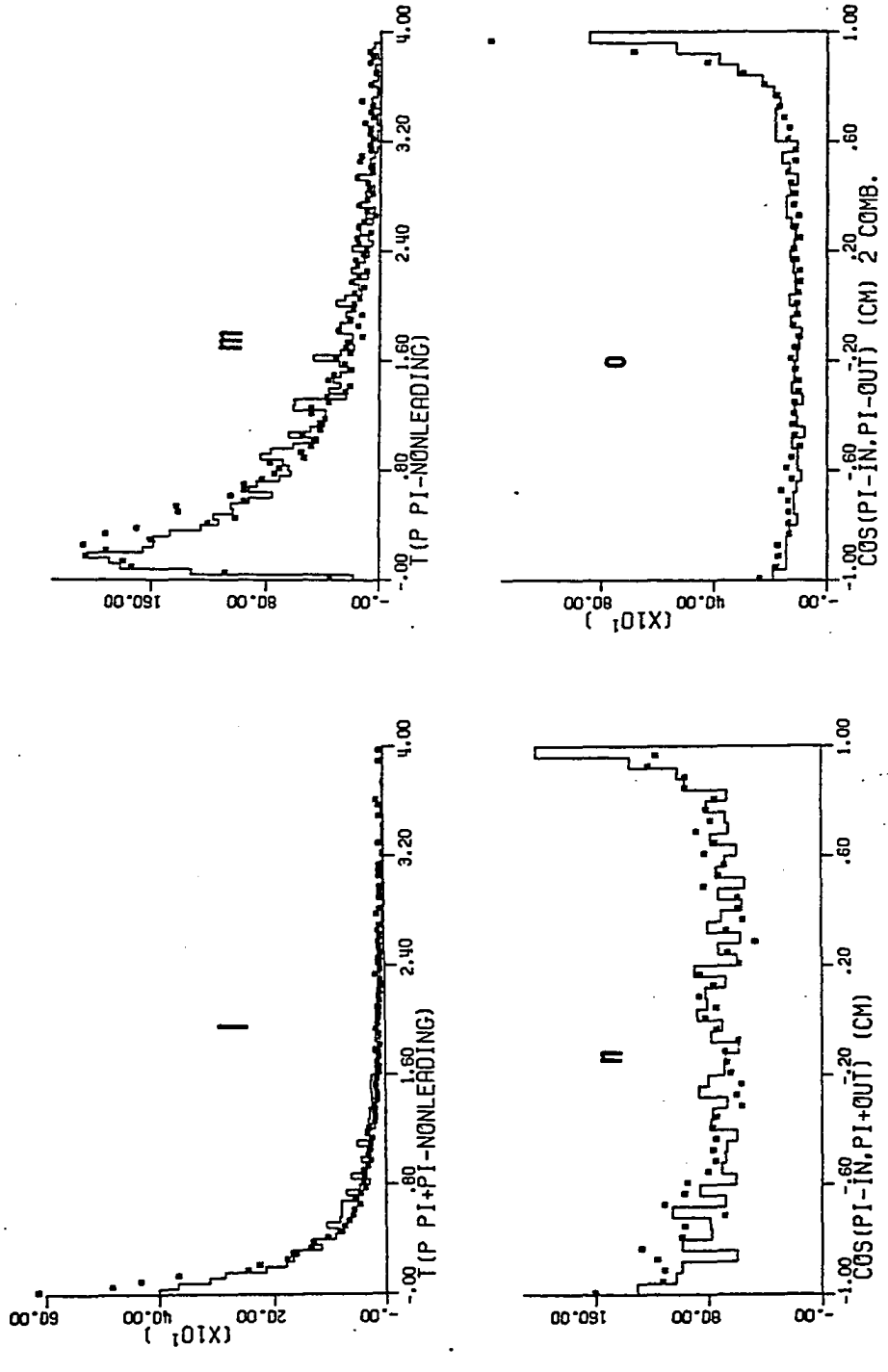

FIG. 1 PART 1 PROTON,3 PI (3.9 GEV/C)

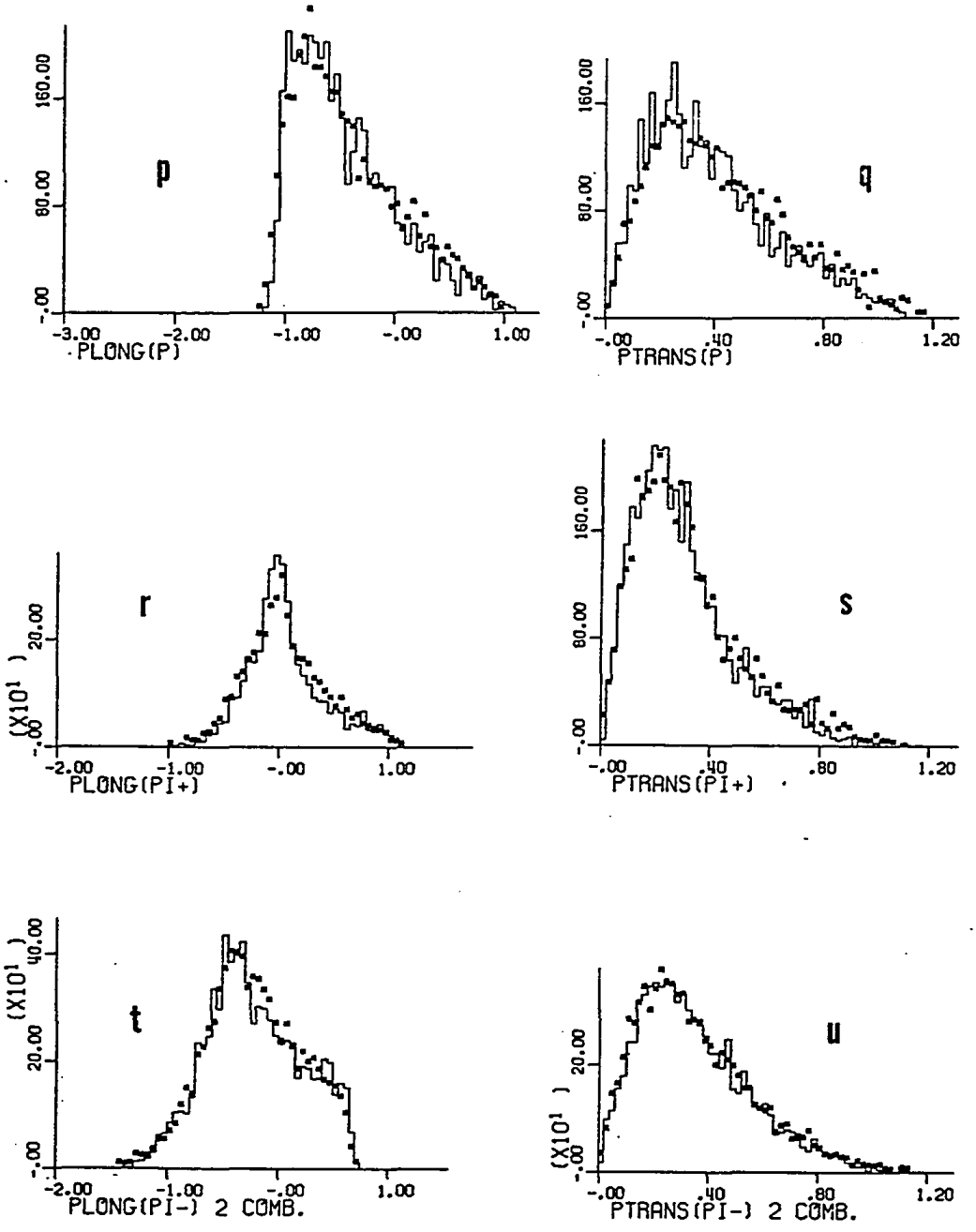

FIG. 1, PART 1 PROTON, 3 PI

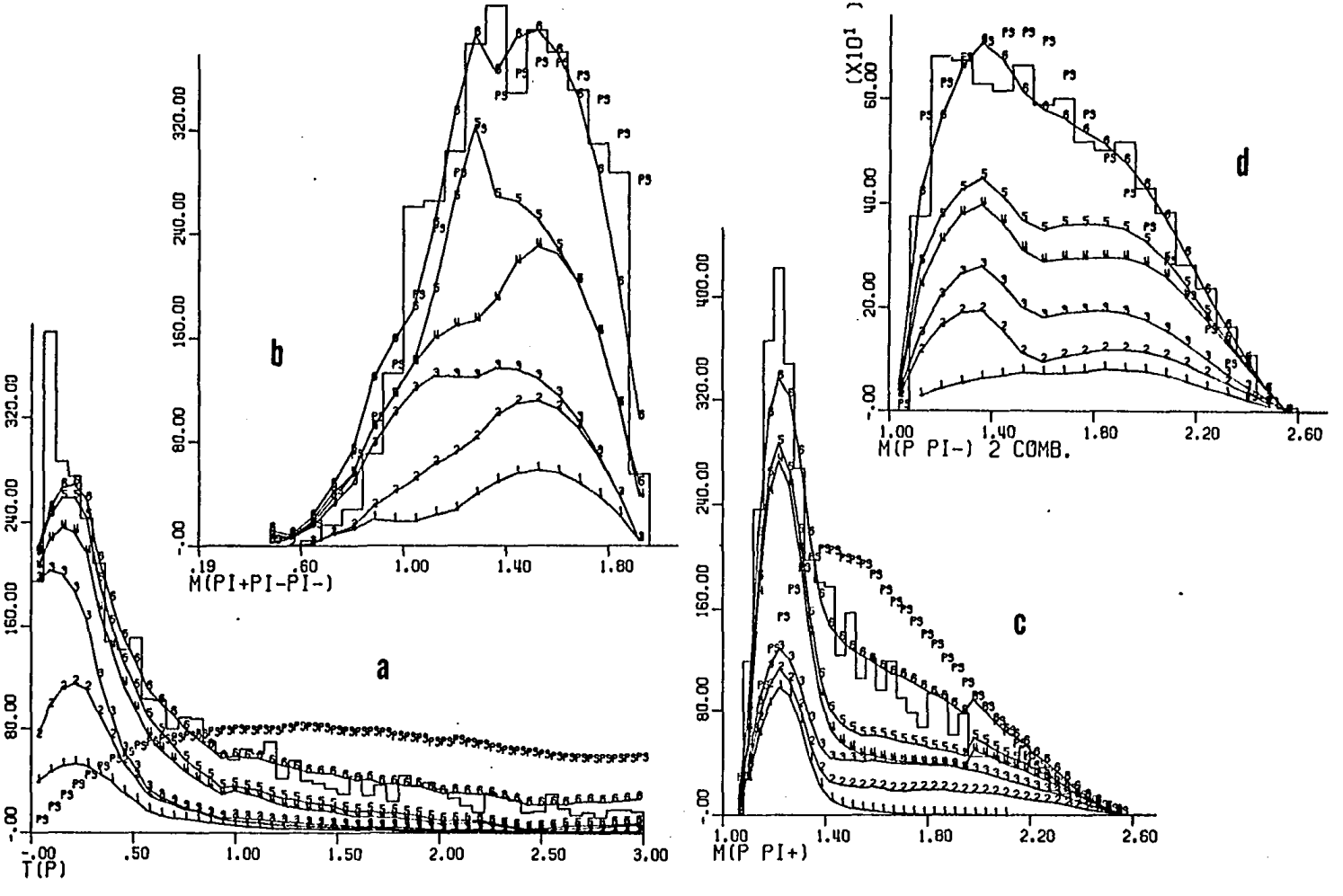

FIG. 1, PART 2 PROTON, 3 PI (3.9 GEV/C)

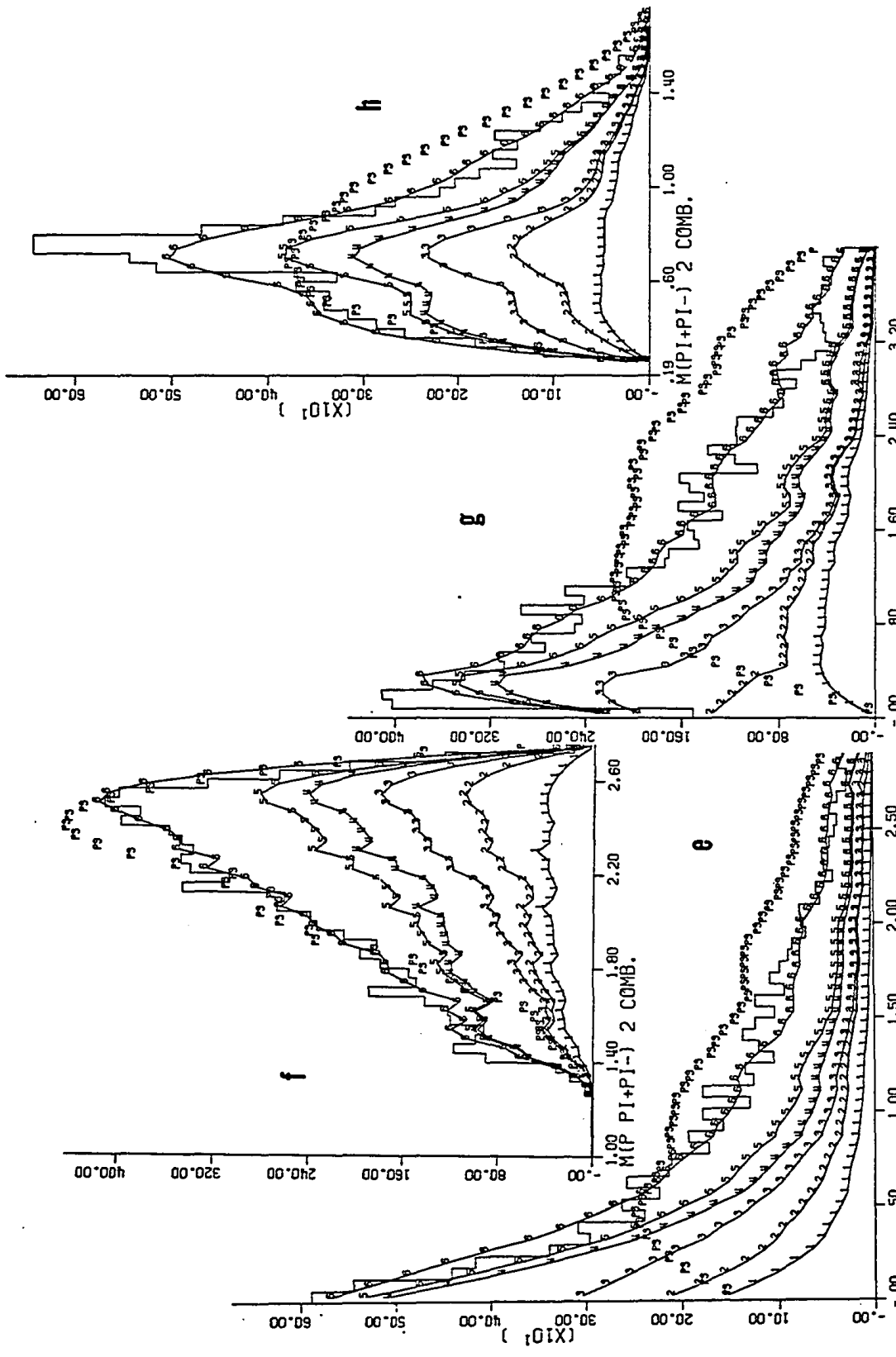

FIG. 1, PART 2 PRØTØN, 3 PI (3.9 GEV/C)

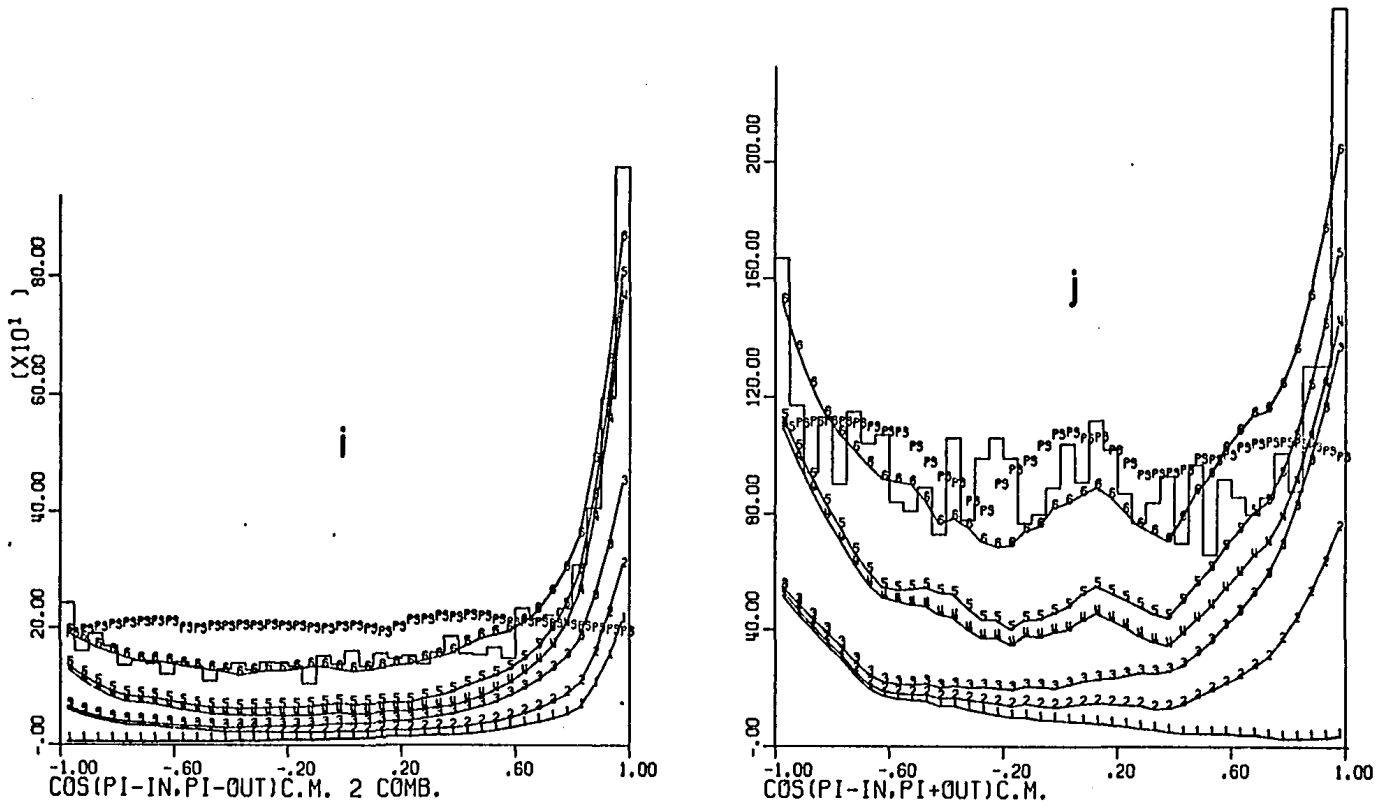

FIG. 1, PART 2 PROTON,3 PI (3.9 GEV/C)

FIGURE 2

Part 1: Overview, $\pi^- p \rightarrow p\pi^+\pi^-\pi^-\pi^0$ at 3.9 GeV/c. The same general comments apply as for Figure 1, Part 1. a-j, masses of selected particle combinations; events/40 mev except g and h which have events/20 mev. k-n, cos(incident, outgoing) for each outgoing particle in cm; events/.04. o-v, longitudinal and transverse components of momentum in laboratory system for each final-state particle; events/40 mev/c. w-z, t to selected particle combinations; events/50 mev.

Part 2: Details, $\pi^- p \rightarrow p\pi^+\pi^-\pi^-\pi^0$ at 3.9 GeV/c. The same general comments apply as for Figure 1, Part 2. a and c, t to proton and t to π^- respectively; events/50 mev^2. b and d-h, masses of selected particle combinations; events/40 mev except f which has events/30 mev. i-j, cos(π^- incident, $\pi^{\pm}$ outgoing) in cm; events/.05.

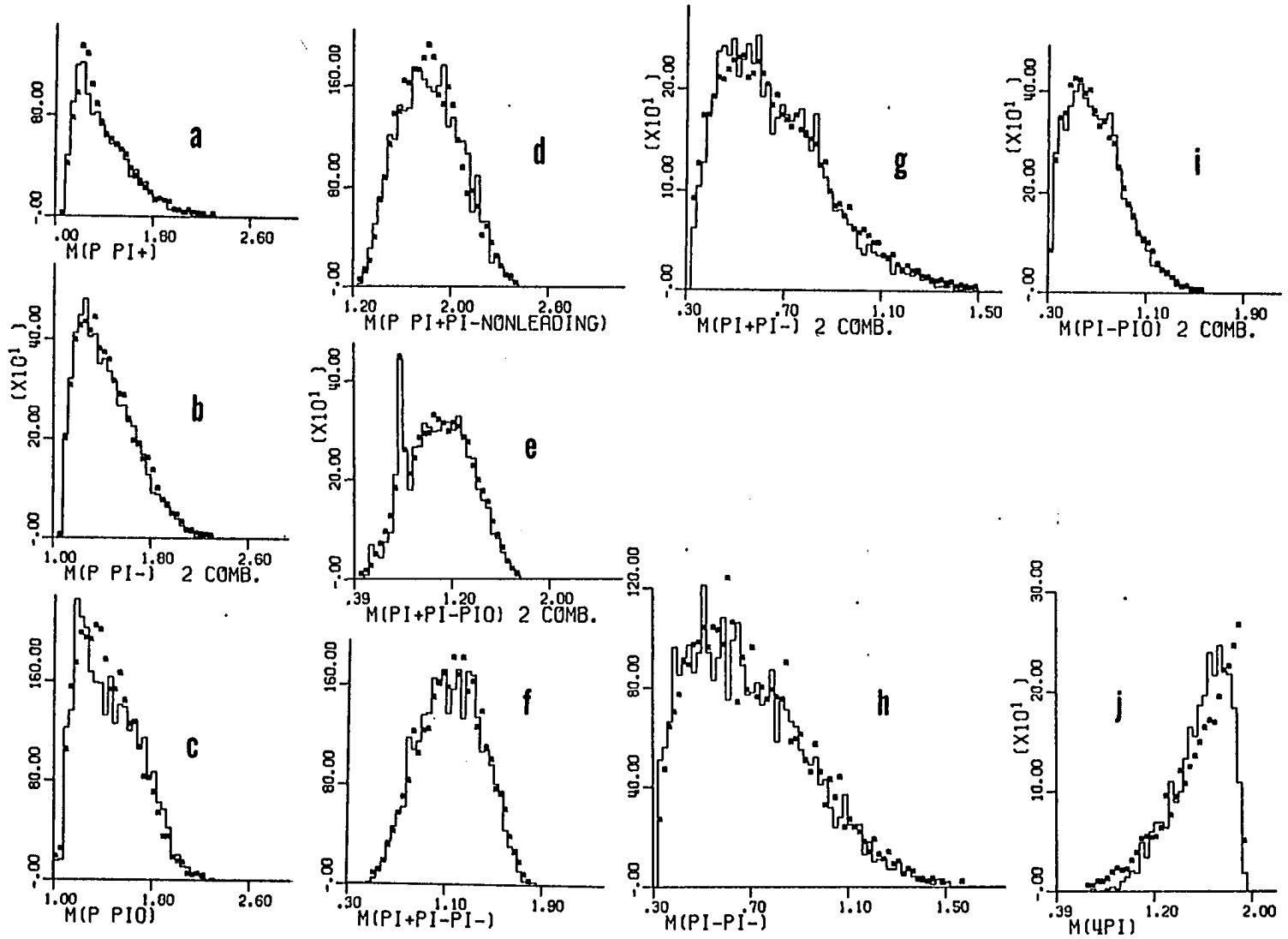

FIG. 2 PART 1 PROTON, 4 PI (3.9 GEV/C)

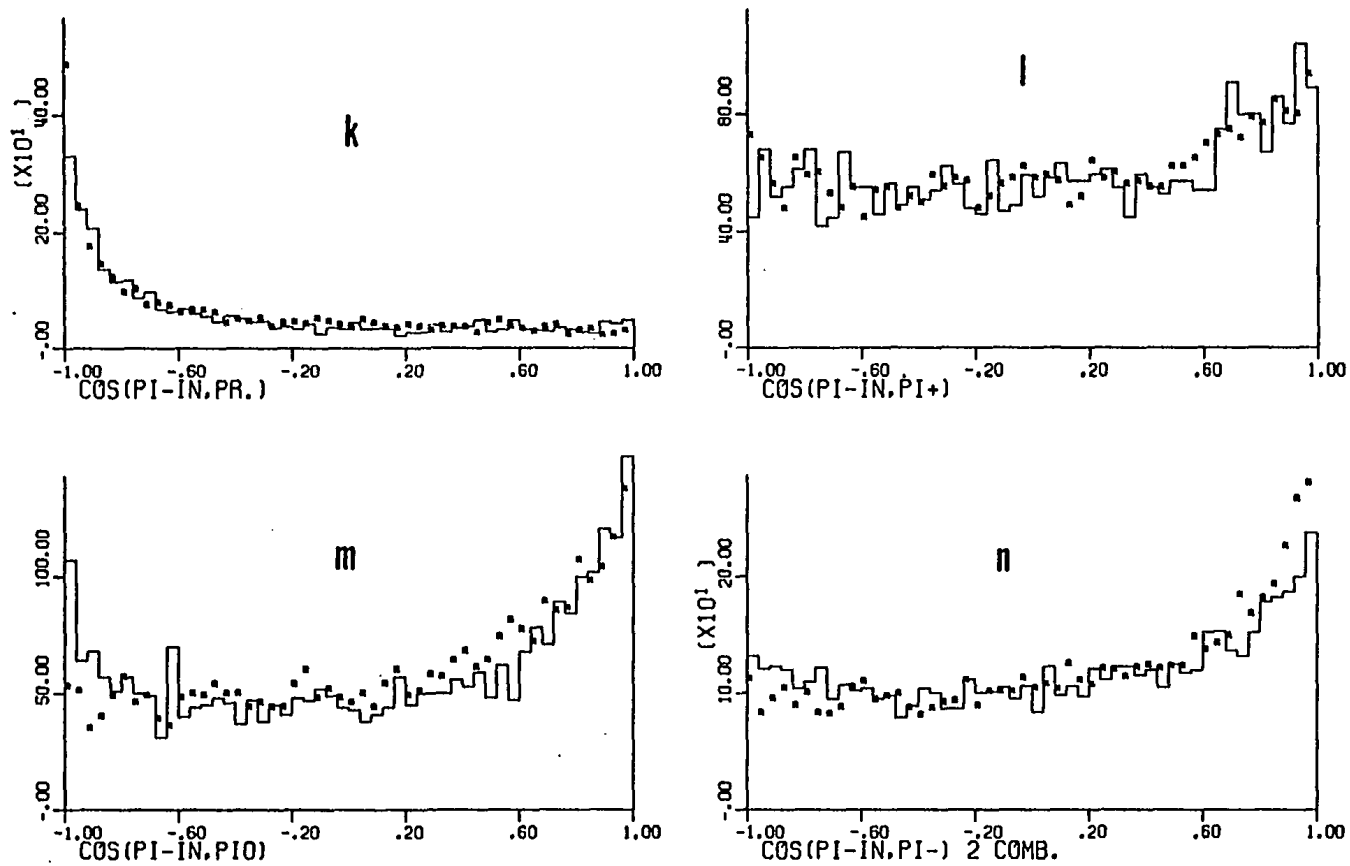

FIG. 2 PART 1 PROTON,4 PI (3.9 GEV/C)

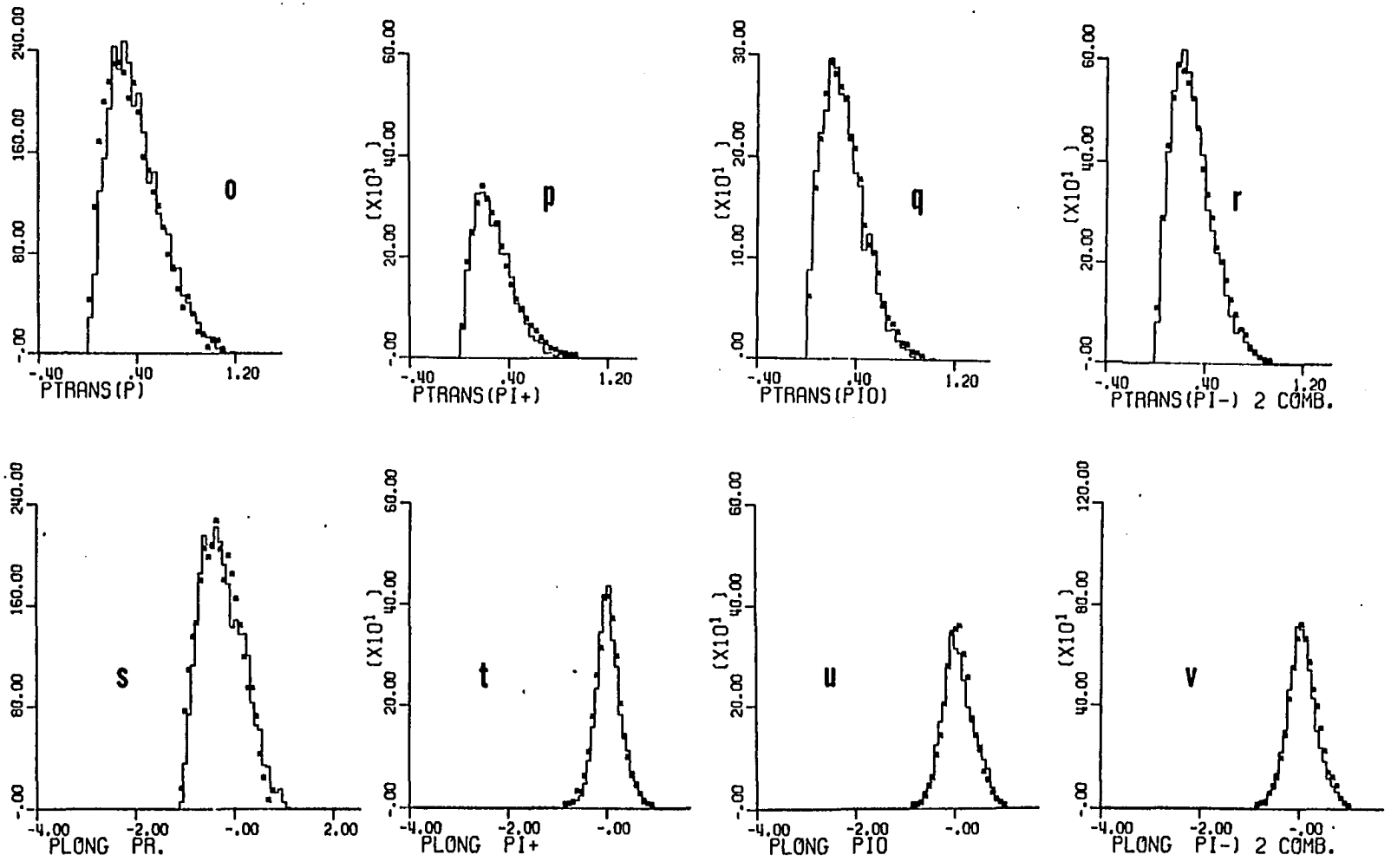

FIG. 2 PART 1 PROTON,4 PI (3.9 GEV/C)

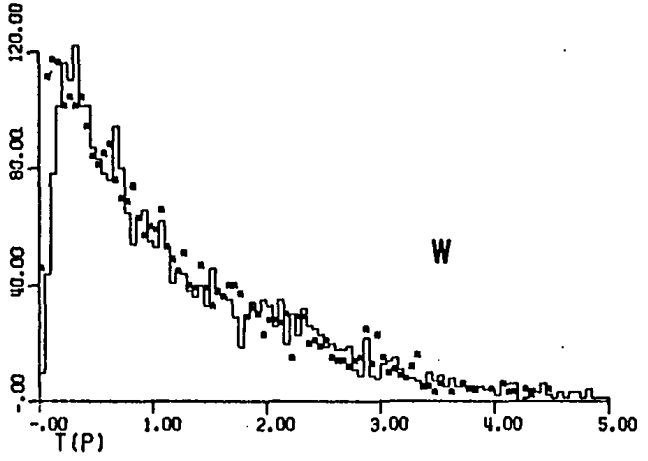

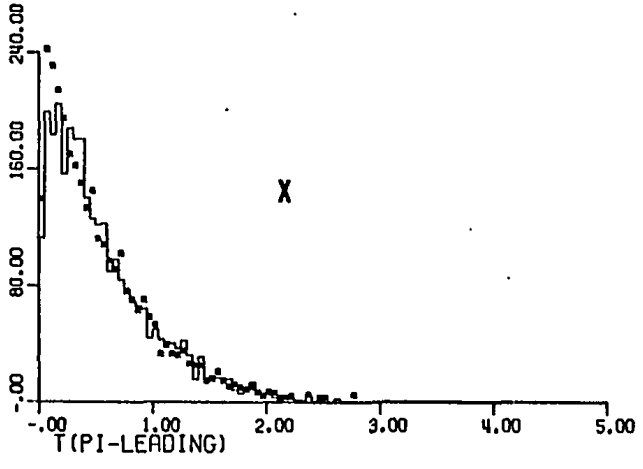

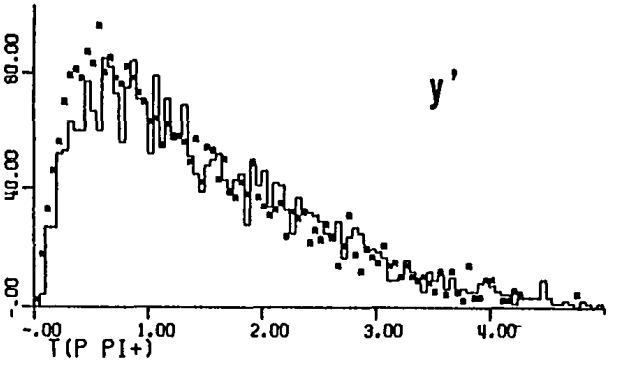

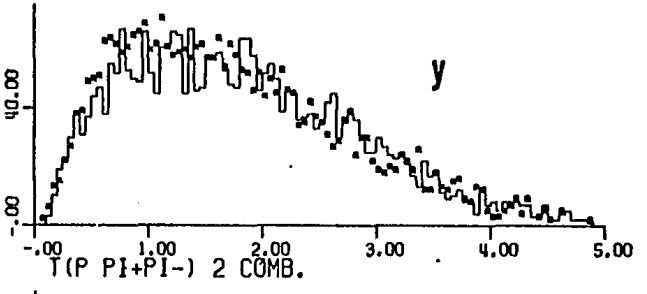

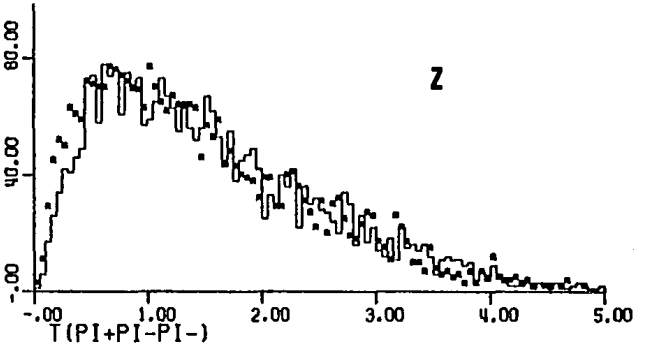

FIG. 2 PART 1 PROTON, 4 PI

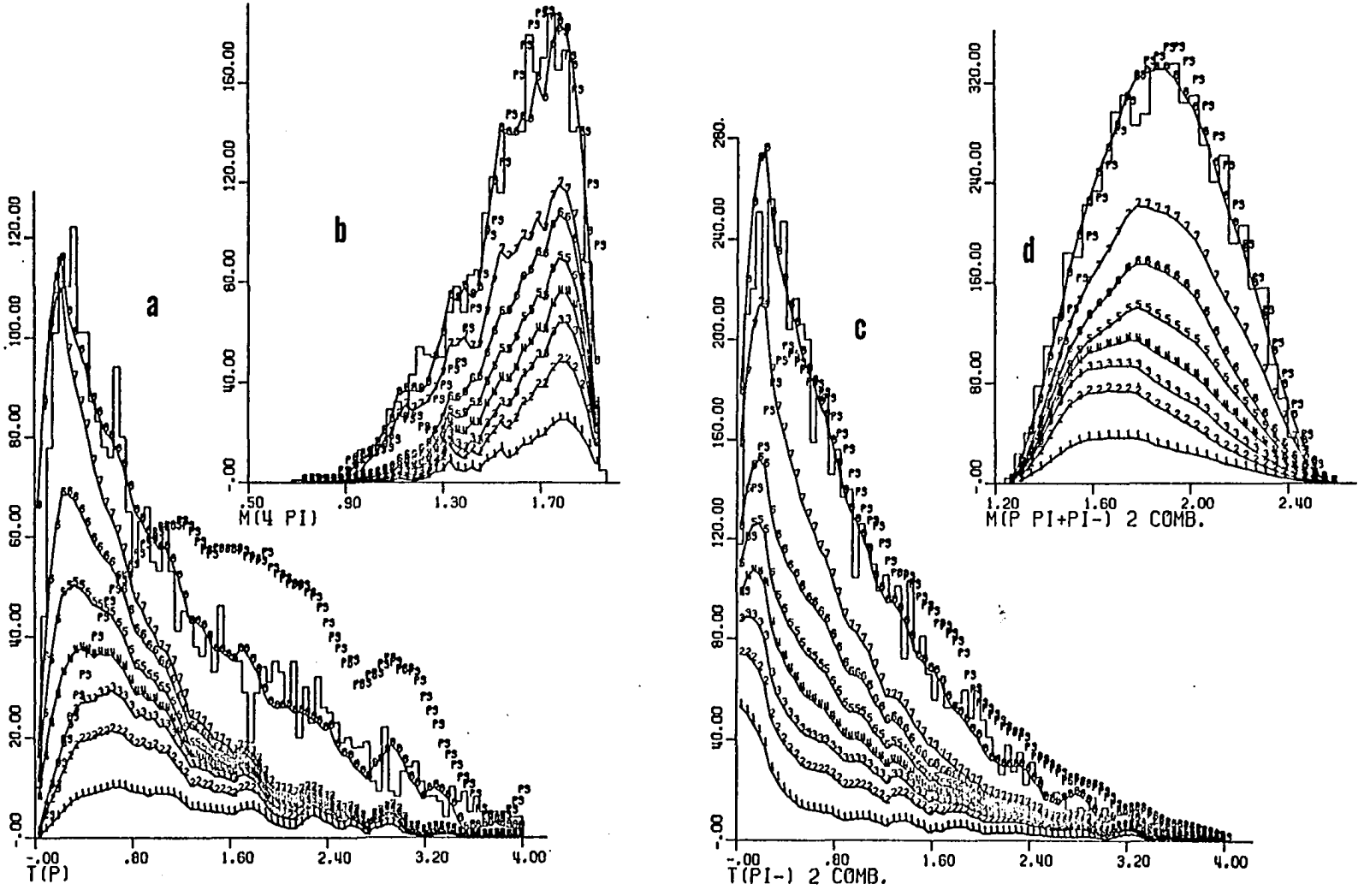

FIG. 2 PART 2 PROTON, 4 PI (3.9 GEV/C)

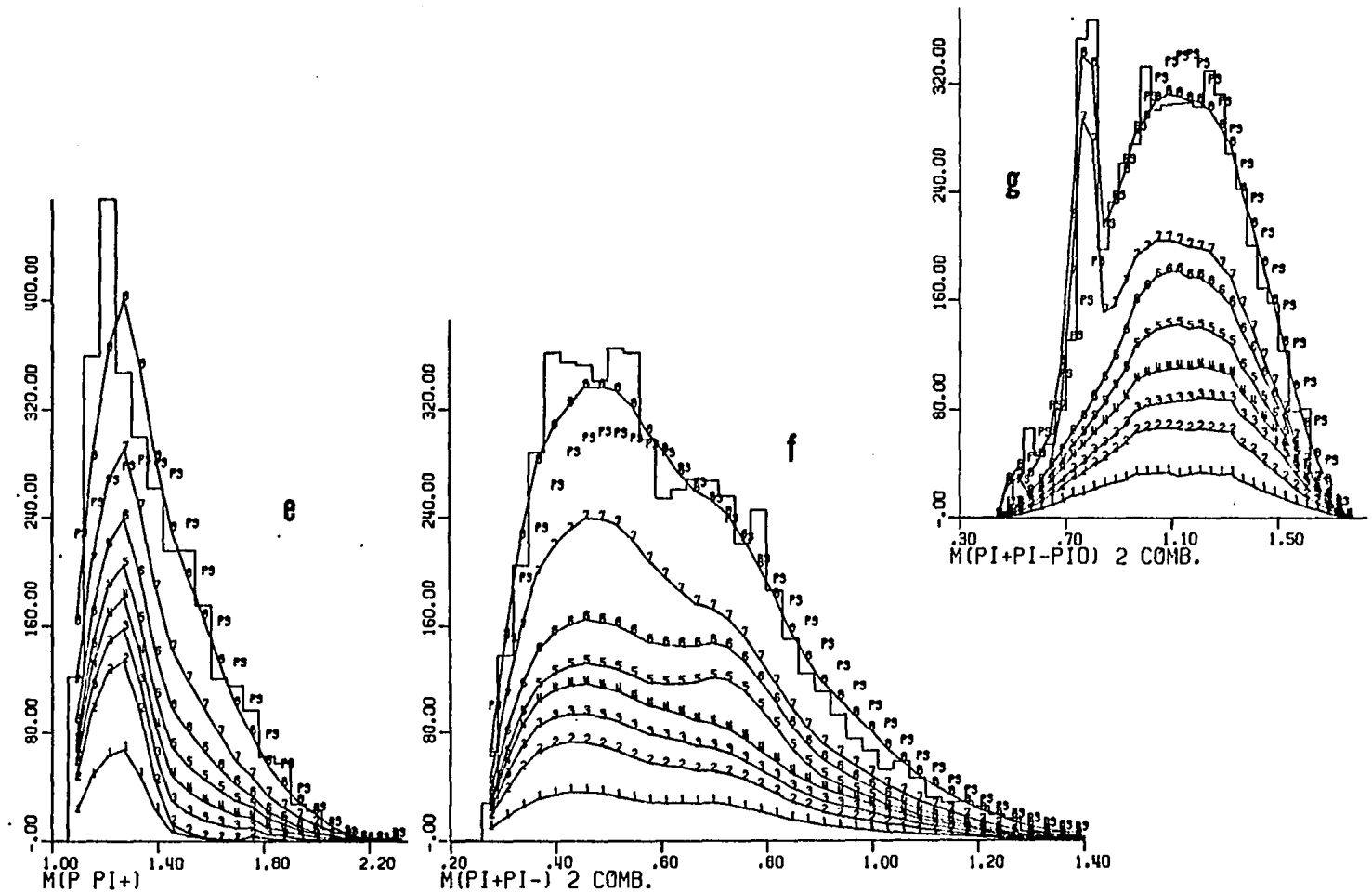

FIG. 2 PART 2 PROTON,4 PI (3.9 GEV/C)

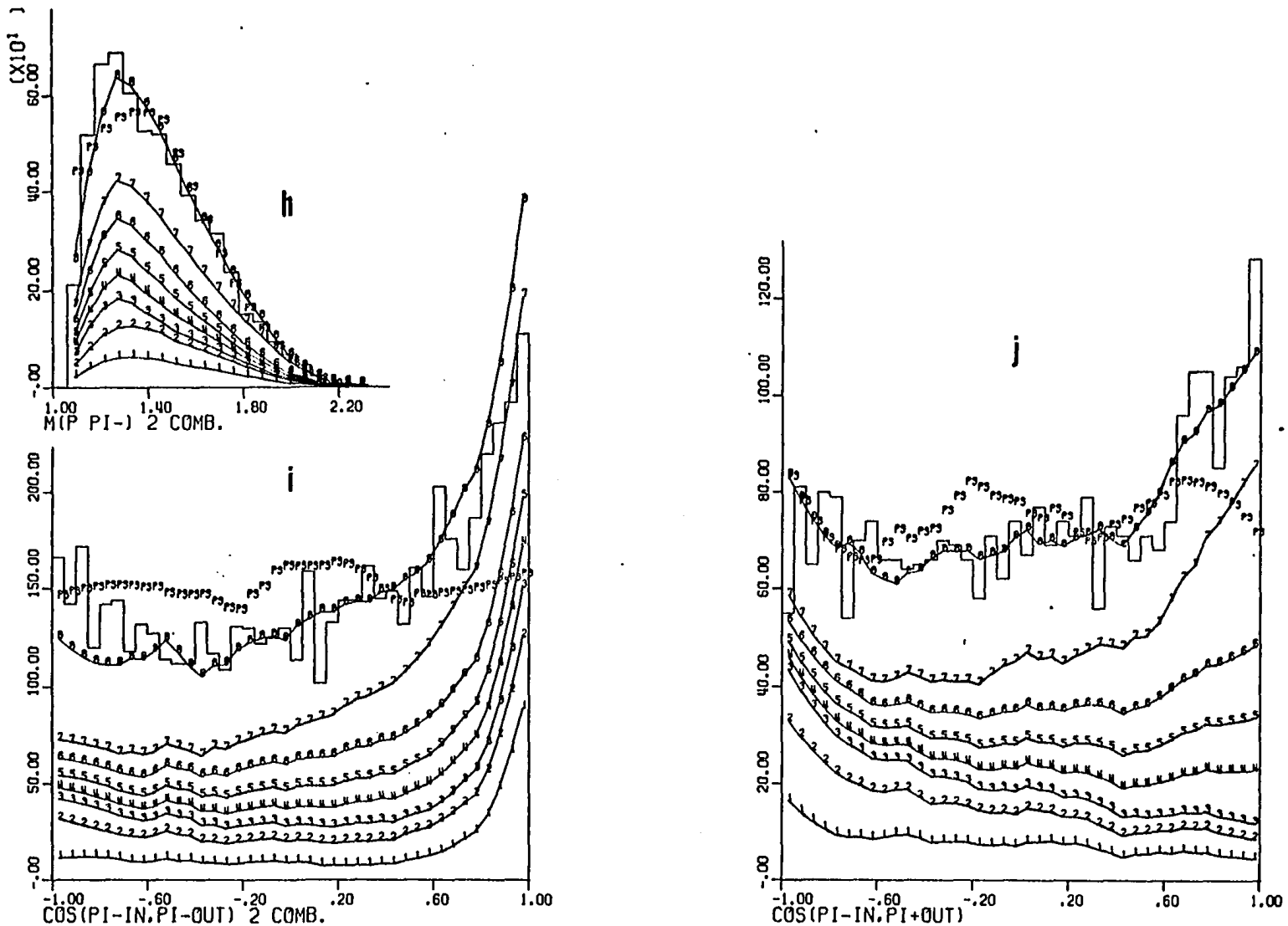

FIG. 2 PART 2 PROTON,4 PI (3.9 GEV/C)

FIGURE 3

Part 1: Overview, $\pi^- p \to p\pi^+\pi^+\pi^-\pi^-$ at 3.9 GeV/c. The same general comments apply as for Figure 1, Part 1. a-h, masses of selected particle combinations; events/40 mev except h which has events/20 mev. i-n, momentum-transfer-squared to selected particle combinations, events/ 50 mev^2. o-t, longitudinal and transverse components of momentum for final-state particles; events/50 mev/c for P_{long}, events/25 mev/c for P_{trans}. u-w, $\cos(\pi^-$ incident, outgoing) for each outgoing particle type.

Part 2: Details, $\pi^- p \to n\pi^+\pi^+\pi^-\pi^-$ at 3.9 GeV/c. The same general comments apply as for Figure 1, Part 2. a, c, and g, momentum-transfer-squared to $n\pi^+\pi^-$, n, and π^- respectively; events/50 mev^2. b, d, h, i, and j, masses of selected particle combinations; events/40 mev. e and f, $\cos(\pi^-$ incident, $\pi^{\pm}$ outgoing) in cm; events/.05.

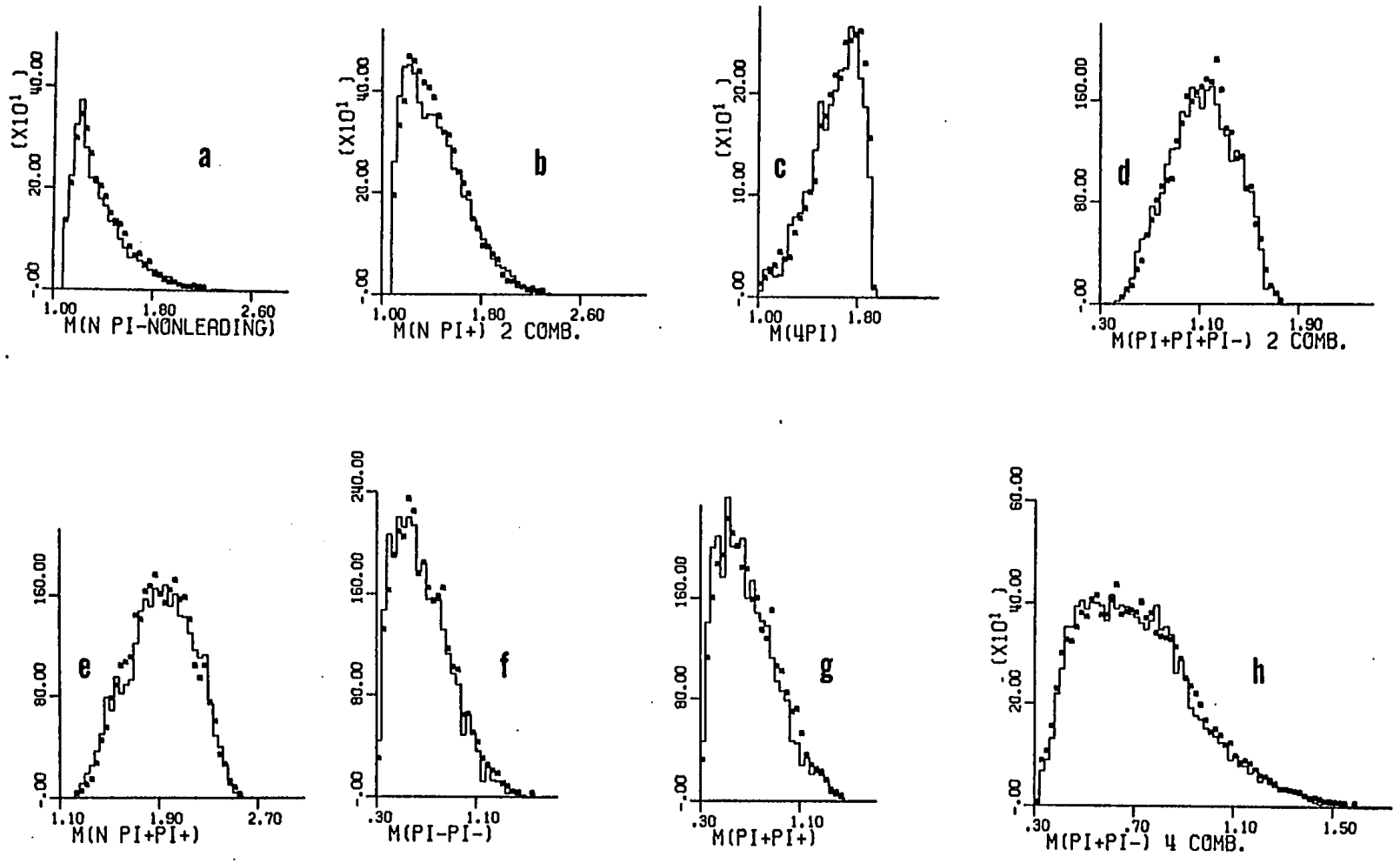

FIG. 3 PART 1 NEUTRON, 4 PI (3.9 GEV/C)

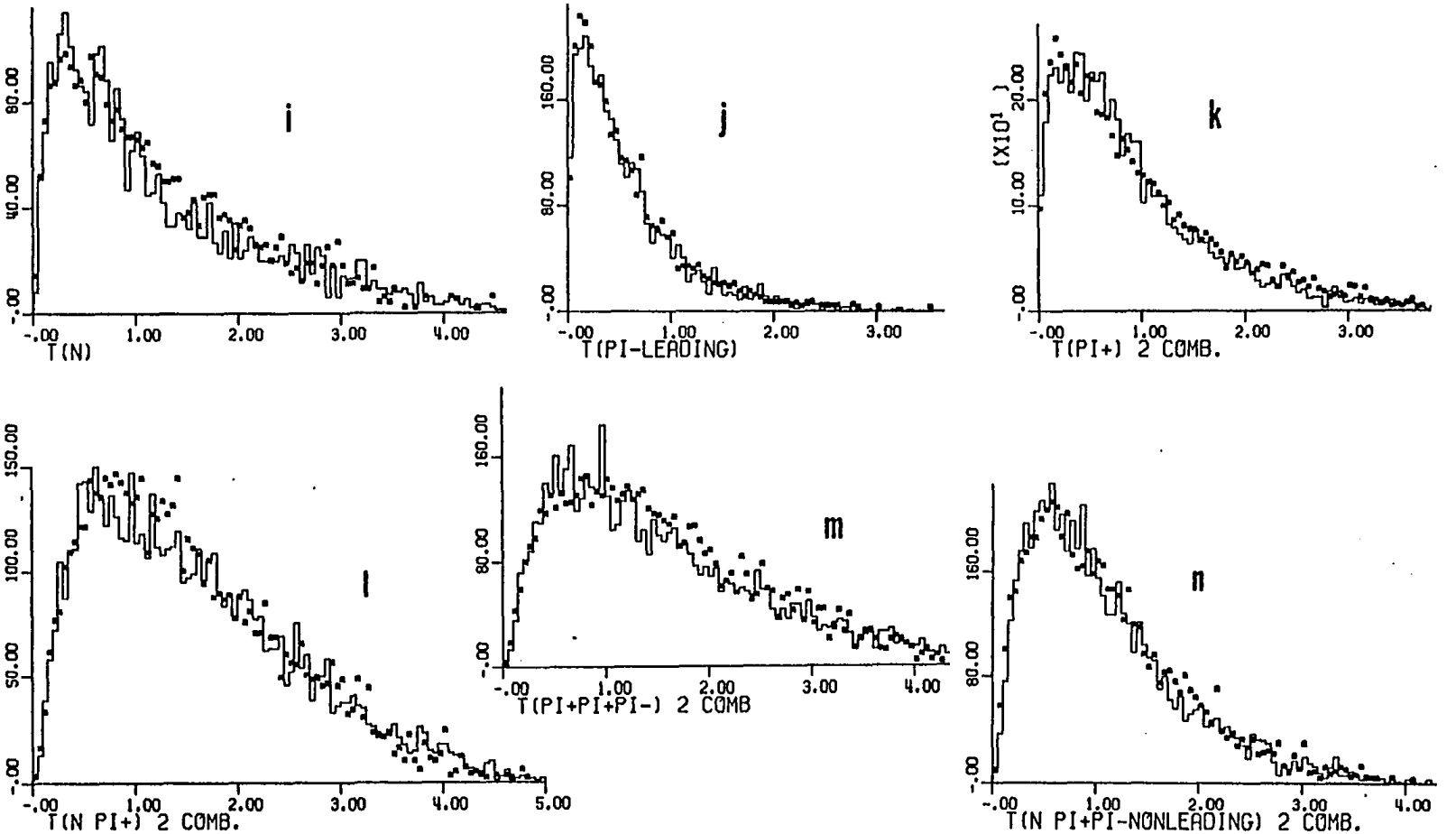

FIG. 3 PART 1 NEUTRON,4 PI (3.9 GEV/C)

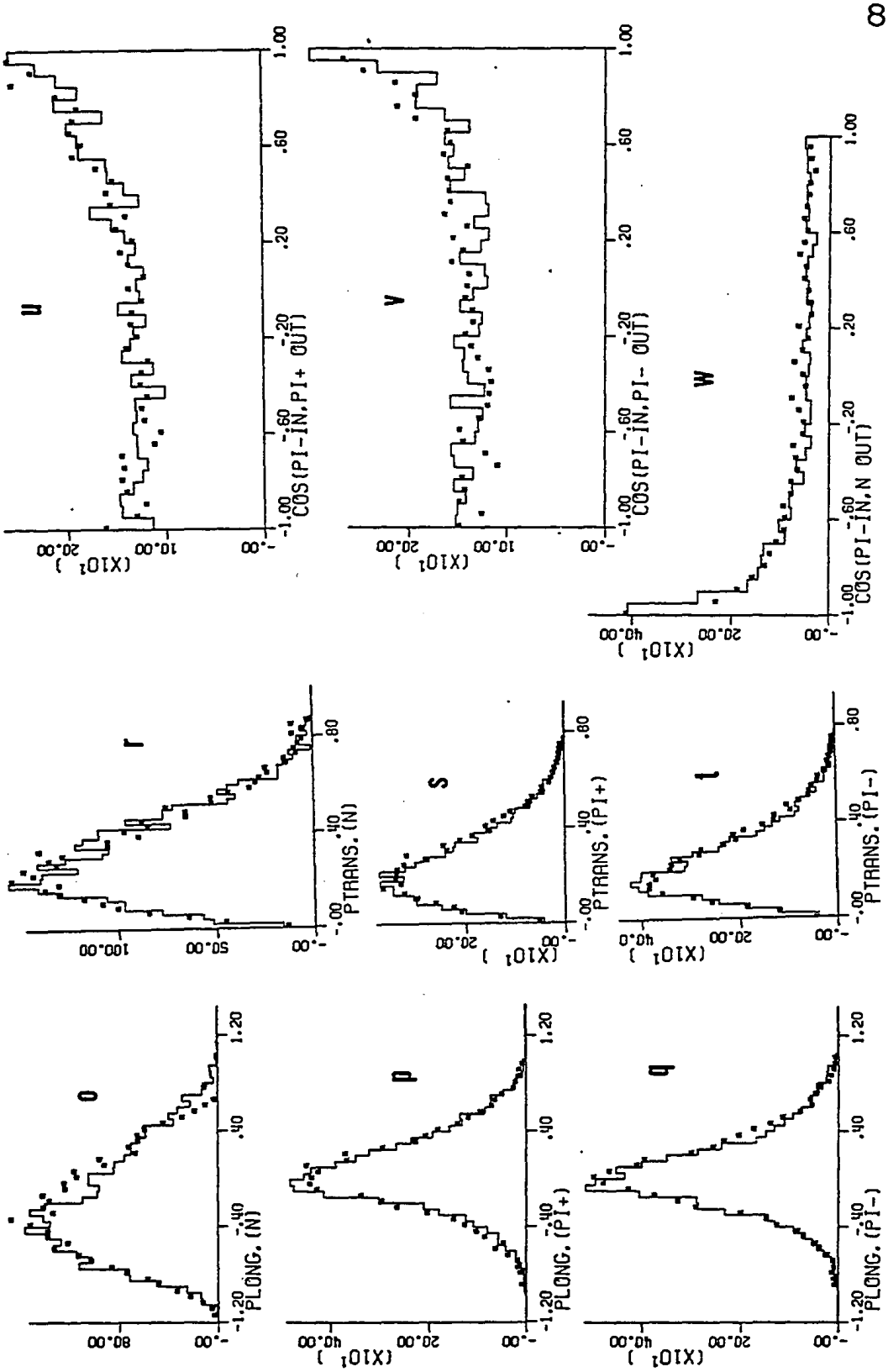

FIG. 3 PART 1 NEUTRON, 4 PI (3.9 GEV/C)

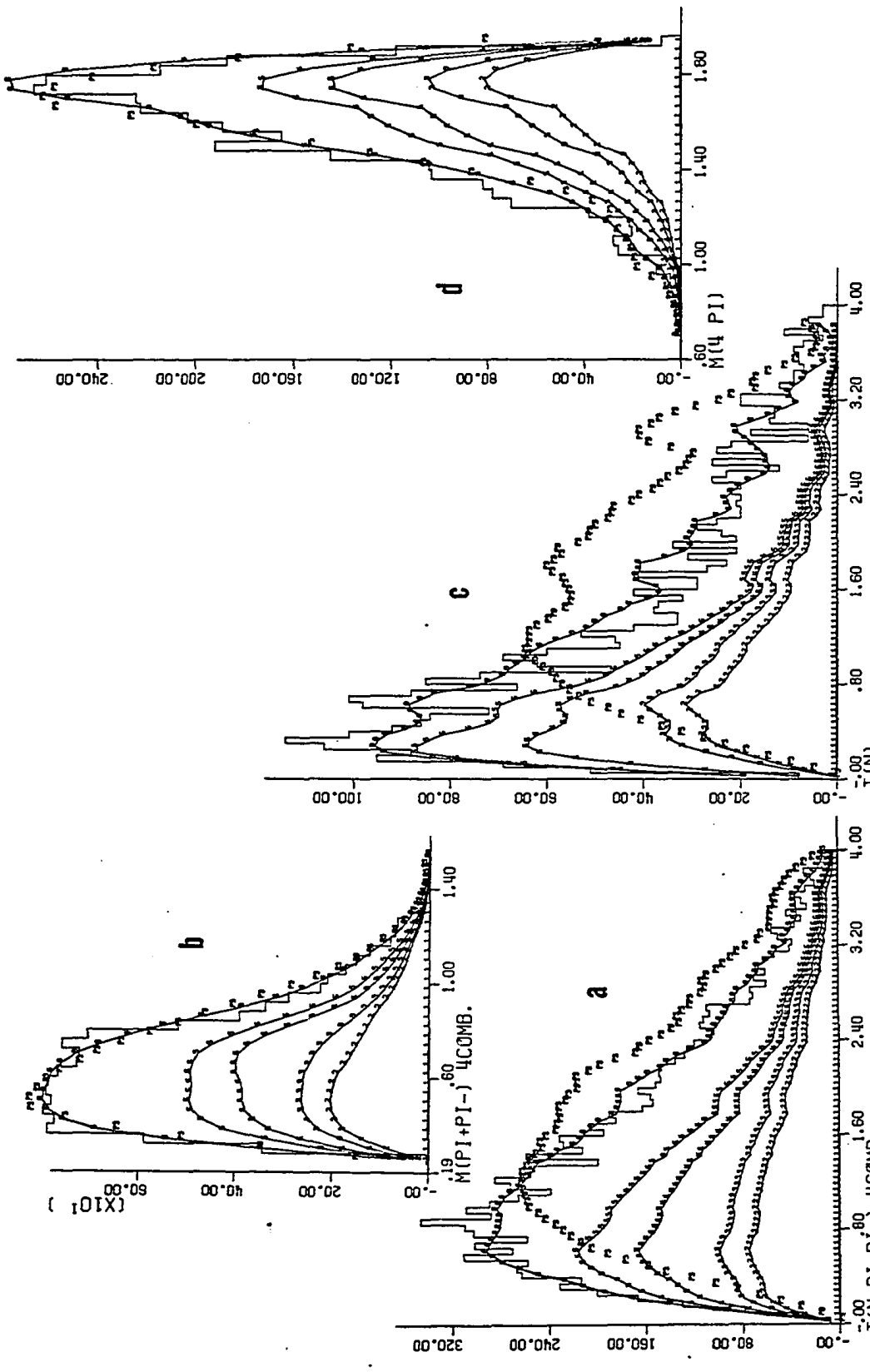

FIG. 3 PART 2 NEUTRON, 4 PI (3.9 GEV/C)

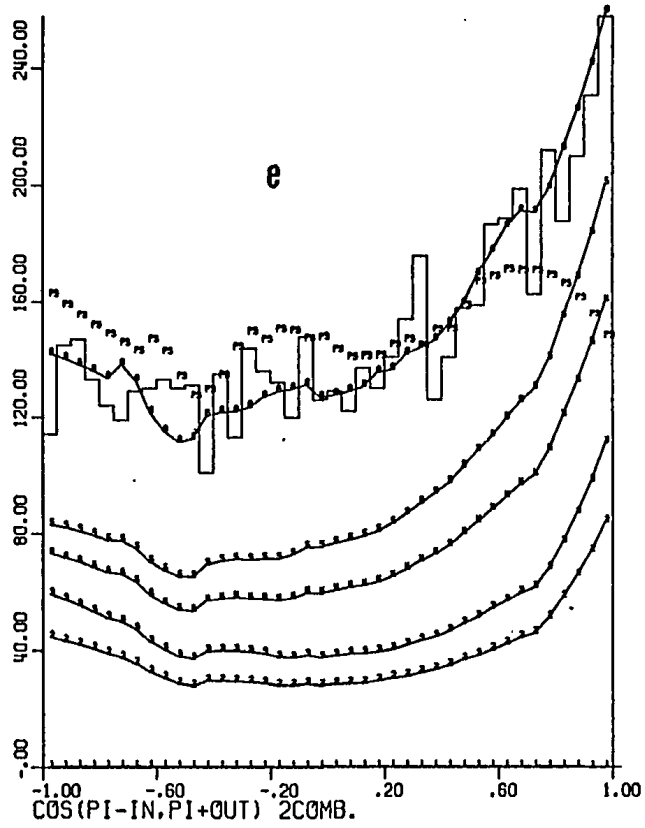

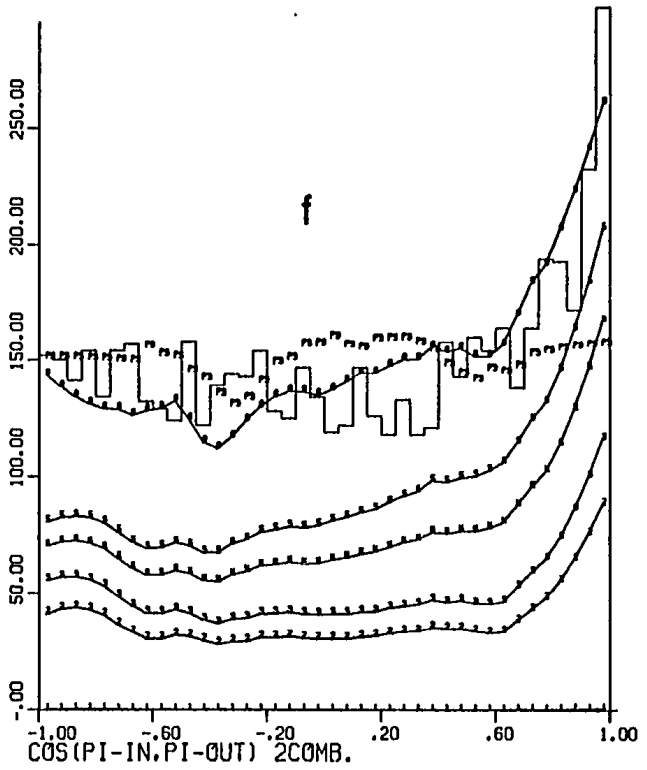

FIG. 3 PART 2 NEUTRON,4 PI (3.9 GEV/C)

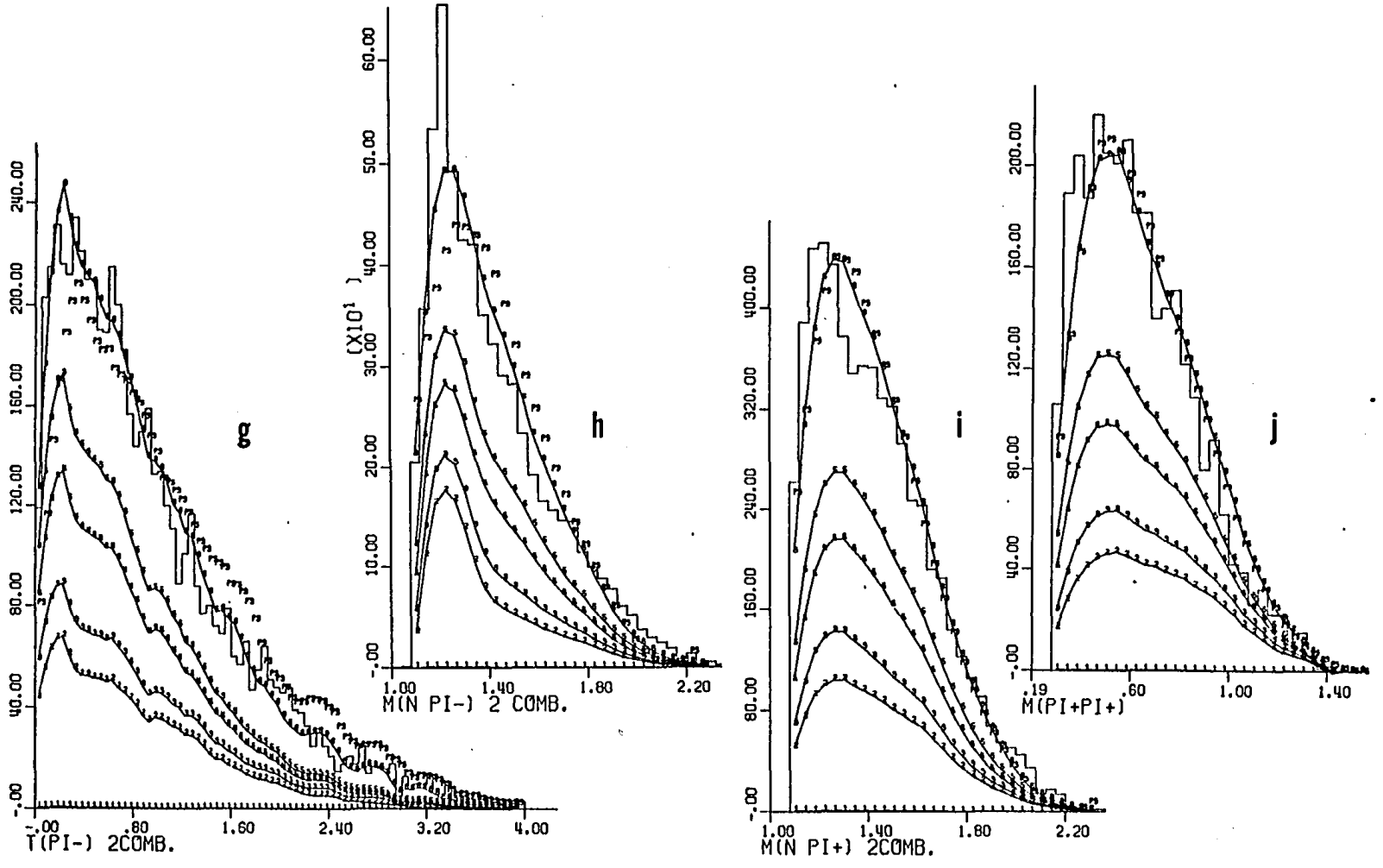

FIG. 3 PART 2 NEUTRON, 4 PI (3.9 GEV/C)

FIGURE 4

Part 1: Overview, $\pi^- p \to p\pi^+\pi^+\pi^-\pi^-\pi^-$ at 3.9 GeV/c. The same general comments apply as for Figure 1, Part 1. a-f, masses of selected particle combinations; events/40 mev. In b and f, the most forward of the $3\pi^-$'s has been excluded. g-i, momentum-transfer-squared to proton, $p\pi^+\pi^-$, and the most forward π^- respectively; events/50 mev^2. j-o longitudinal and transverse components of momentum for the three types of final-state particles; events/20 mev/c for P_{trans}, events/40 mev for P_{long}. p-u, cos(π^- incident, outgoing particle) for each type of final-state particle in cm. n, u, cos(π out, π out) in cm of five outgoing pions. In t, the most forward π^- has been excluded; events/.025.

Part 2: Details, $\pi^- p \to p\pi^+\pi^+\pi^-\pi^-\pi^-$ at 3.9 GeV/c. The same general comments apply as for Figure 1, Part 2. a-c, momentum-transfer-squared to selected particle combinations; events/100 mev^2. 1-g, masses of selected particle combinations, events/40 mev.

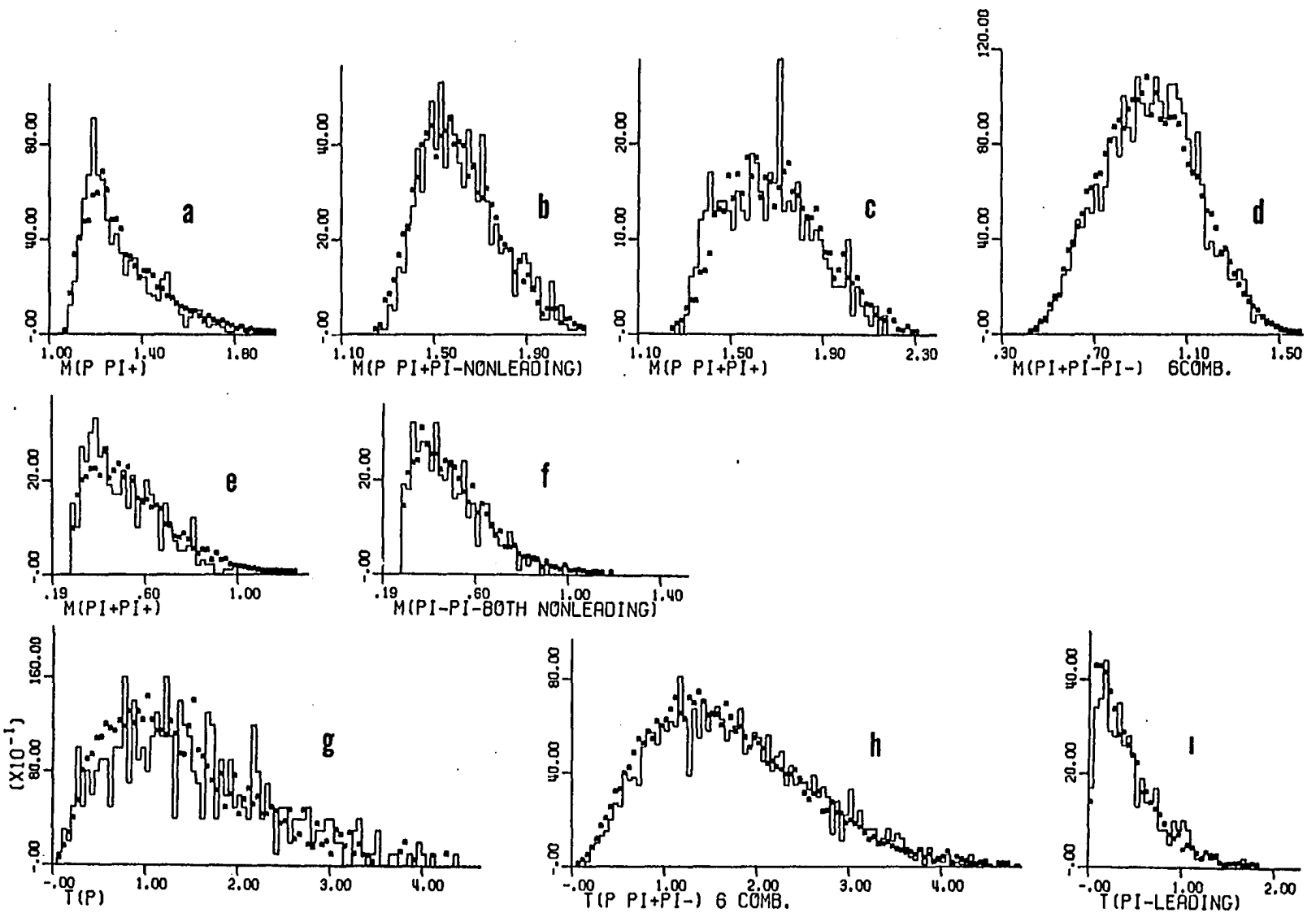

FIG. 4 PART 1 PROTON,5 PI (3.9 GEV/C)

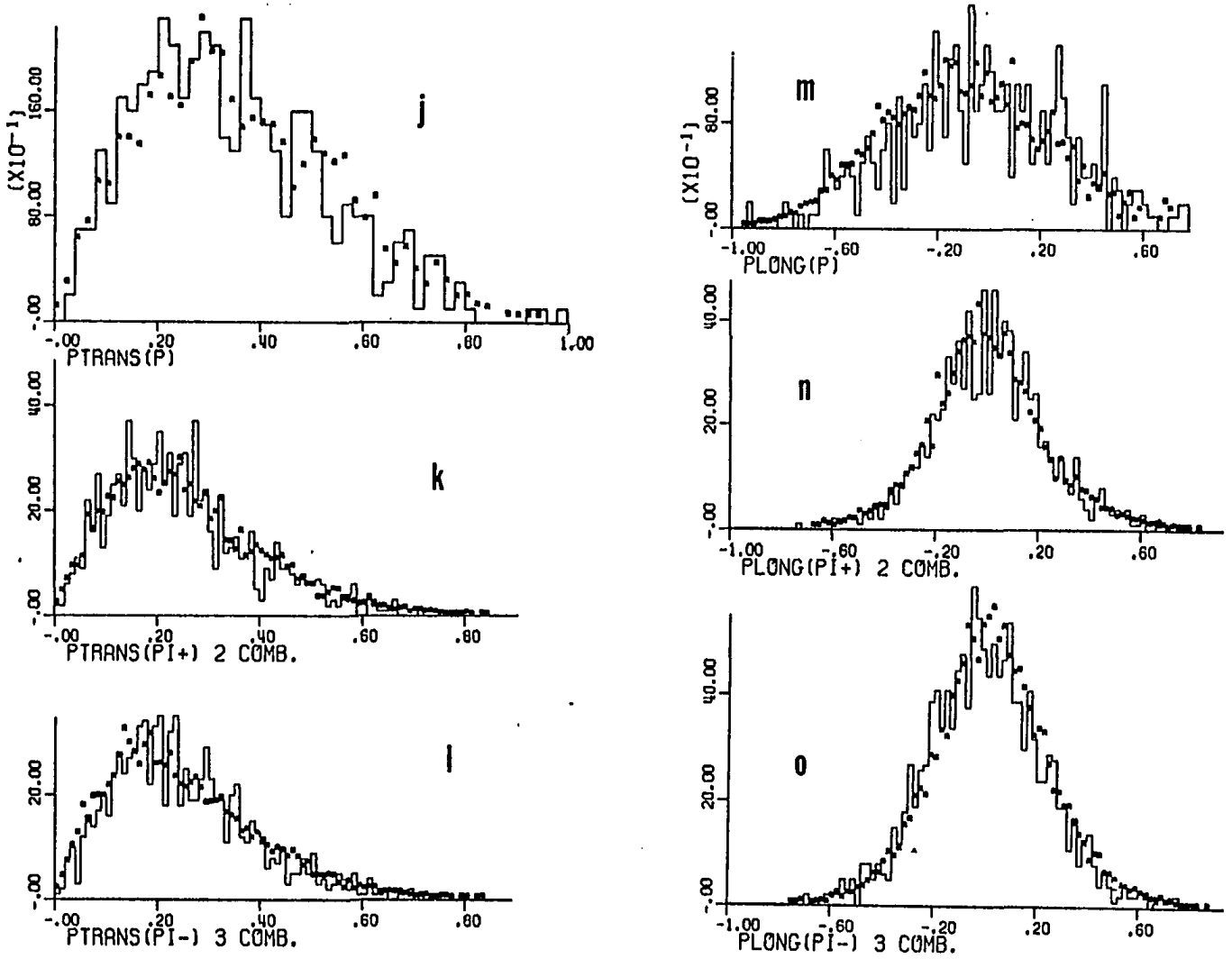

FIG. 4 PART 1 PROTON,5 PI (3.9 GEV/C)

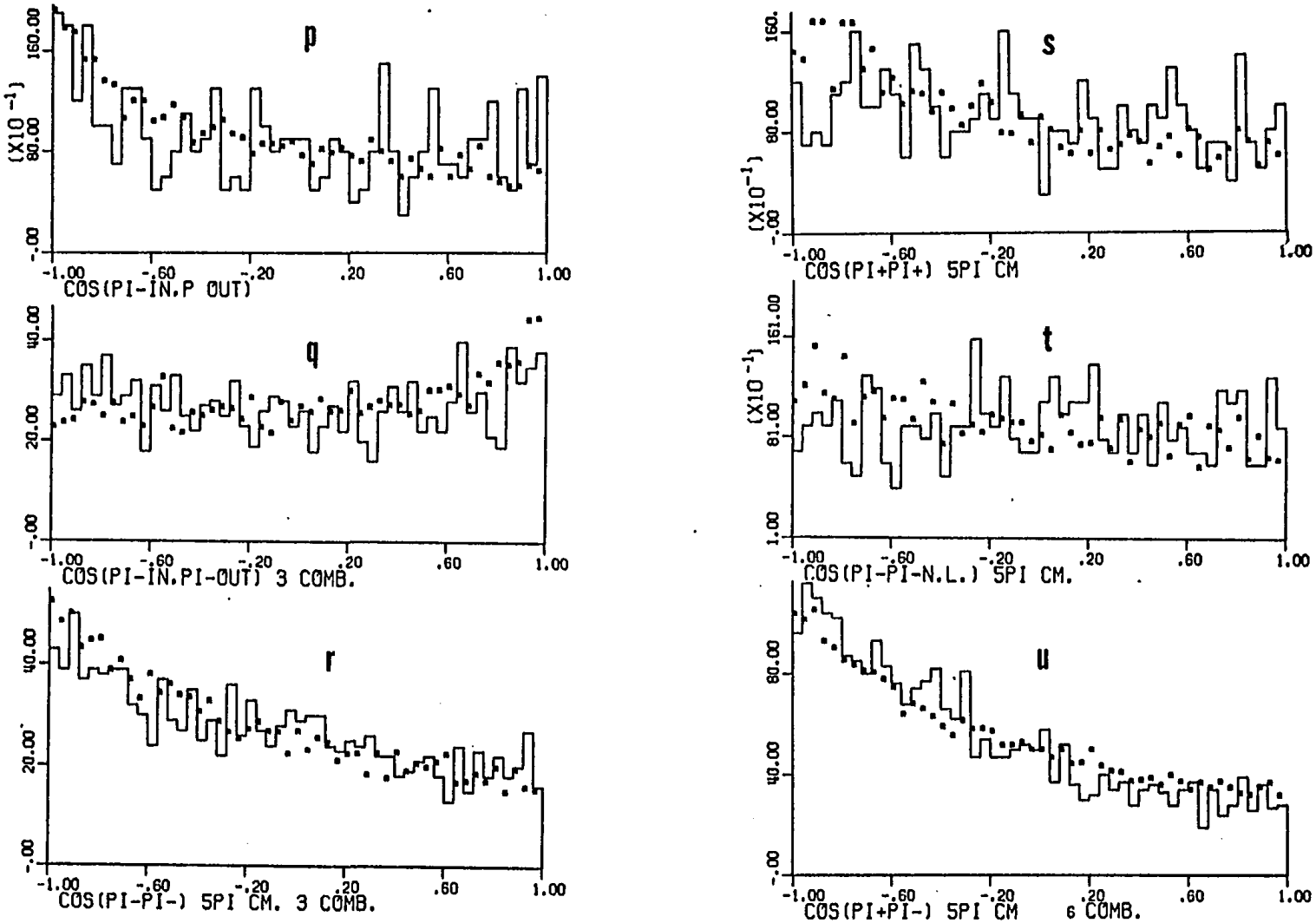

FIG. 4 PART 1 PROTON,5 PI (3.9 GEV/C)

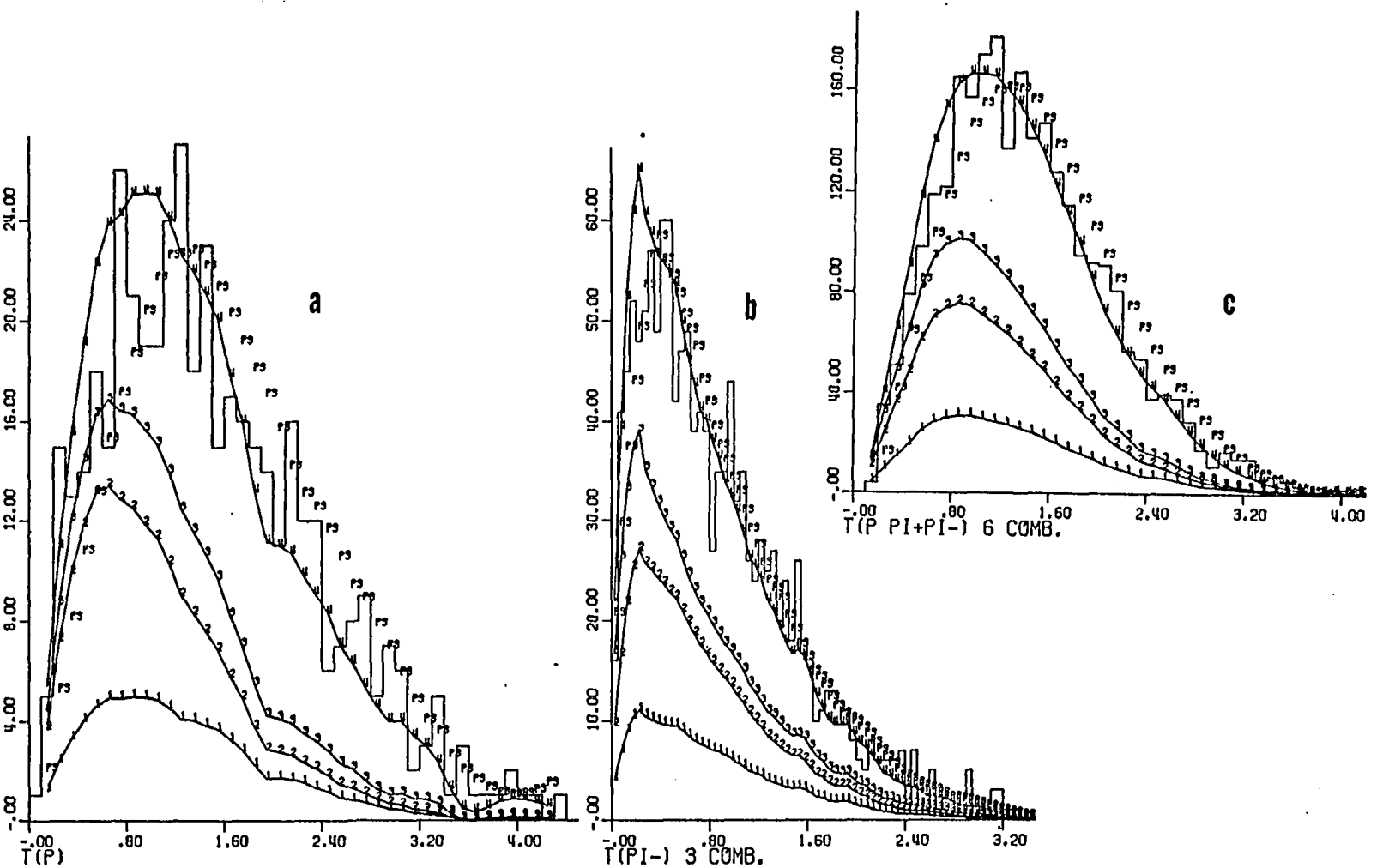

FIG. 4 PART 2 · PROTON,5 PI (3.9 GEV/C)

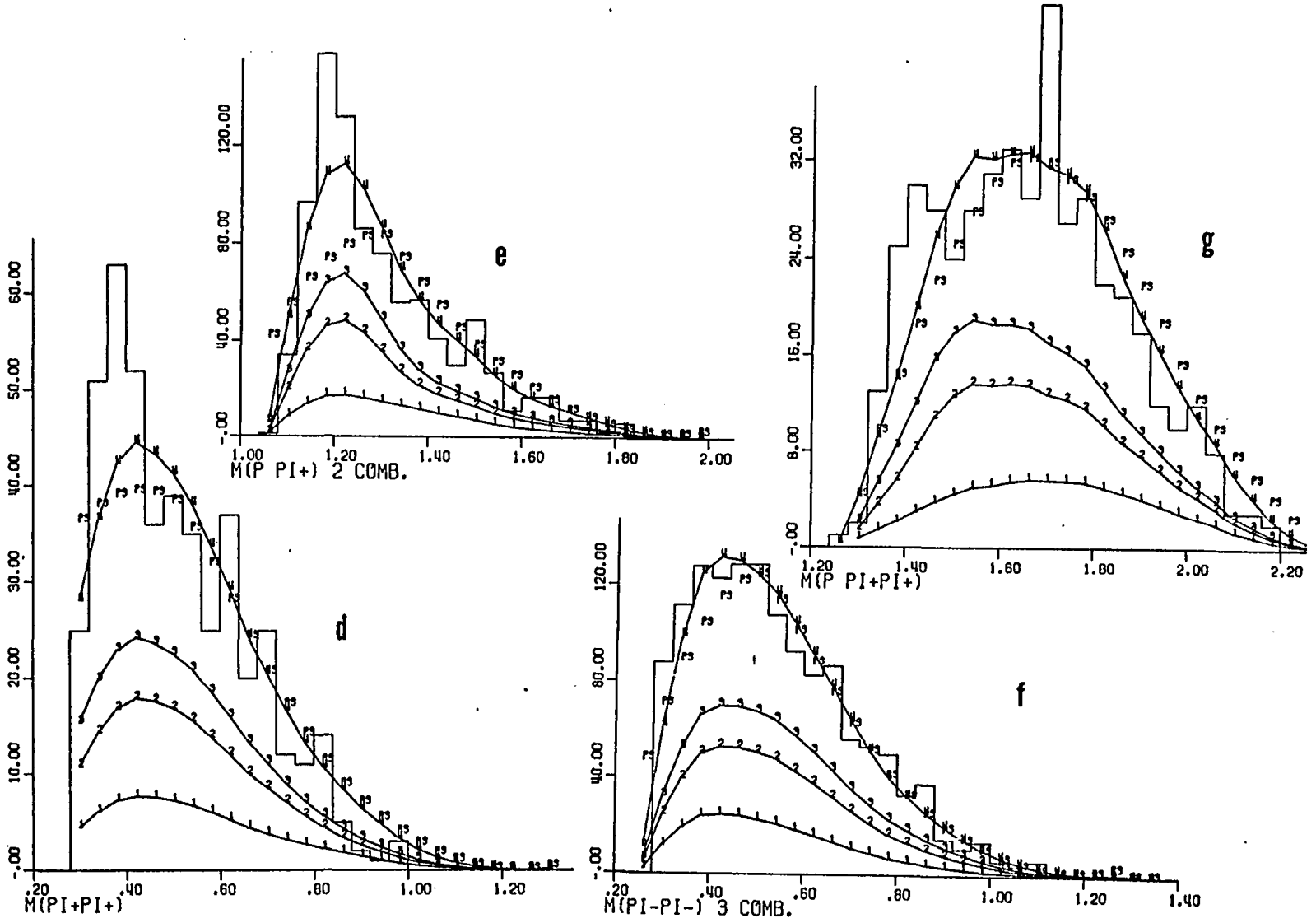

FIG. 4 PART 2 PROTON,5 PI (3.9 GEV/C)

FIGURE 5

Part 1: Overview, $\pi^- p \rightarrow p\pi^+\pi^+\pi^-\pi^-\pi^-\pi^0$ at 3.9 GeV/c. The same general comments apply as for Figure 1, Part 1. a-d, masses of selected particle combinations; events/40 mev. e-g, momentum-transfer-squared to selected particle combinations; events/40 mev^2.

Part 2: Details, $\pi^- p \rightarrow p\pi^+\pi^+\pi^-\pi^-\pi^-\pi^0$ at 3.9 GeV/c. The same general comments apply as for Figure 1, Part 2. a and c, momentum-transfer-squared to proton and $p\pi^+\pi^-$ respectively; events/100 mev^2. b, d, e, and f, masses of selected particle combinations; events/40 mev. g, cos(π^- incident, π^0 outgoing) in cm; events/.05.

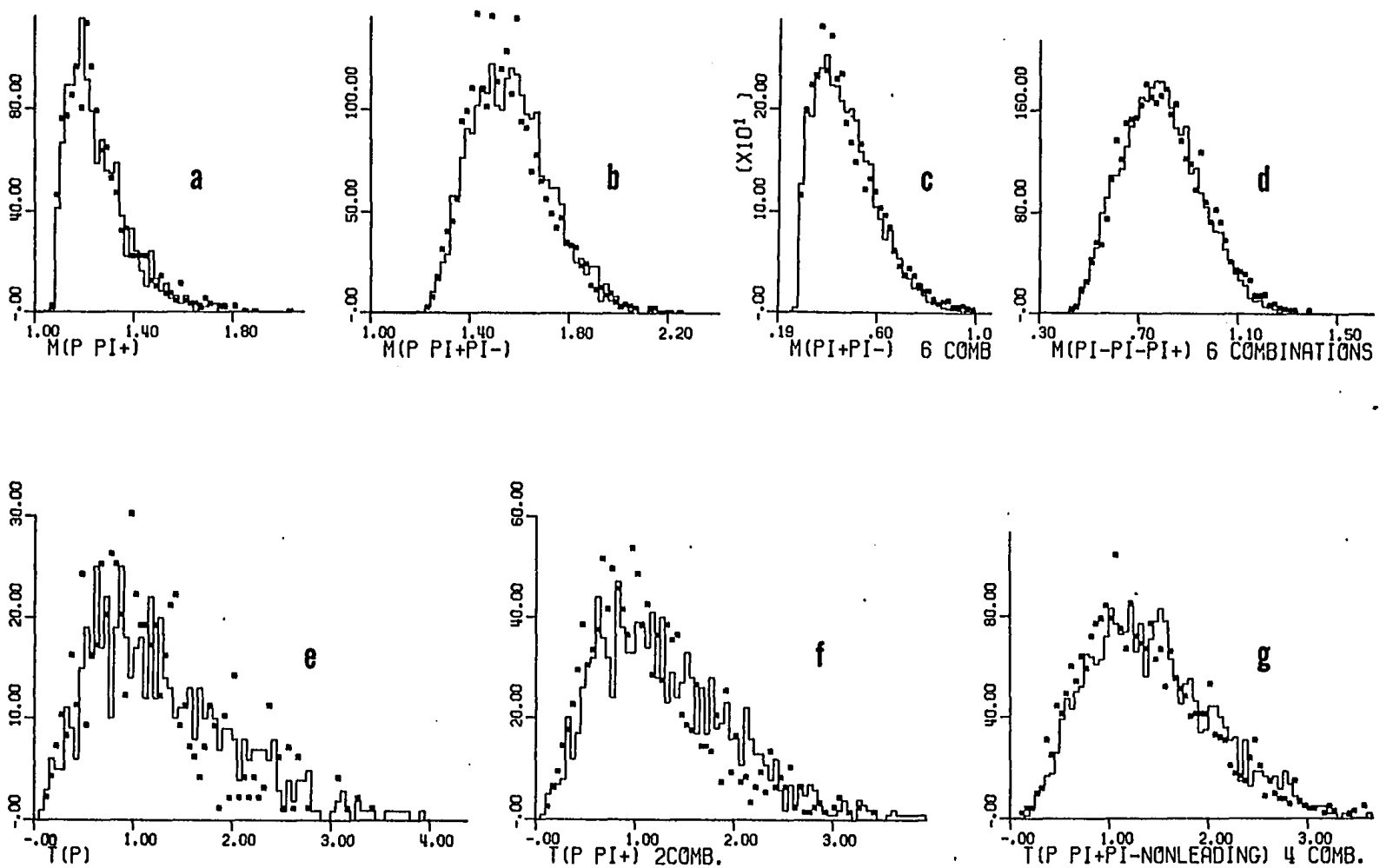

FIG. 5 PART 1 PROTON,6 PI (3.9 GEV/C)

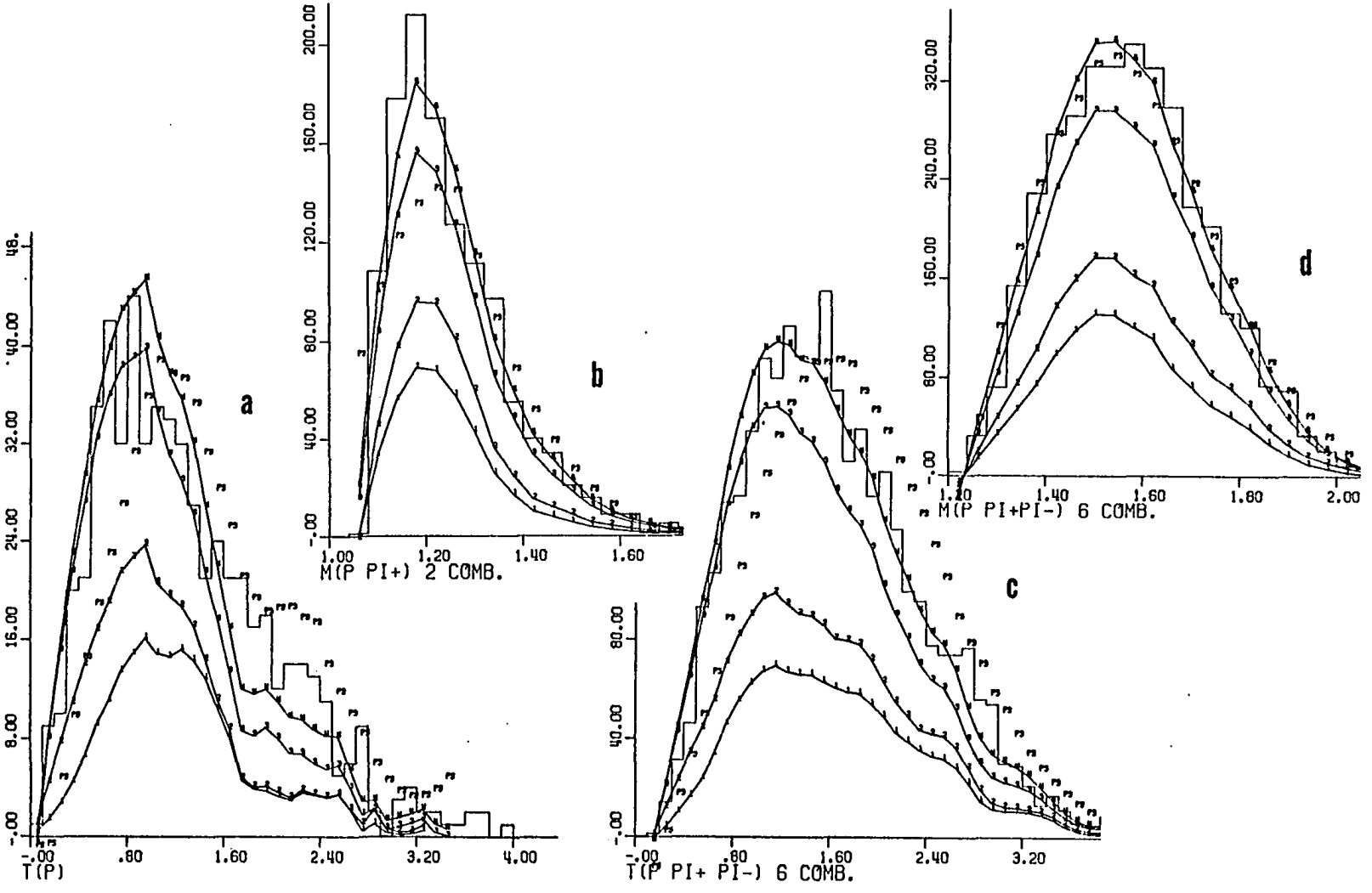

FIG. 5 PART 2 PROTON,6 PI (3.9 GEV/C)

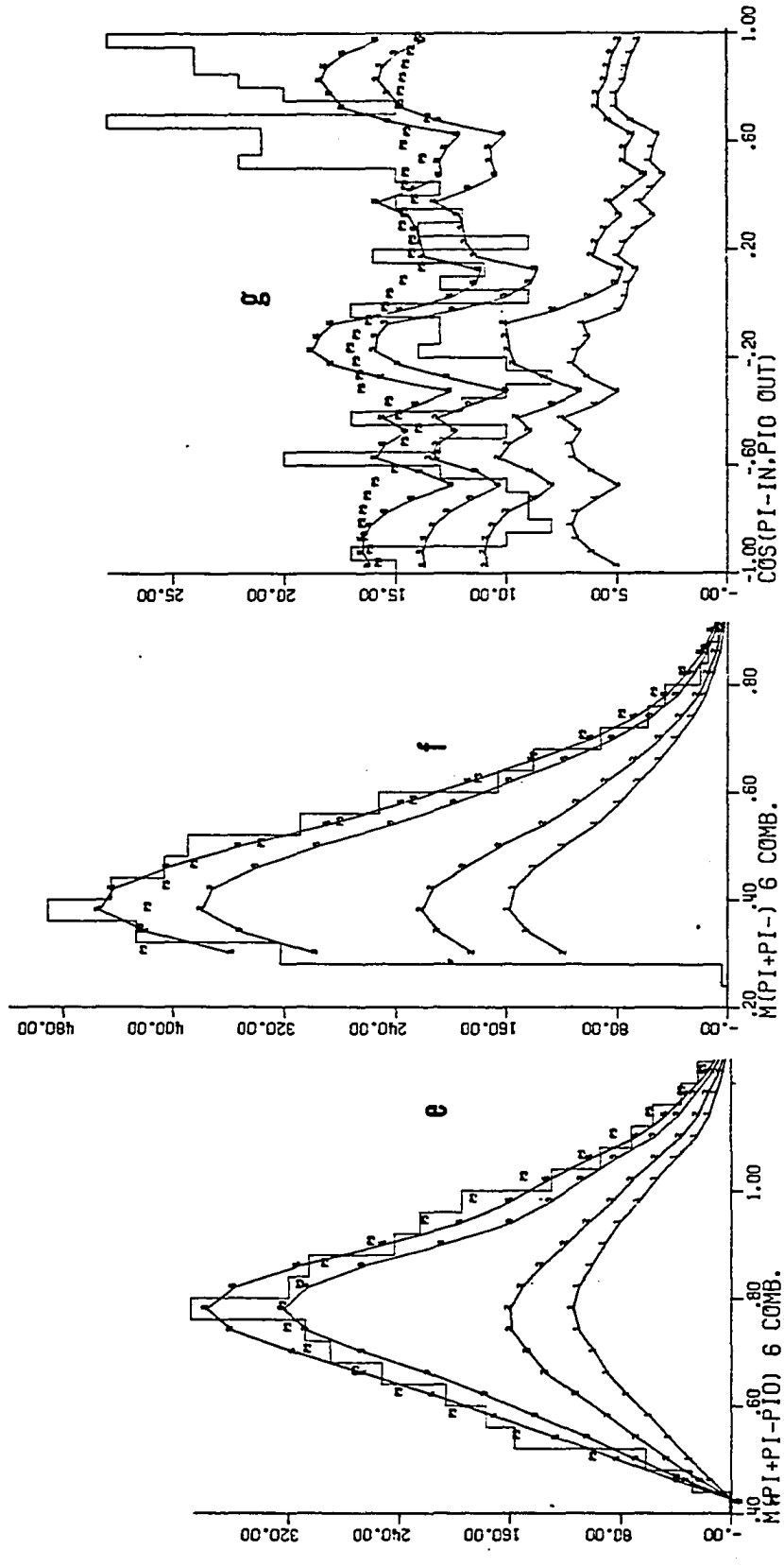

FIG. 5 PART 2 PROTON,6 PI (3.9 GEV/C)

FIGURE 6

Part 1: Overview, $\pi^- p \rightarrow n\pi^+\pi^+\pi^+\pi^-\pi^-\pi^-$ at 3.9 GeV/c. The same general comments apply as for Figure 1, Part 2. a-c, masses of selected particle combinations; events/40 mev. d, n, o, and p, momentum-transfer-squared to selected combinations; events/50 mev^2. In c and d, the most forward π^- and π^+ have been excluded, giving four combinations/event. e, f, g, cos(π^- incident, outgoing particle) for each type of final-state particle; events/.04. h-m, longitudinal and transverse components of momentum for final-state particles; events/20 mev/c for P_{trans}, events/40 mev/c for P_{long}.

Part 2: Details, $\pi^- p \rightarrow n\pi^+\pi^+\pi^+\pi^-\pi^-\pi^-$ at 3.9 GeV/c. a, c, d, momentum-transfer-squared to the three types of final-state particles; events/40 mev^2. b, mass of n, π^- combination; events/40 mev.

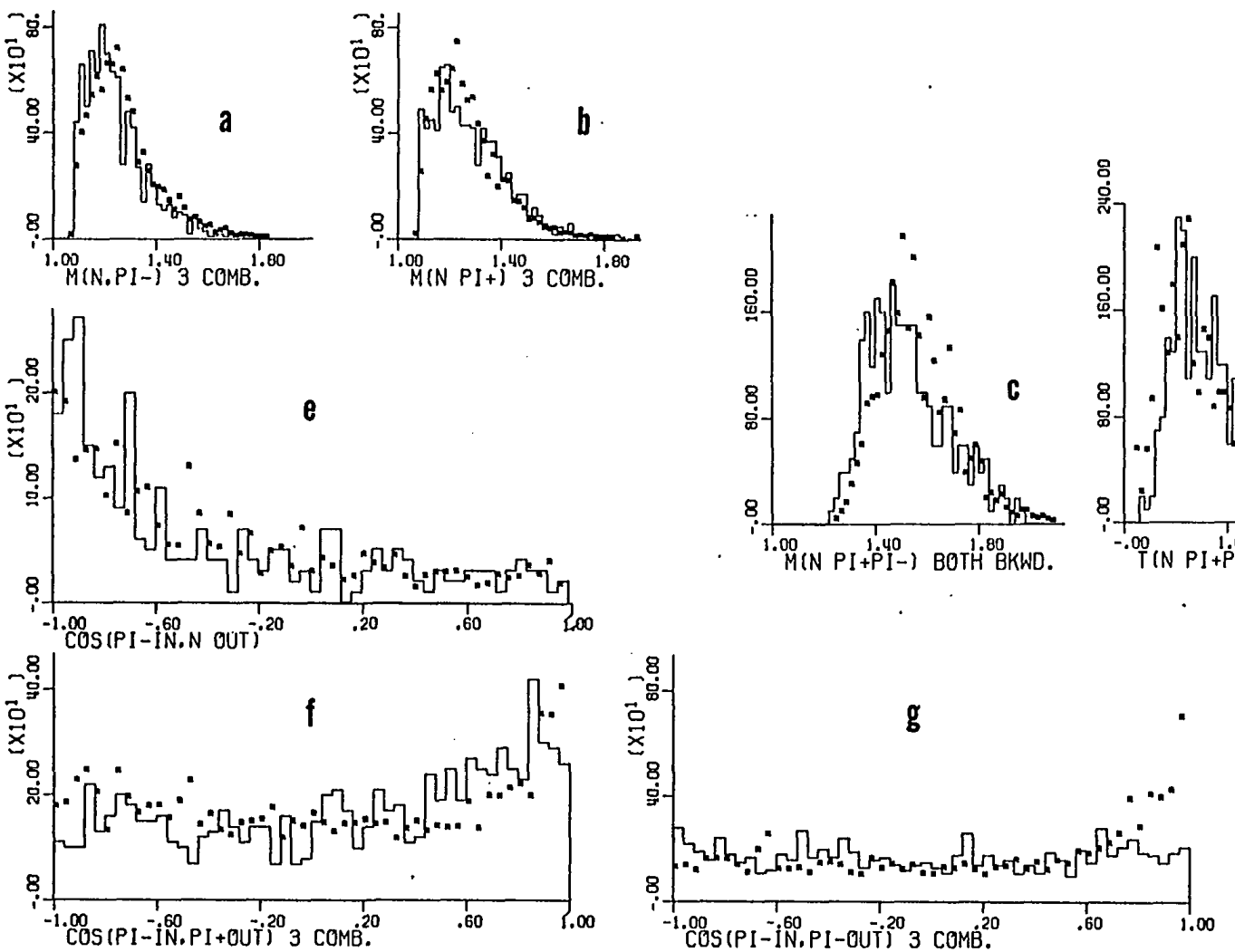

FIG. 6 PART 1 NEUTRON, 6 PI (3.9 GEV/C)

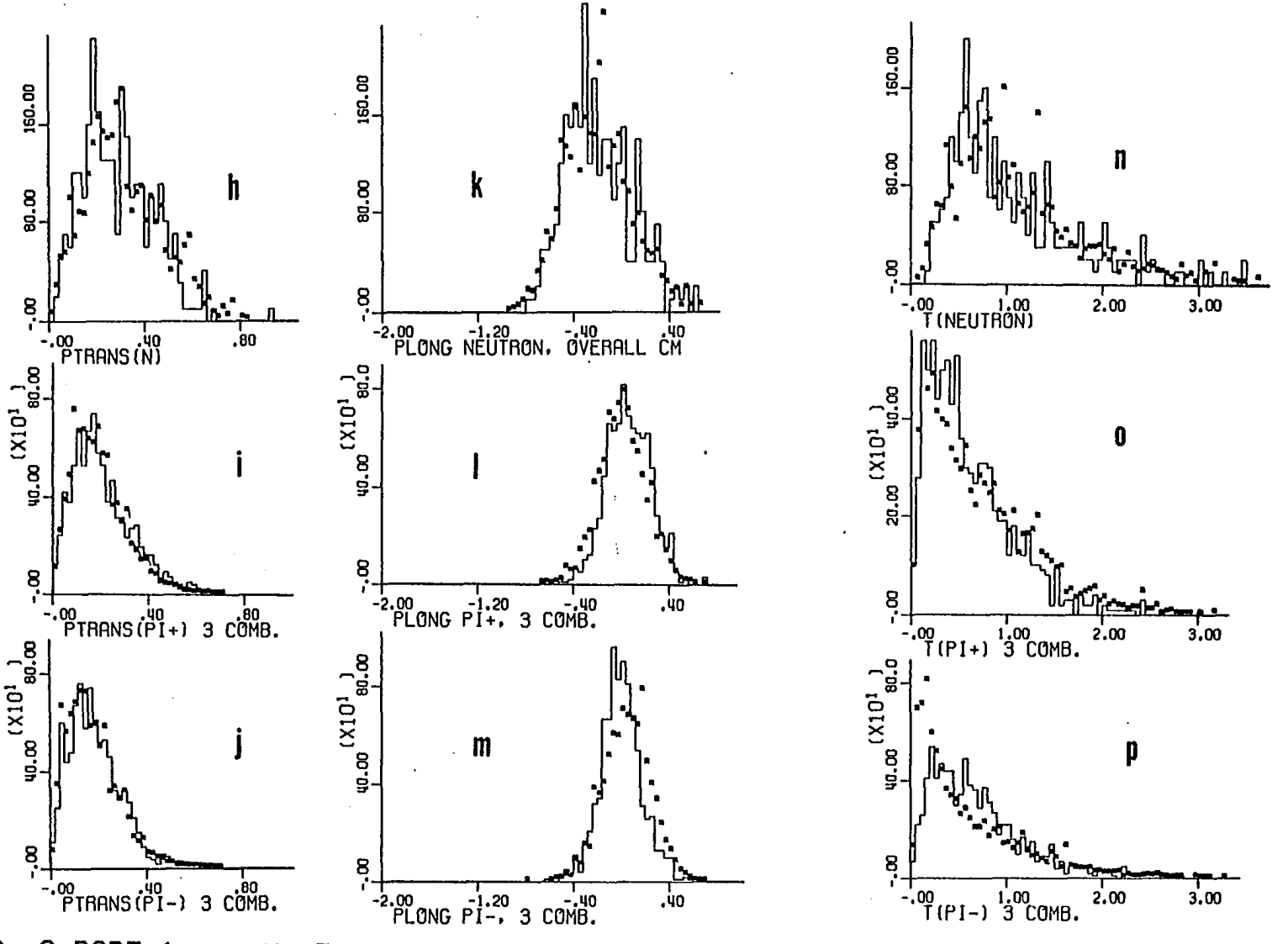

FIG. 6 PART 1 NEUTRON, 6 PI (3.9 GEV/C)

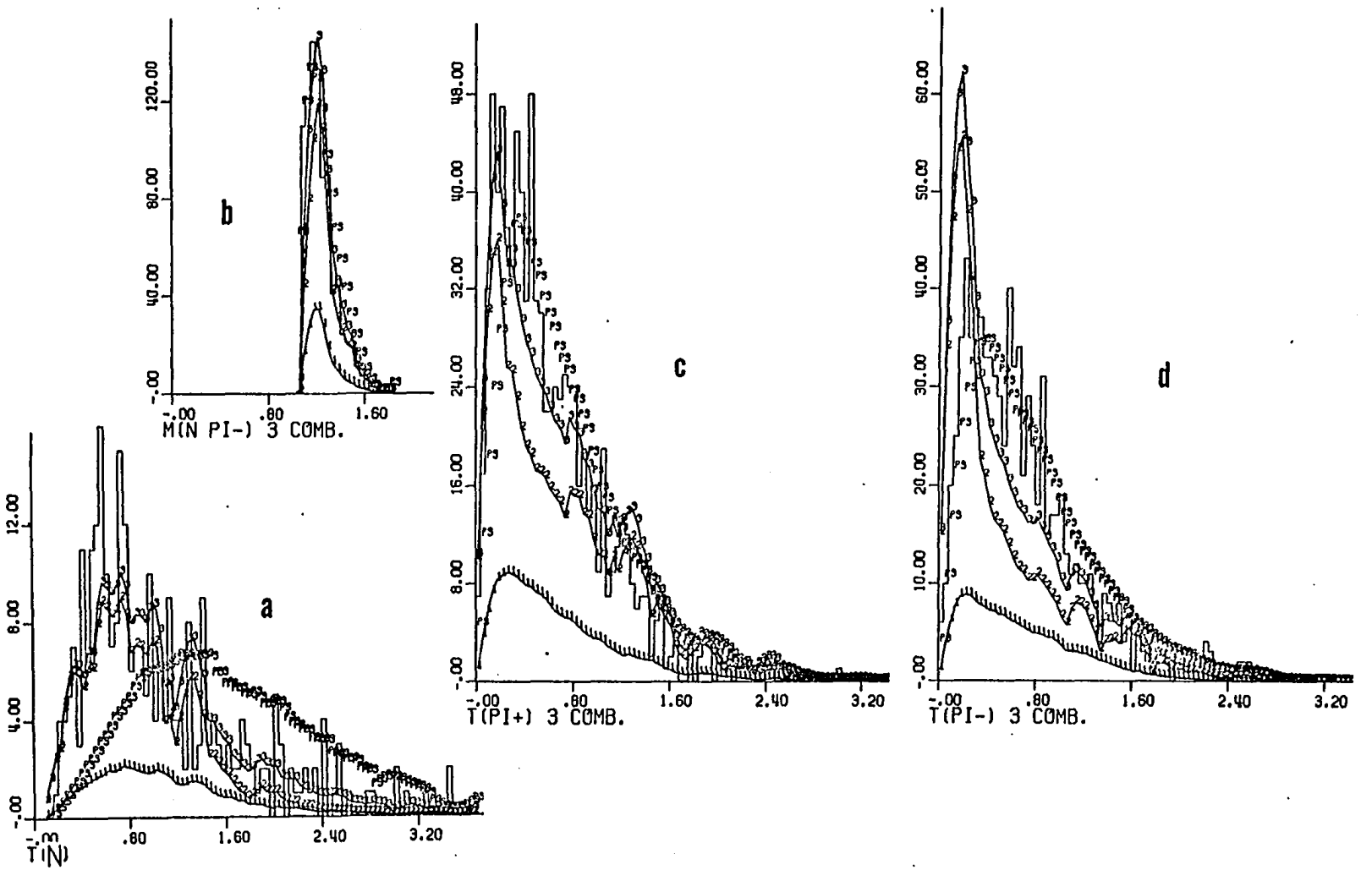

FIG. 6 PART 2 NEUTRON, 6 PI (3.9 GEV/C)

FIGURE 7

Part 1: Overview, $\pi^- p \rightarrow p\pi^+\pi^-\pi^-$ at 11.9 GeV/c. The same general comments apply as for Figure 1, Part 1. a, b, c, g, masses of selected particle combinations; events/40 mev. d, e, f, h, i, momentum-transfer-squared to selected particle combinations; events/40 mev^2. j, k, cos(π^- incident, π outgoing) in cm; events/.04. l-q, longitudinal and transverse components of momentum for final-state particles in laboratory system; events/50 mev/c for P_{long}, events/20 mev/c for P_{trans}.

Part 2: Details, $\pi^- p \rightarrow p\pi^+\pi^-\pi^-$ at 11.9 GeV/c. The same general comments apply as for Figure 1, Part 2. a, c, e, momentum-transfer-squared to selected particle combinations; events/60 mev^2. b, d, f, masses of selected particle combinations; events/40 mev. g, h, cos(π^- incident, $\pi^\pm$ outgoing) in cm; events/.05.

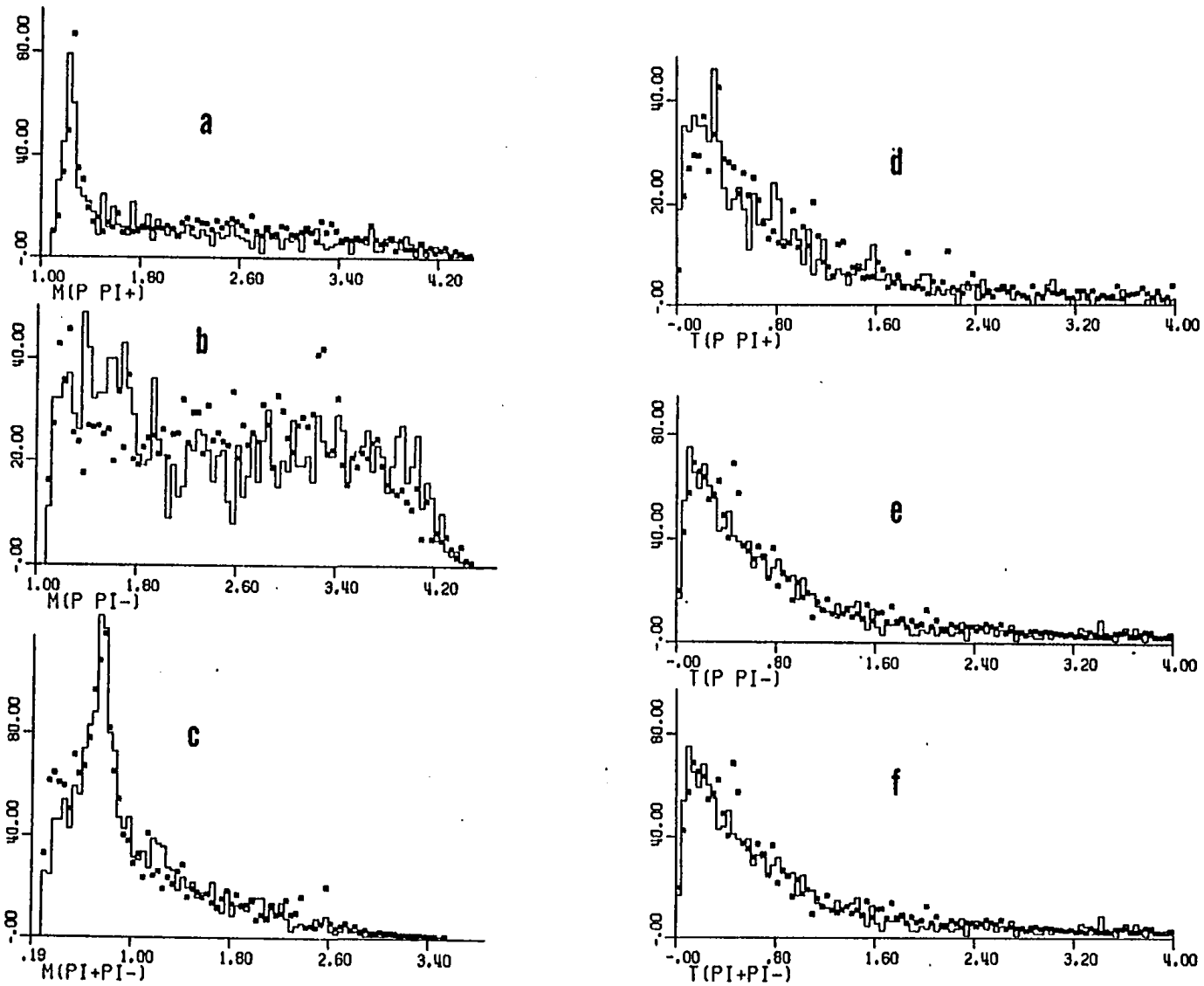

FIG. 7 PART 1 PROTON, 3 PI (11.9 GEV/C)

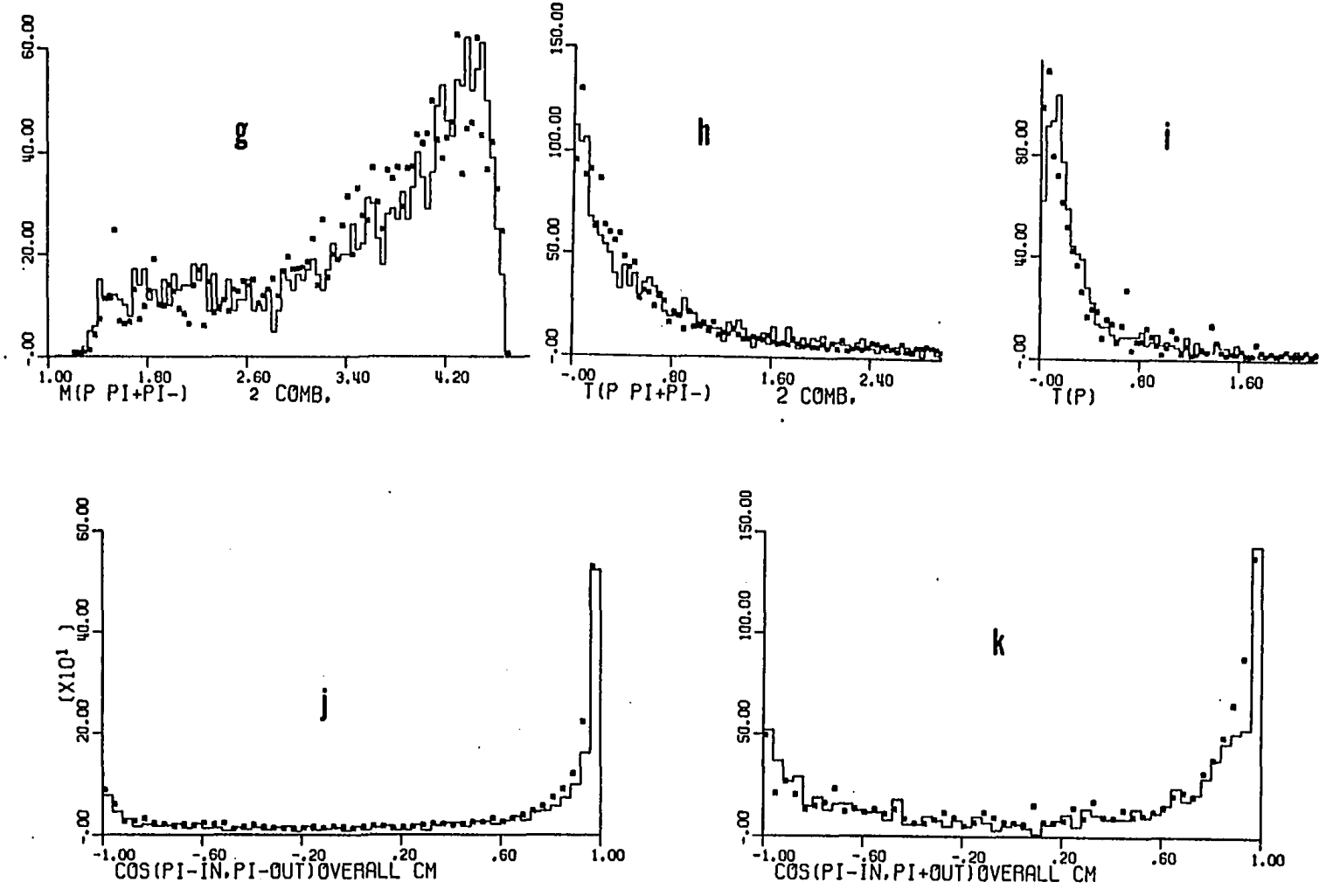

FIG. 7 PART 1 PROTON,3 PI (11.9 GEV/C)

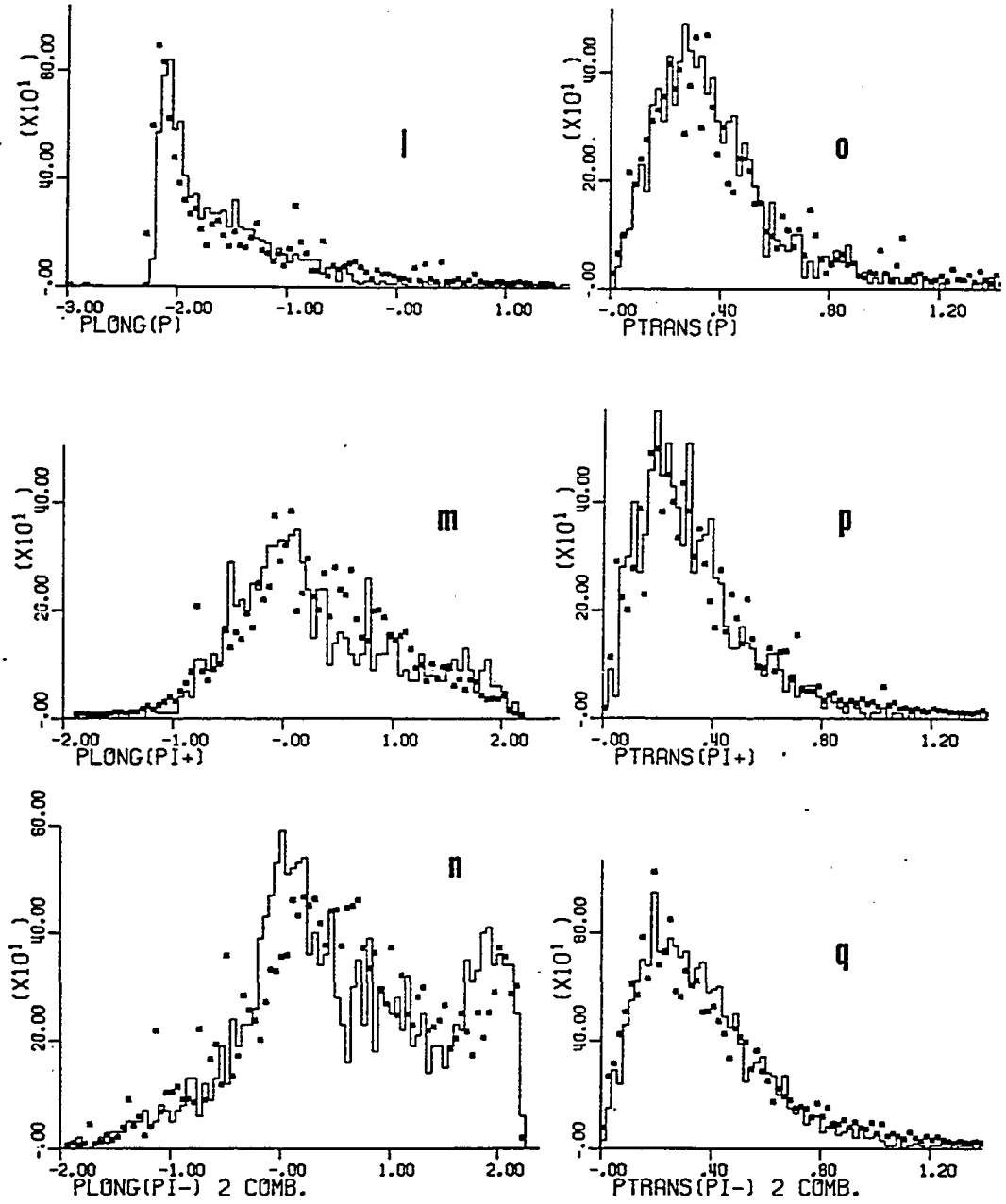

FIG. 7 PART 1 PROTON, 3 PI

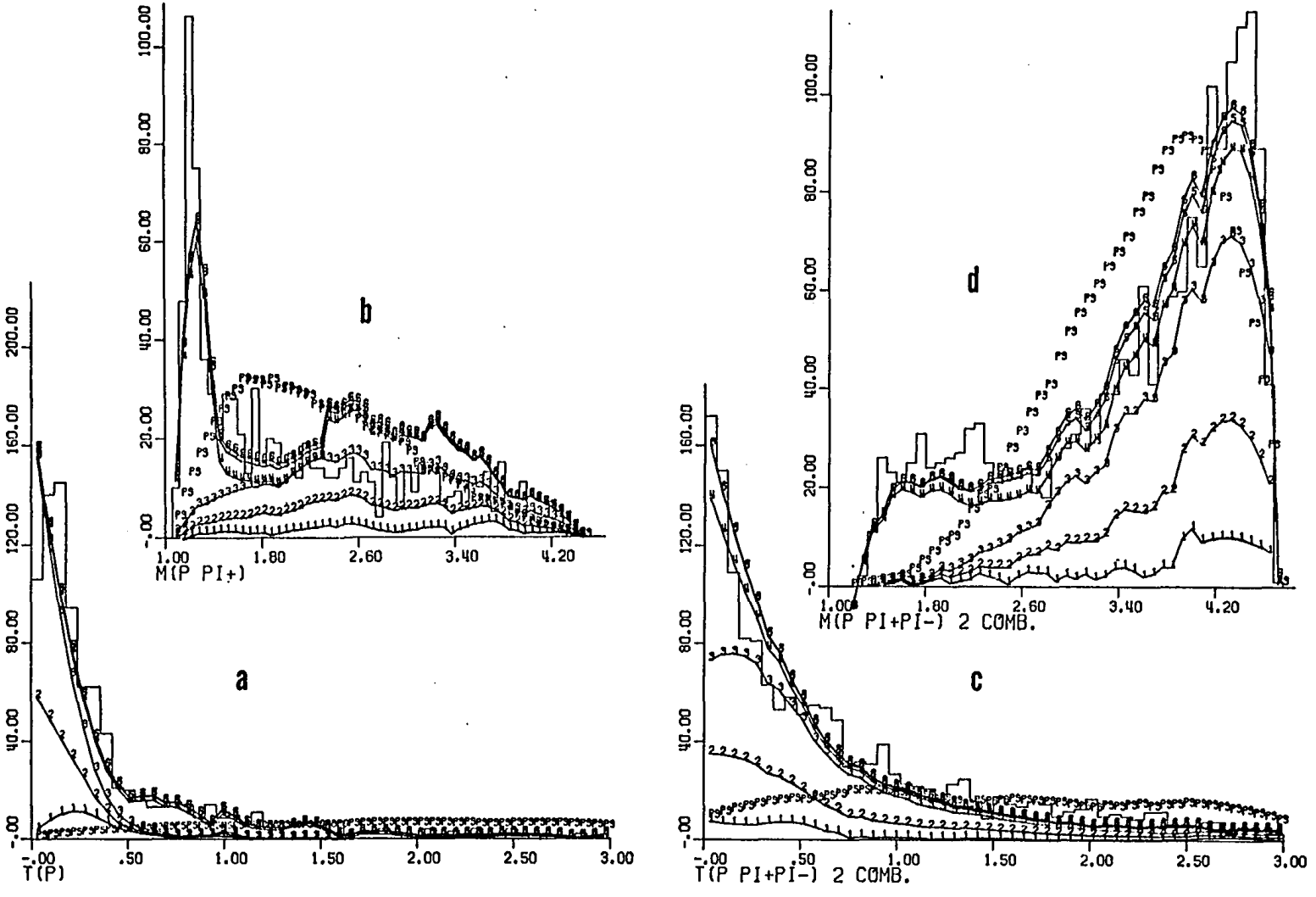

FIG. 7 PART 2 PROTON, 3 PI (11.9 GEV/C)

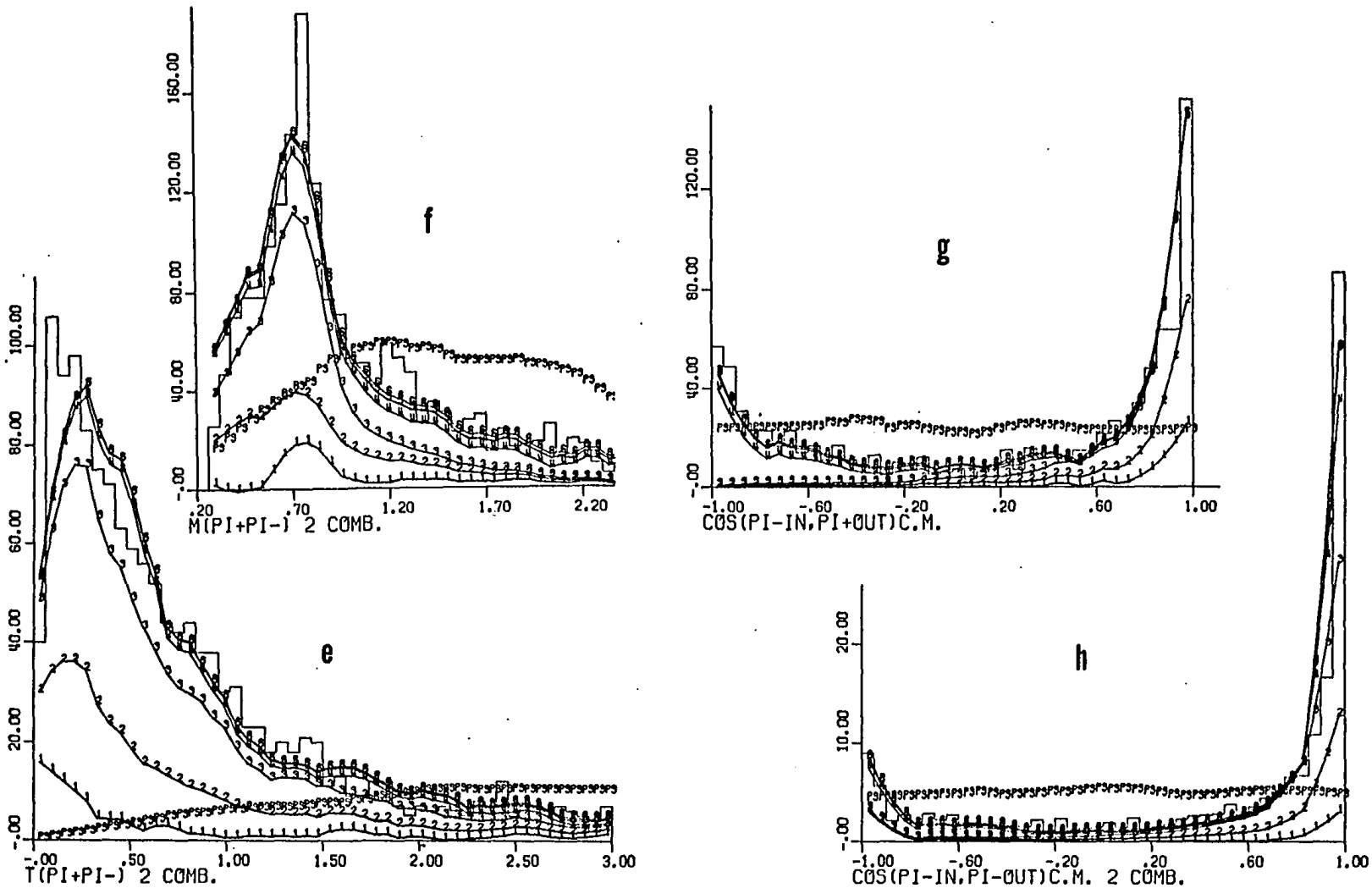

FIG. 7 PART 2 PROTON, 3 PI (11.9 GEV/C)

FIGURE 8

Part 1: Overview, $\pi^- p \to p\pi^+\pi^-\pi^-\pi^0$ at 11.9 GeV/c. The same general comments apply as for Figure 1, Part 1. a-f, masses of selected particle combinations; events/40 mev except c which has events/20 mev. g-i, cos(π^- incident, π outgoing) in cm. In i, the more forward π^- has been excluded. j-l, momentum-transfer-squared to various particle combinations; events/50 mev^2. m-t, longitudinal and transverse components of momentum for particles in final state, in laboratory system; events/80 mev/c for P_{long}, events/40 mev/c.

Part 2: Details, $\pi^- p \to p\pi^+\pi^-\pi^-\pi^0$ at 11.9 GeV/c. The same general comments apply as for Figure 1, Part 2. a, momentum-transfer-squared to proton; events/50 mev^2. b, c, e-g, masses of selected particle combinations; b, c, and g have 40 mev bins; e, f have 60 mev bins. d, cos(π^- incident, π^- outgoing) in cm; events/.05.

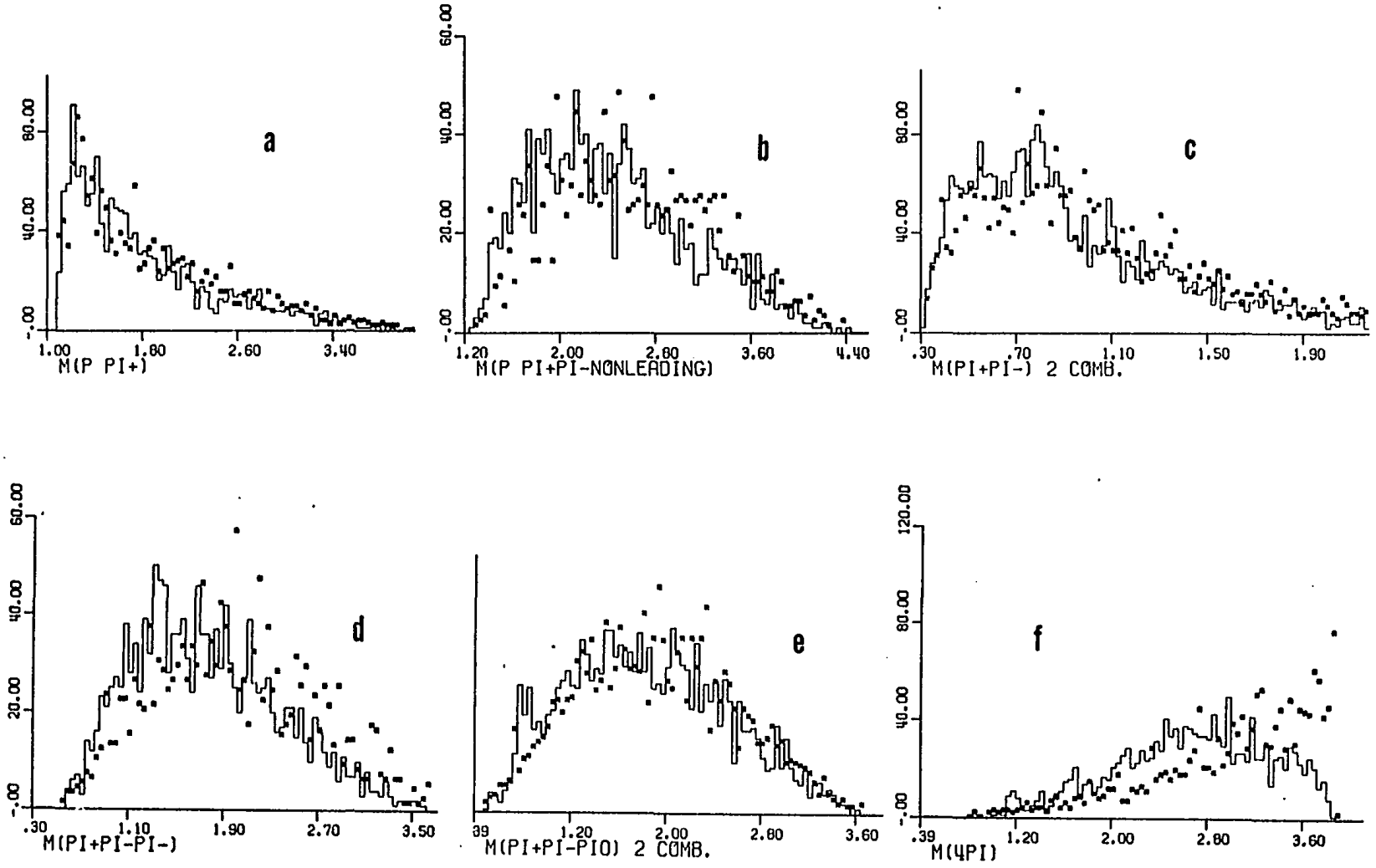

FIG. 8 PART 1 PROTON, 4 PI (11.9 GEV/C)

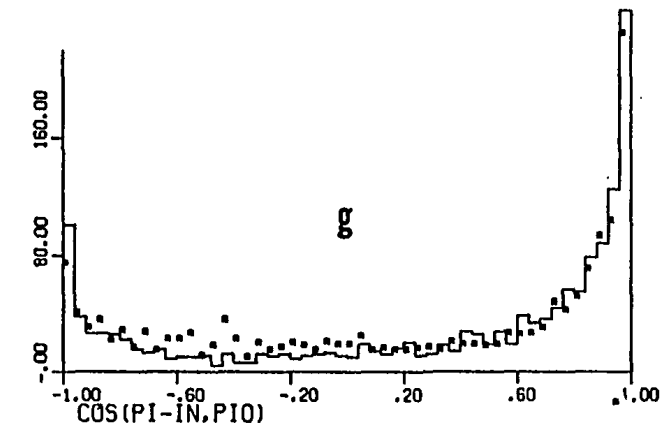

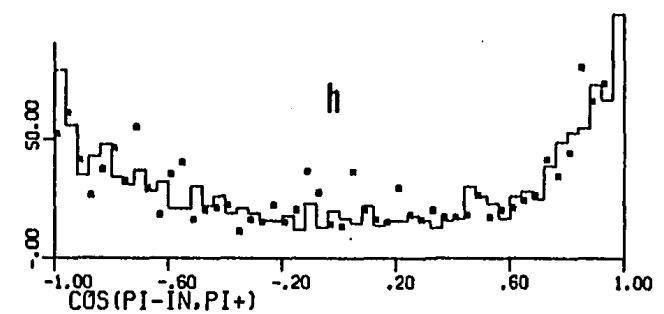

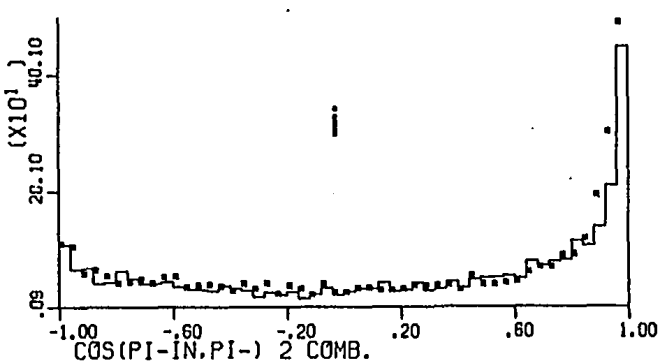

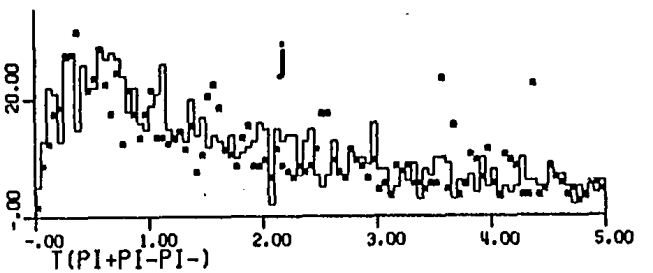

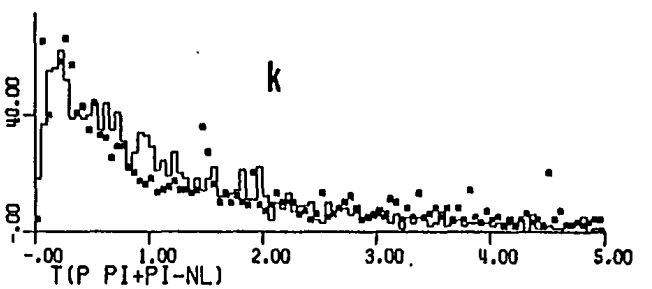

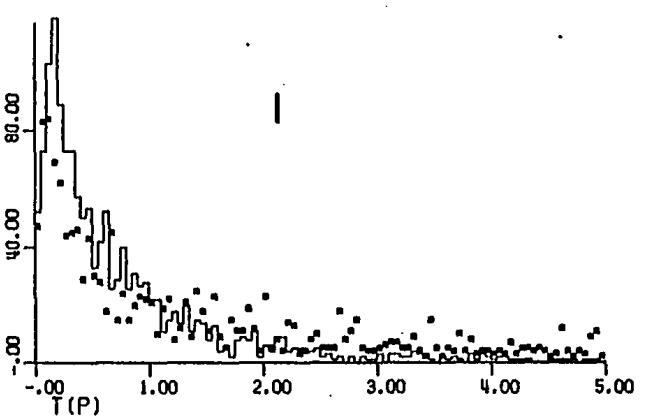

FIG. 8 PART 1 PROTON,4 PI (11.9 GEV/C)

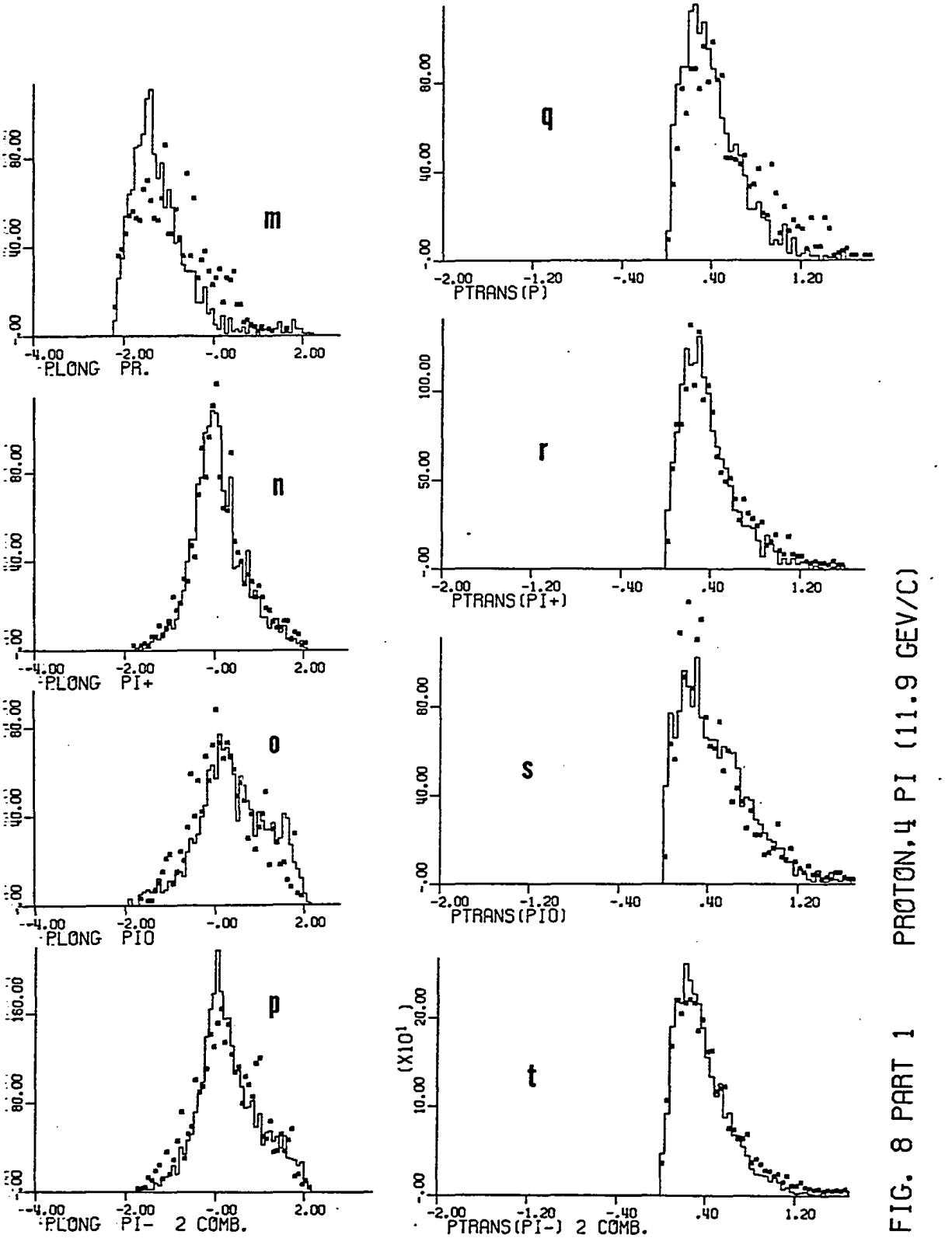

FIG. 8 PART 1 PROTON, 4 PI (11.9 GEV/C)

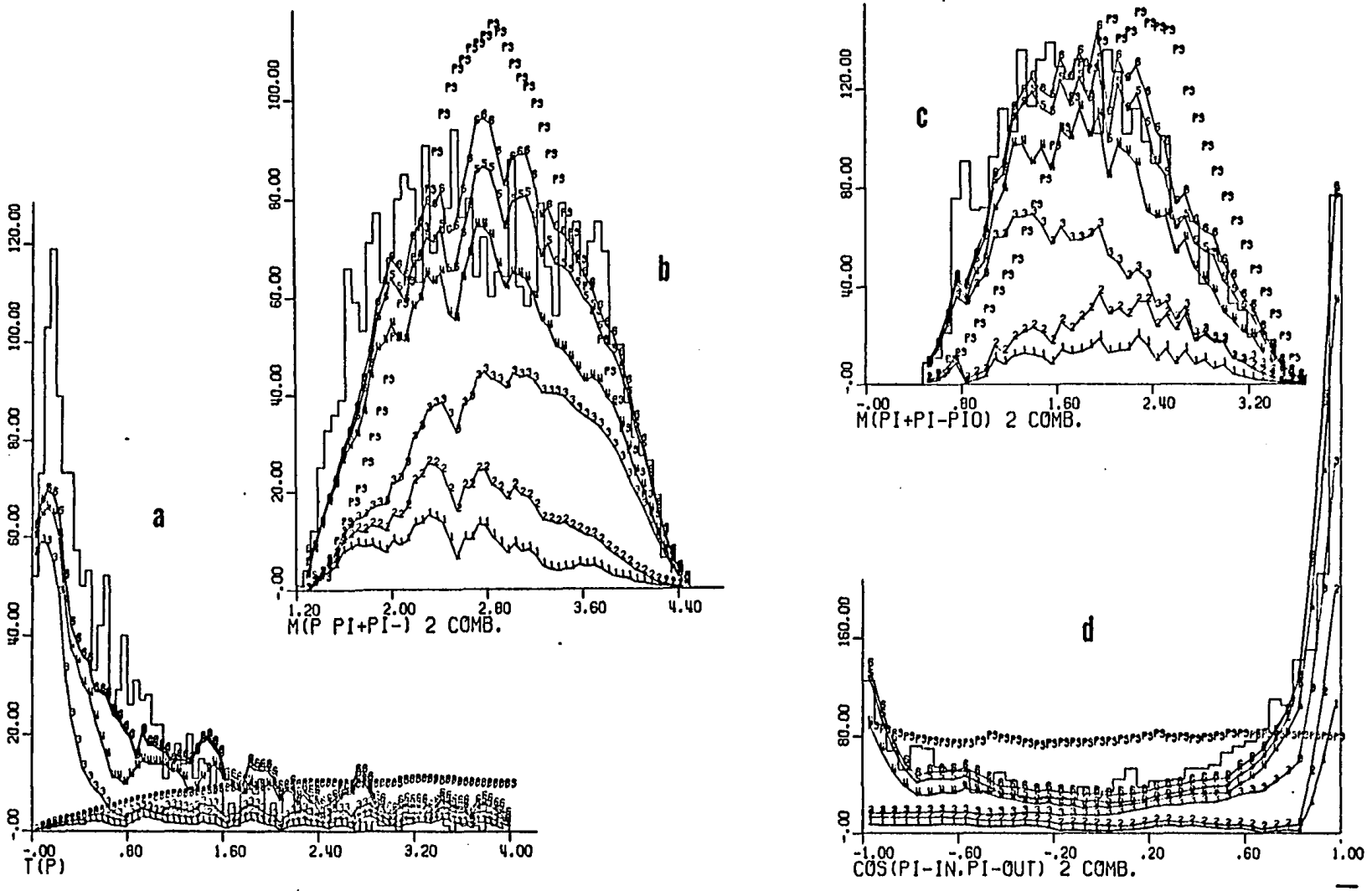

FIG. 8 PART 2 PROTON,4 PI (11.9 GEV/C)

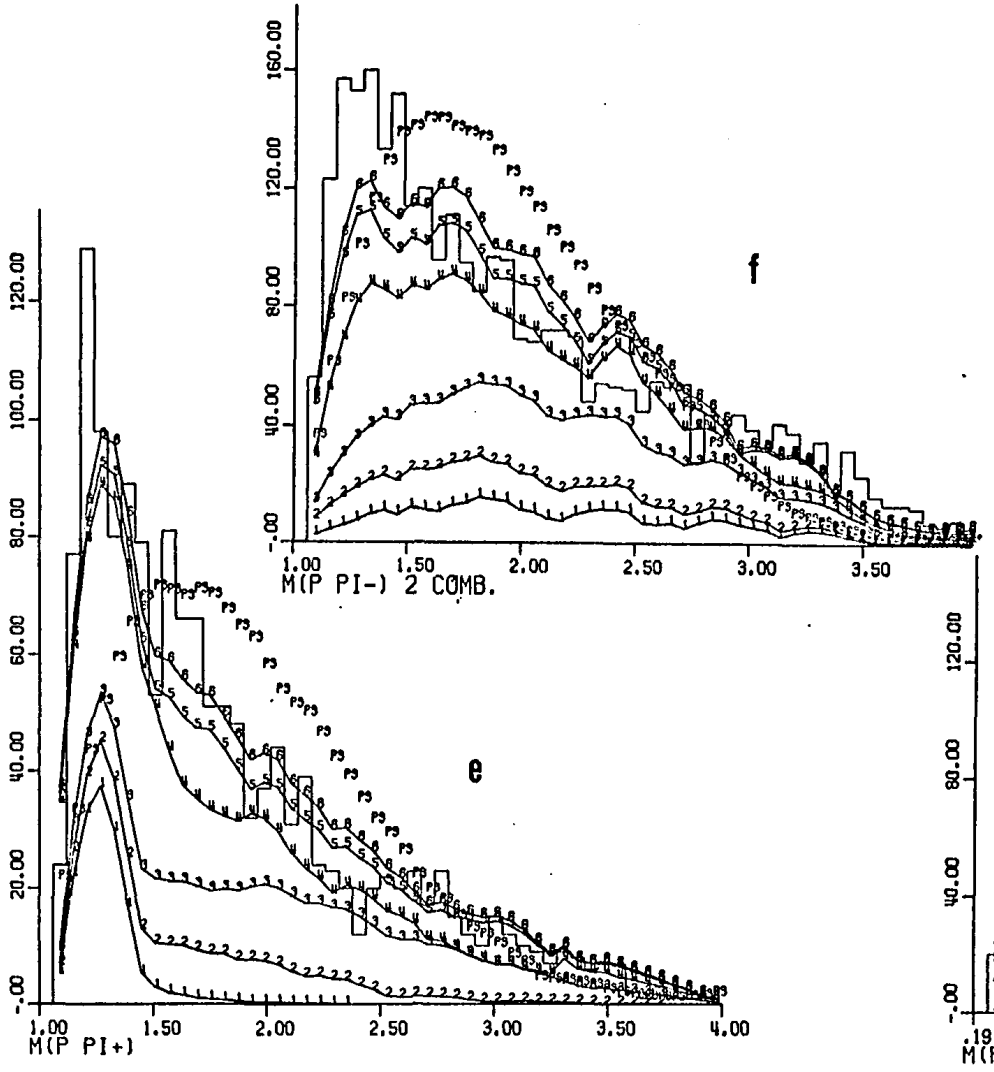

FIG. 8 PART 2 PROTON,4 PI (11.9 GEV/C)

FIGURE 9

Part 1: Overview, $\pi^- p \rightarrow n\pi^+\pi^+\pi^-\pi^-$ at 11.9 GeV/c. The same general comments apply as for Figure 1, Part 1. a-e, g, h, masses of selected particle combinations; events/40 mev. f, momentum-transfer-squared to neutron; events/50 mev^2. i-n, longitudinal and transverse components of momentum for final-state particles in laboratory system; events/.04.

Part 2: Details, $\pi^- p \rightarrow n\pi^+\pi^+\pi^-\pi^-$ at 11.9 GeV/c. The same general comments apply as for Figure 1, Part 2. a, c, momentum-transfer-squared to neutron and $n\pi^+\pi^-$ combination, respectively; events/50 mev^2. b, d, e, f, masses of selected particle combinations; events/50 mev. g, h, cos(π^- incident, π outgoing) in cm; events/.05.

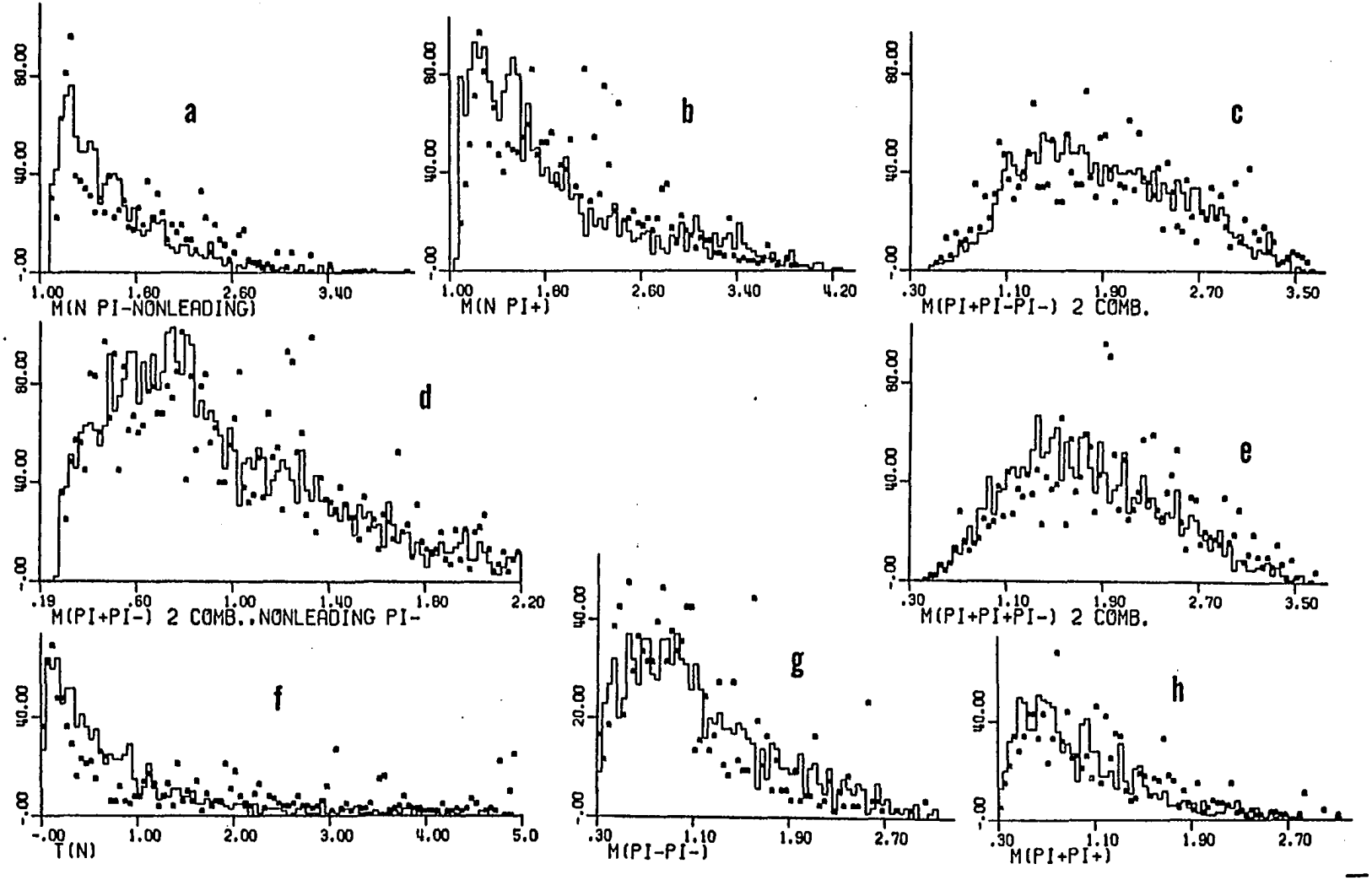

FIG. 9 PART 1 NEUTRON,4 PI (11.9 GEV/C)

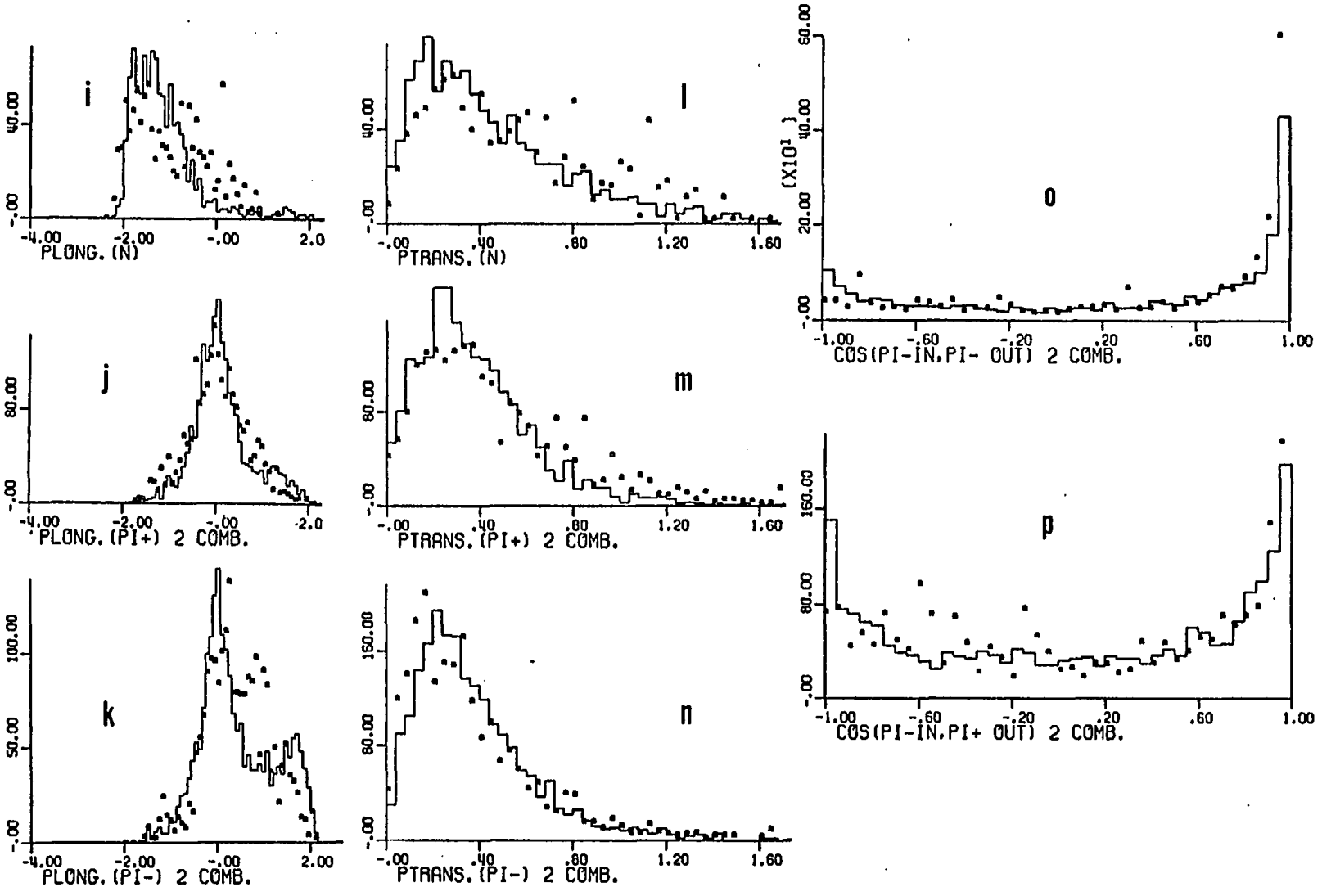

FIG. 9 PART 1 NEUTRON, 4 PI (11.9 GEV/C)

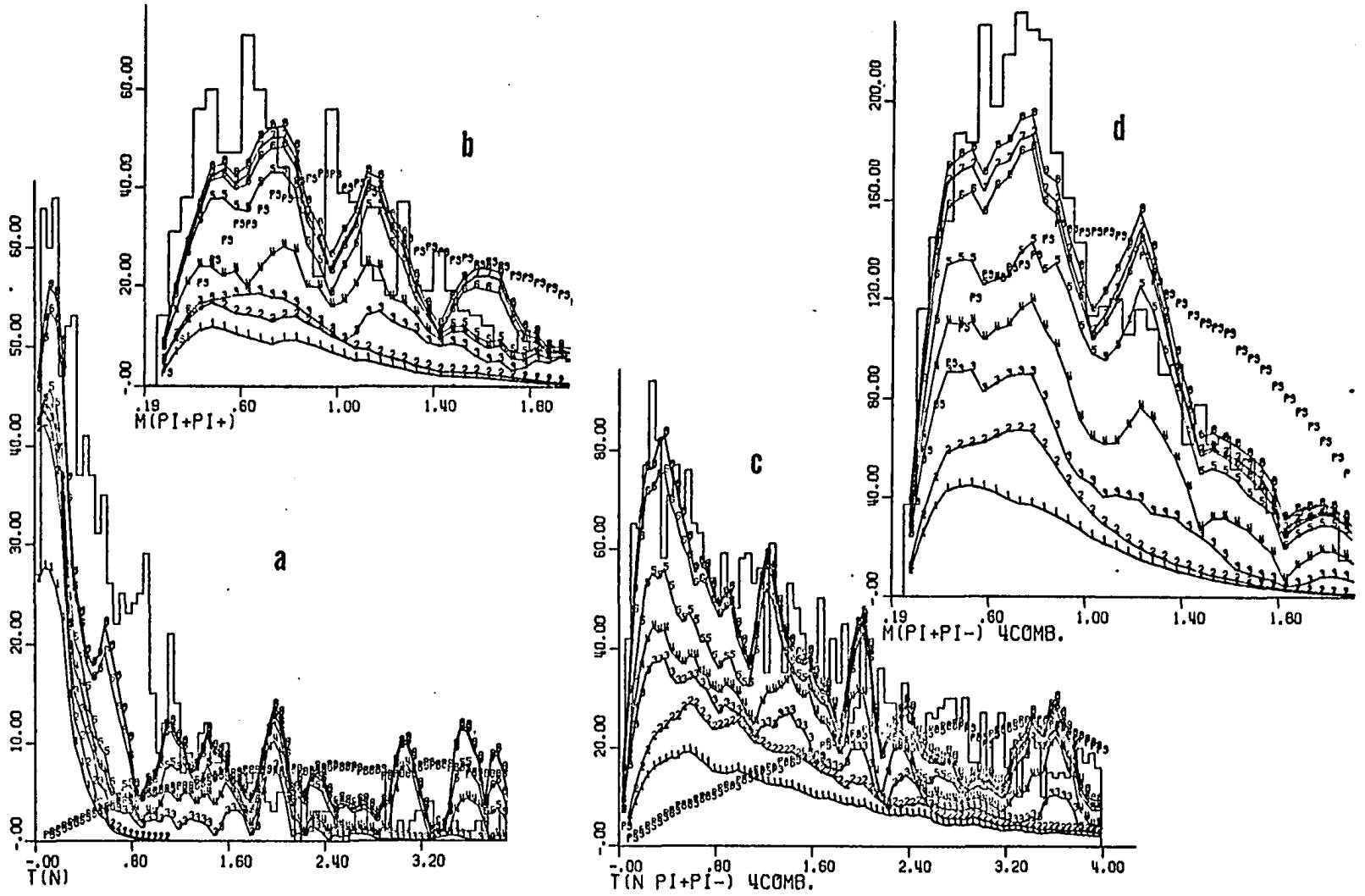

FIG. 9 PART 2 NEUTRON, 4 PI (11.9 GEV/C)

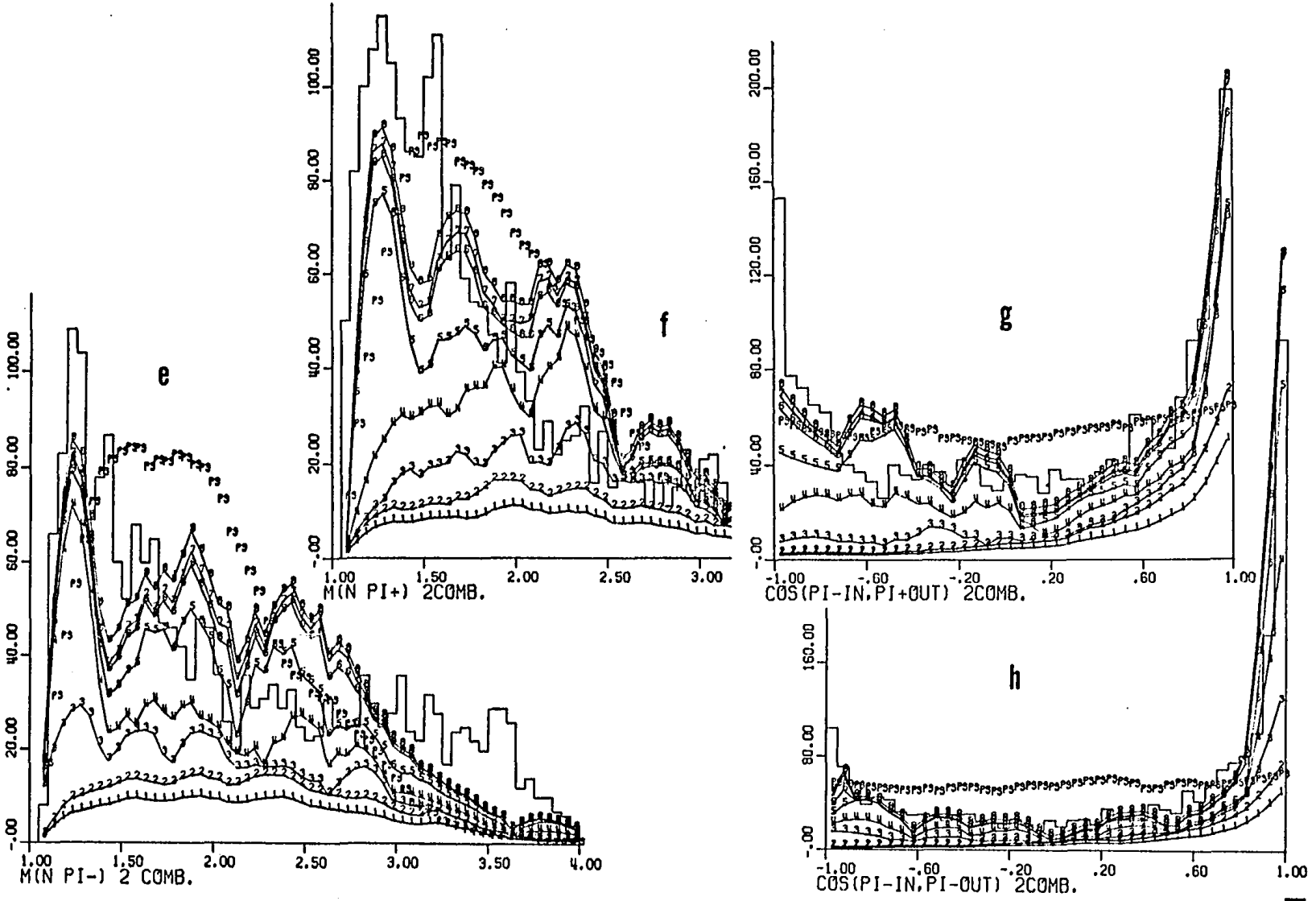

FIG. 9 PART 2 NEUTRON,4 PI (11.9 GEV/C)

FIGURE 10

Part 1: Overview, $\pi^- p \rightarrow p\pi^+\pi^+\pi^-\pi^-\pi^-$ at 11.9 GeV/c. The same general comments apply as for Figure 1, Part 1. a-g, masses of selected particle combinations; events/20 mev. h-l, momentum-transfer-squared to selected particle combinations; events/50 mev^2. m-r, longitudinal and transverse components of momentum for final-state particles in laboratory system; events/40 mev/c for P_{long}, events/20 mev/c for P_{trans}. s-v, cos(π^- incident, outgoing particle) for the three types of outgoing particles, in cm; events/.04. w, x, cos(π outgoing, π outgoing) in 5π cm; events/.04.

Part 2: Details, $\pi^- p \rightarrow p\pi^+\pi^+\pi^-\pi^-\pi^-$ at 11.9 GeV/c. a, d, f, momentum-transfer-squared to selected particle combinations; events/50 mev^2. b, c, e, g, masses of selected particle combinations; b and g have 50 mev bins, c and e have 40 mev bins. h, i, cos(π^- incident, π outgoing) in cm; events/40 mev.

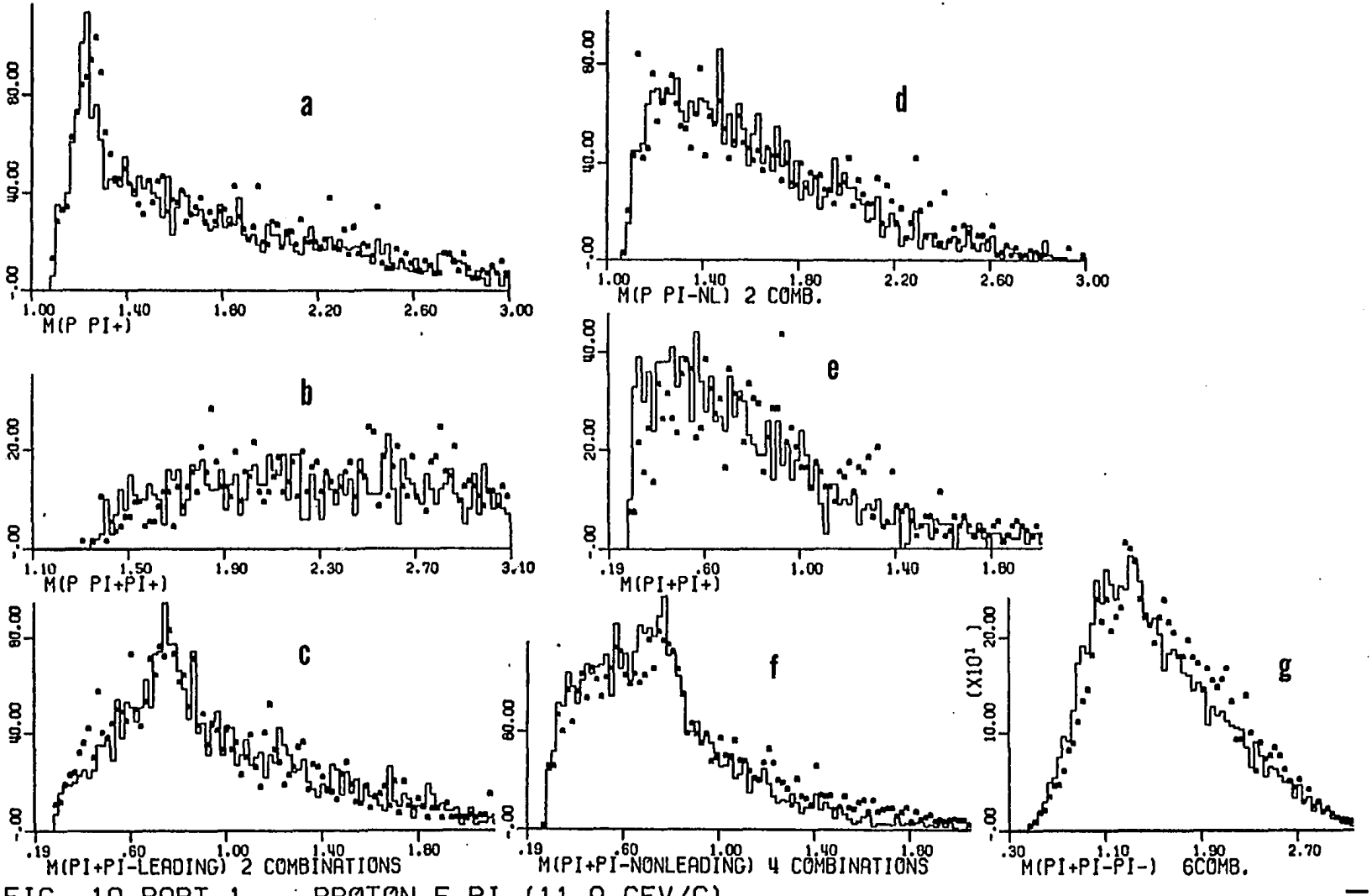

FIG. 10 PART 1 PROTON,5 PI (11.9 GEV/C)

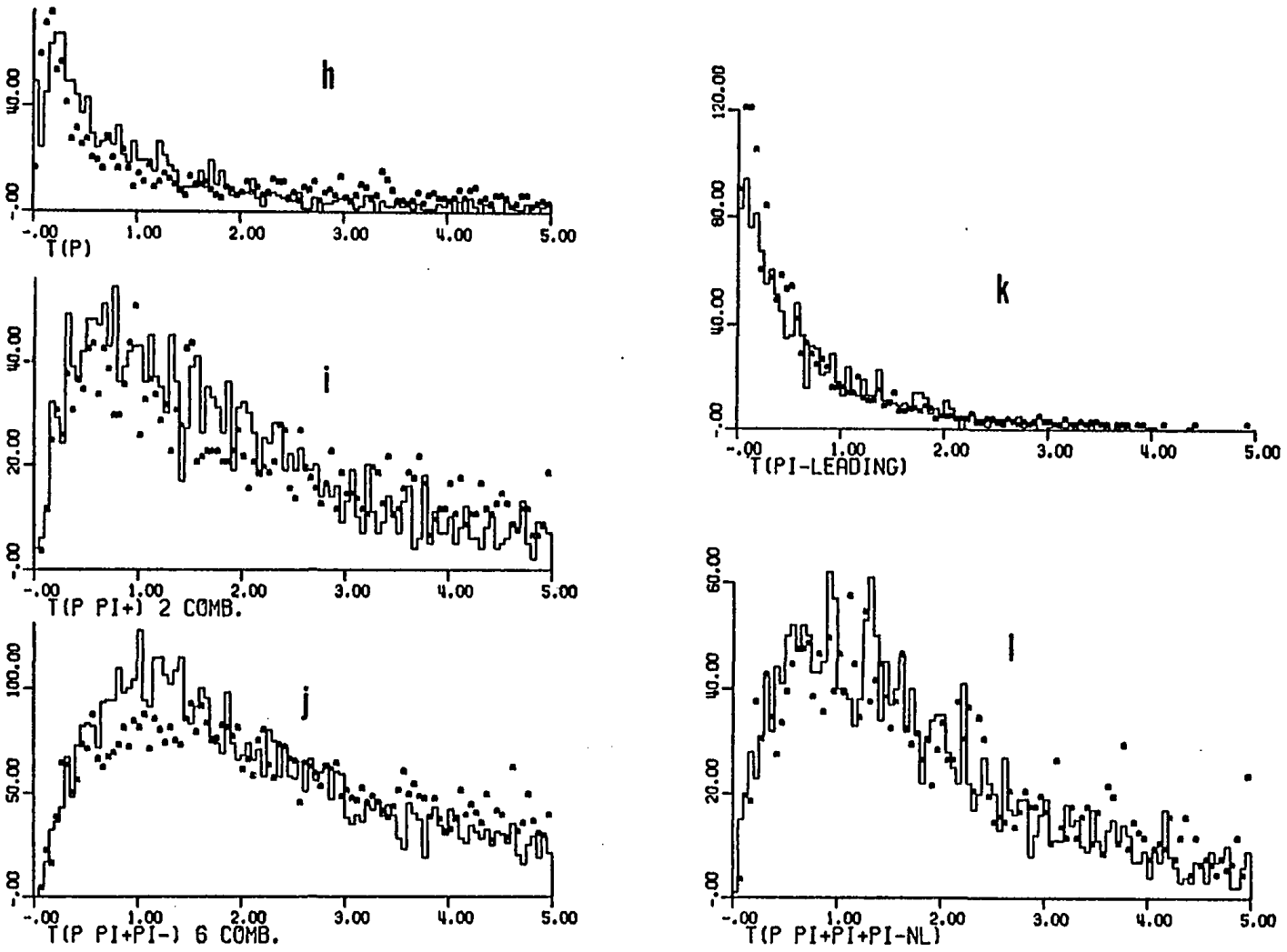

FIG. 10 PART 1 PROTON.5 PI (11.9 GEV/C)

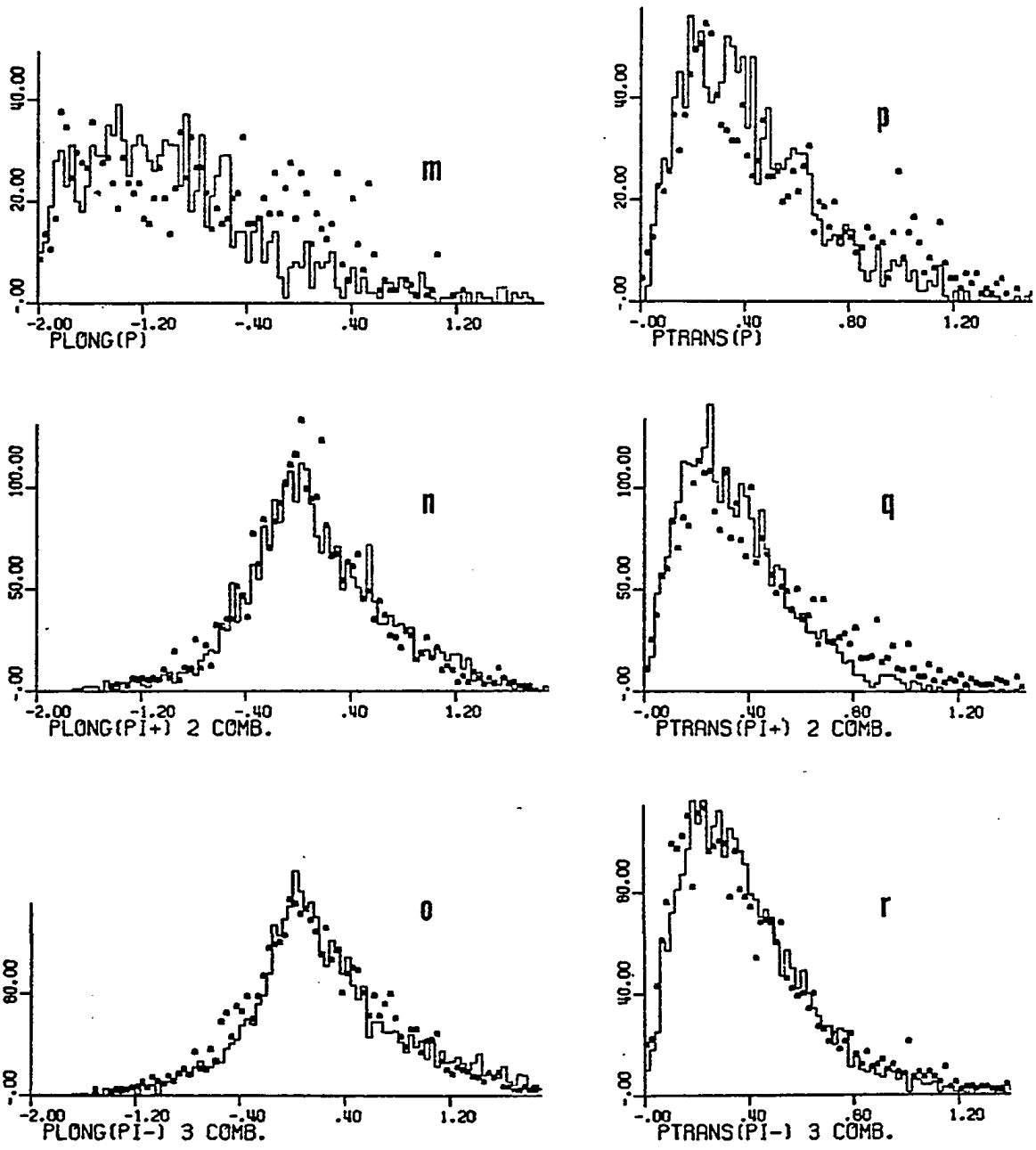

FIG. 10 PART 1 PROTON,5 PI (11.9 GEV/C)

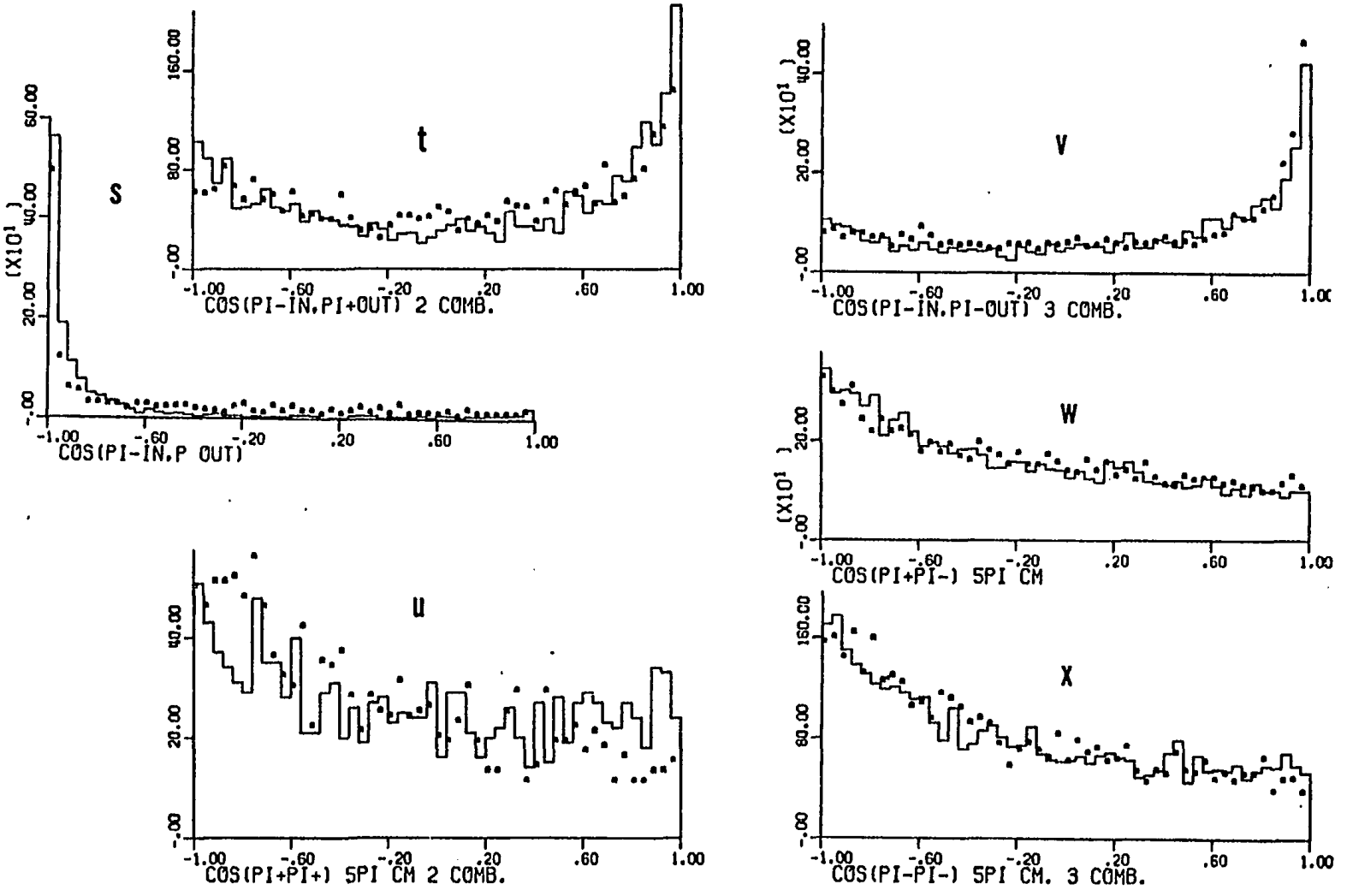

FIG. 10 PART 1 PROTON, 5 PI

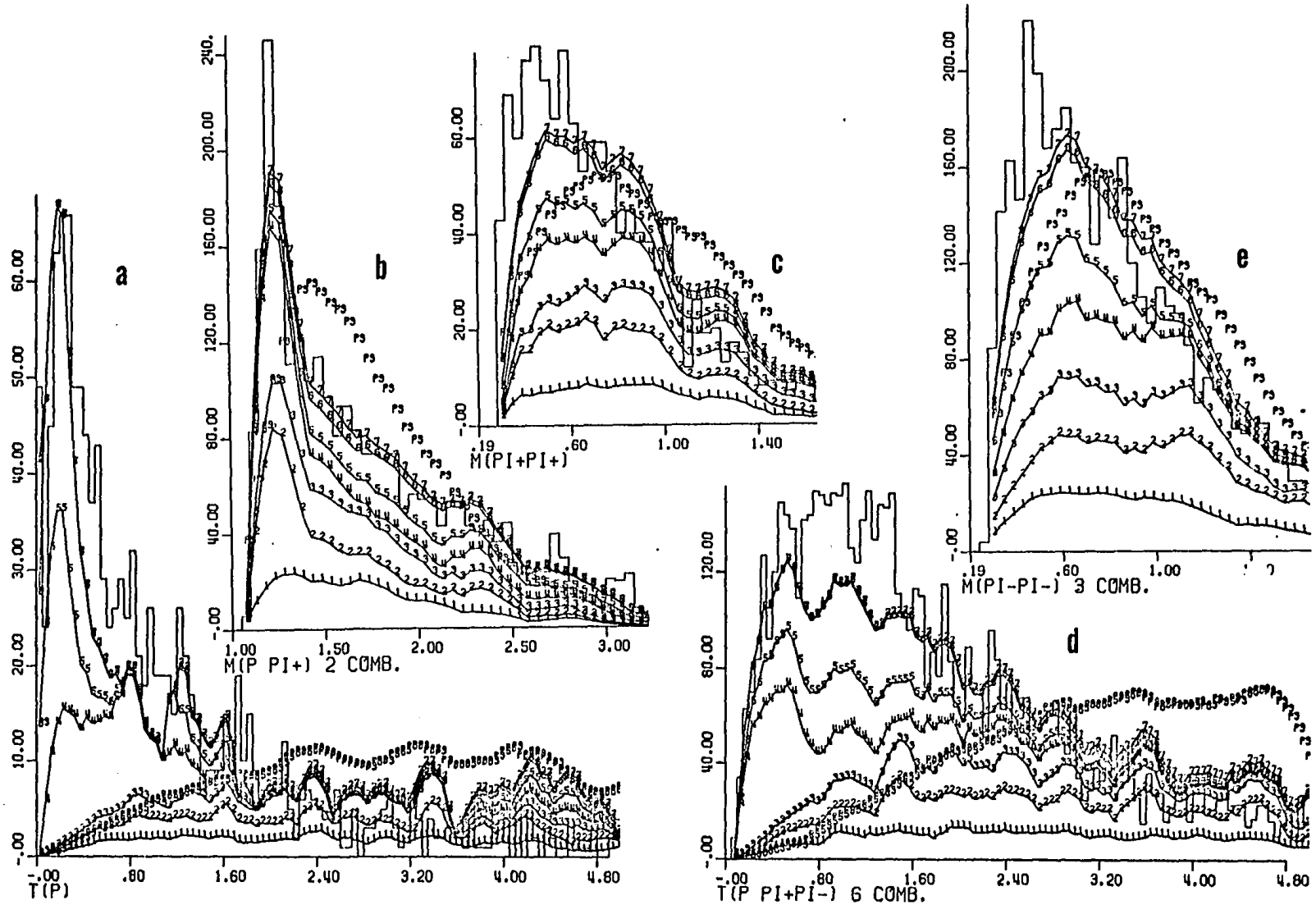

FIG. 10 PART 2 PROTON,5 PI (11.9 GEV/C)

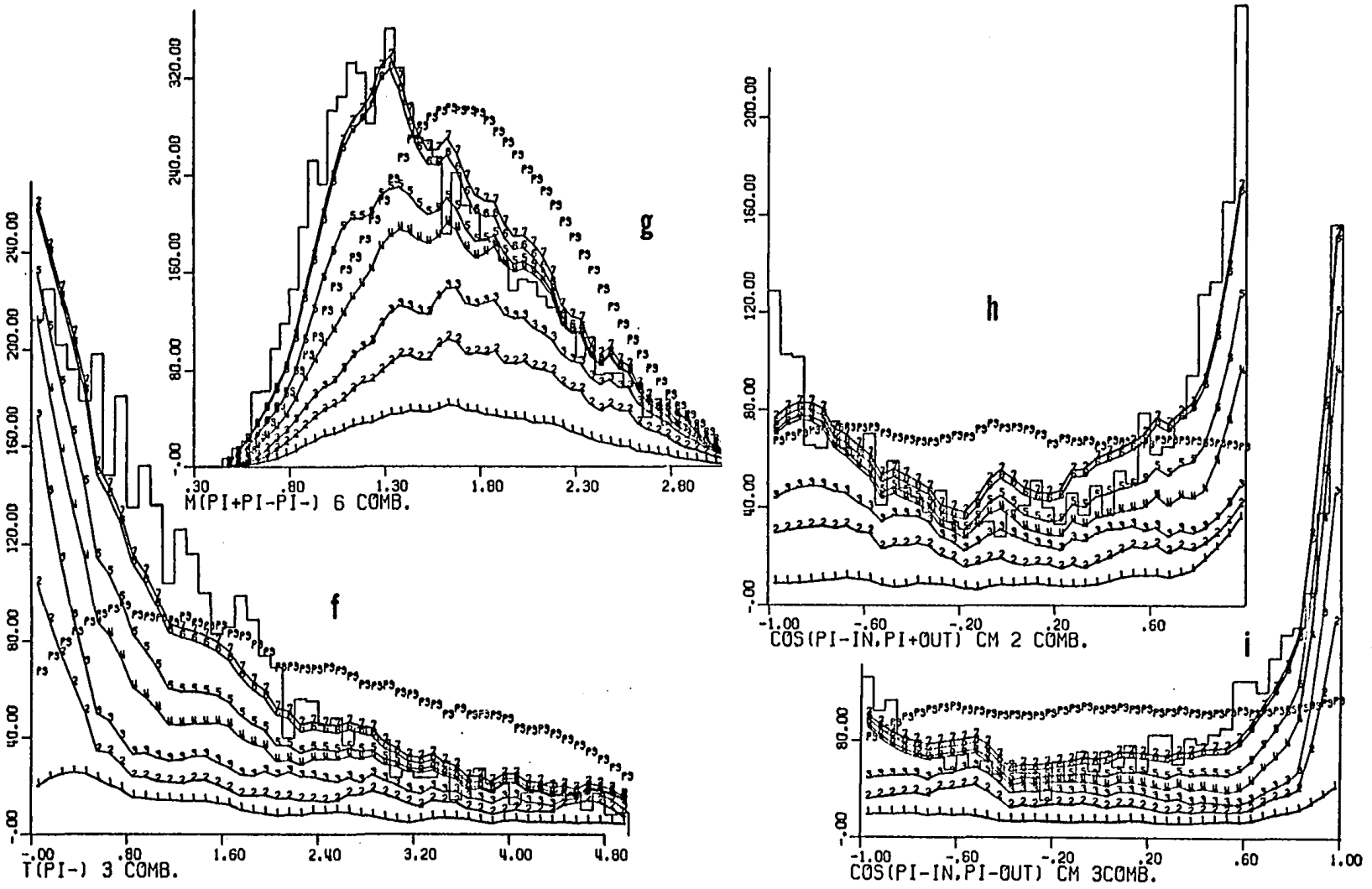

FIG. 10 PART 2 PROTON,5 PI (11.9 GEV/C)

FIGURE 11

Part 1: Overview, $\pi^- p \rightarrow p\pi^+\pi^+\pi^-\pi^-\pi^-\pi^0$ at 11.9 GeV/c. The same general comments apply as for Figure 1, Part 1. a, b, c, l, masses of selected particle combinations; events/40 mev. d, g, cos(π^- incident, outgoing particle) for the four types of final-state particles; events/.04. h-k, longitudinal component of momentum for final-state particles in laboratory system; events/40 mev/c. m, momentum-transfer-squared to proton; events/ 50 mev^2.

Part 2: Details, $\pi^- p \rightarrow p\pi^+\pi^+\pi^-\pi^-\pi^-\pi^0$ at 11.9 GeV/c. The same general comments apply as for Figure 1, Part 2. a-d, masses of selected particle combinations; events/40 mev.

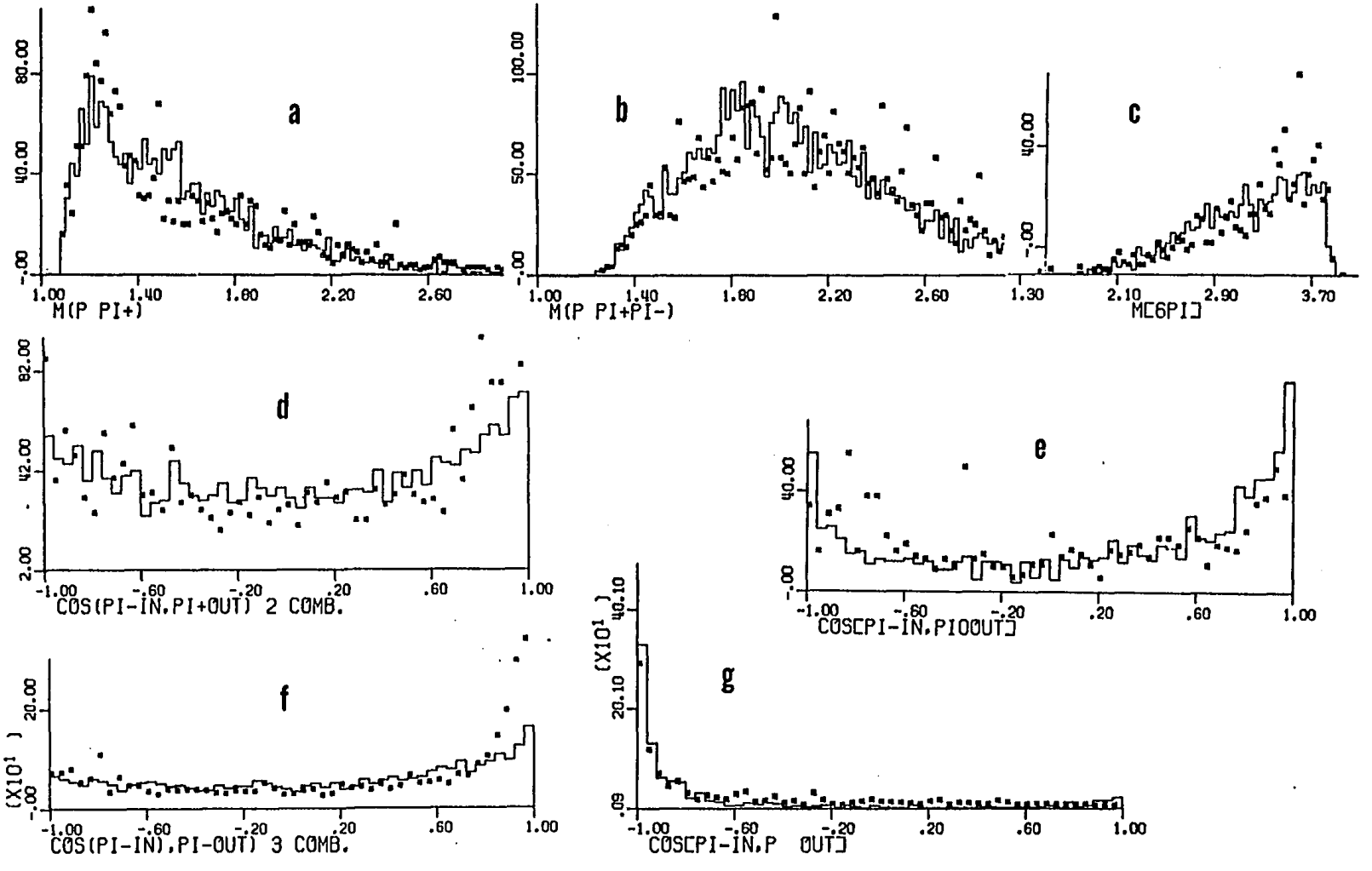

FIG. 11 PART 1 PROTON,6 PI (11.9 GEV/C)

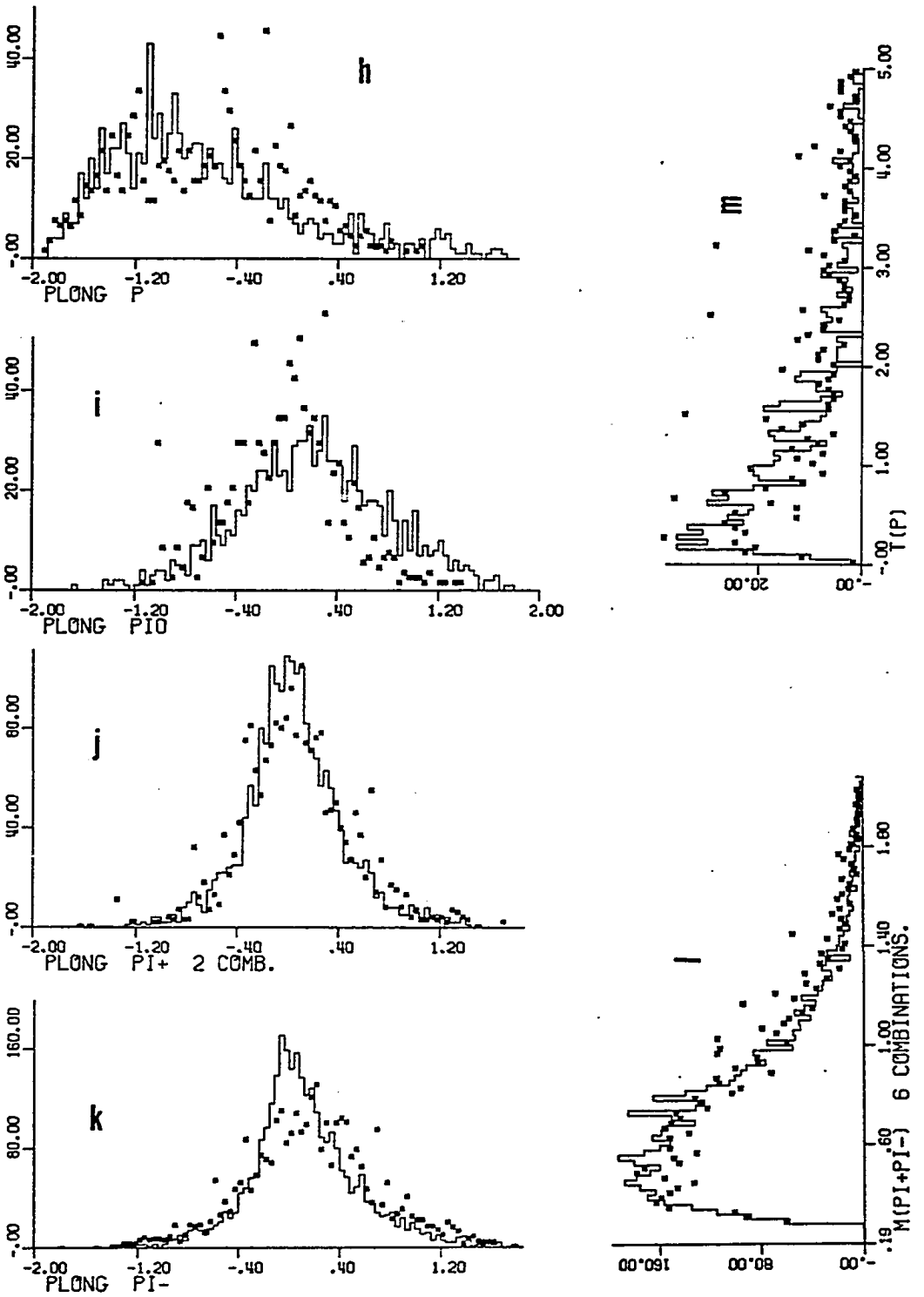

FIG. 11 PART 1 PROTON,6 PI (11.9 GEV/C)

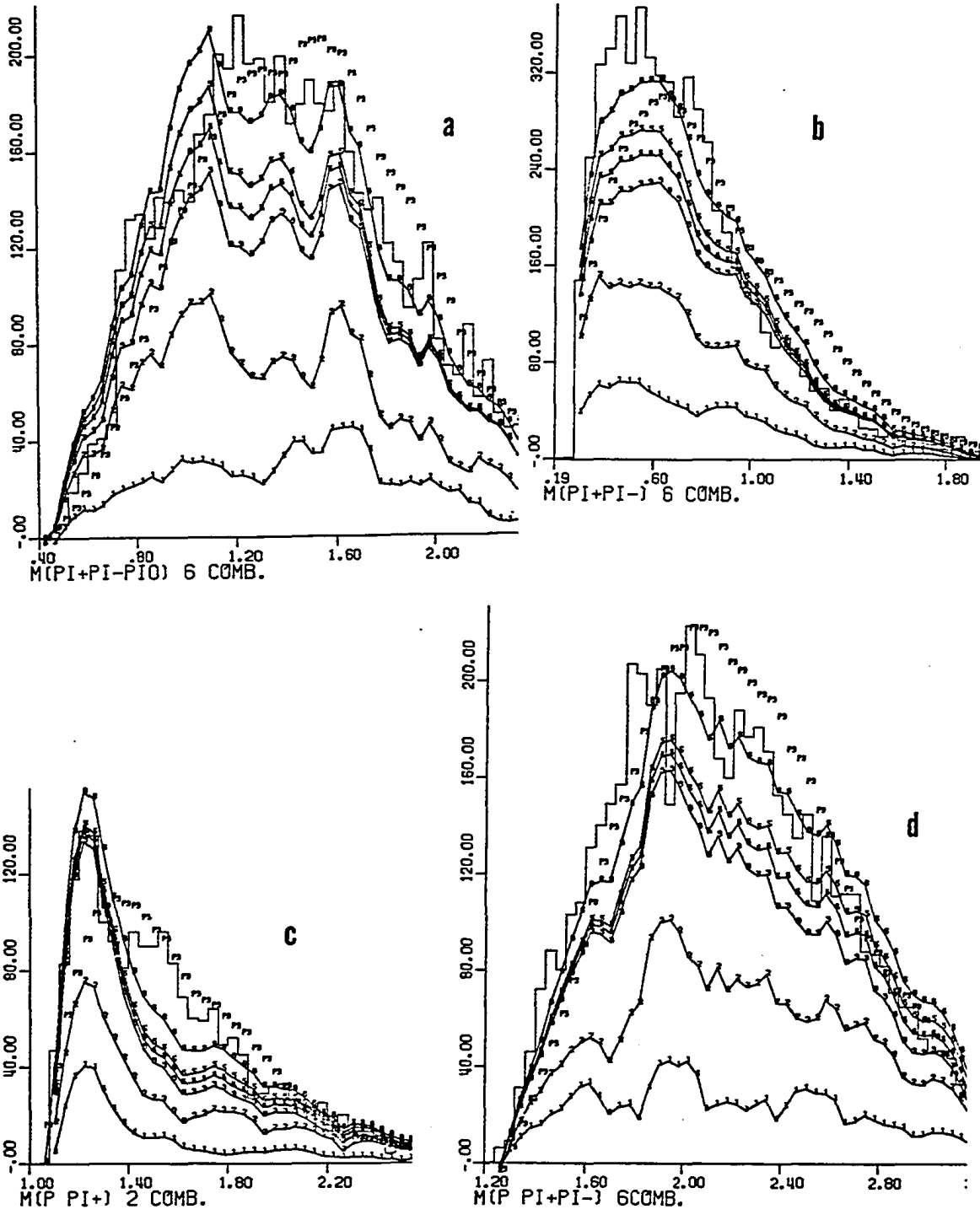

FIG. 11 PART 2 PROTON,6 PI (11.9 GEV/C)

FIGURE 12

Part 1: Overview, $\pi^- p \to n\pi^+\pi^+\pi^+\pi^-\pi^-\pi^-$ at 11.9 GeV/c. The same general comments apply as for Figure 1, Part 1. a-c, masses of selected particle combinations; events/40 mev. d-g, momentum-transfer-squared to selected particle combinations; events/50 mev^2. h-l, longitudinal and transverse components of momentum for final-state particles in laboratory system; events/40 mev/c. m-o, cos(π^- incident, outgoing particle) in cm; events/.04.

Part 2: Details, $\pi^- p \to n\pi^+\pi^+\pi^+\pi^-\pi^-\pi^-$ at 11.9 GeV/c. The same general comments apply as for Figure 1, Part 2. a, mass of $n\pi^+$ system; events/40 mev. b, c, momentum-transfer-squared to π^+, n respectively; events/50 mev^2.

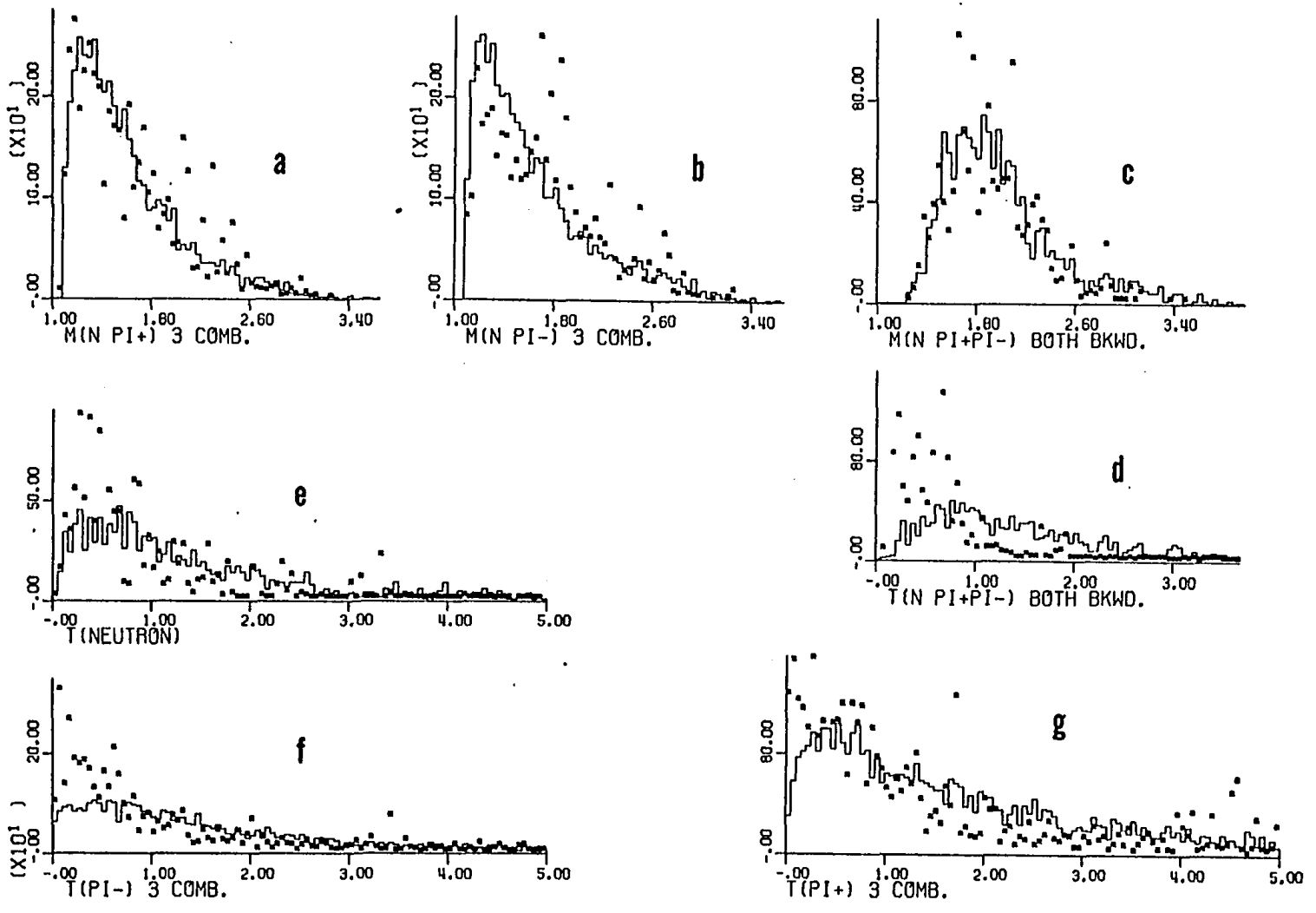

FIG. 12 PART 1 NEUTRON, 6 PI (11.9 GEV/C)

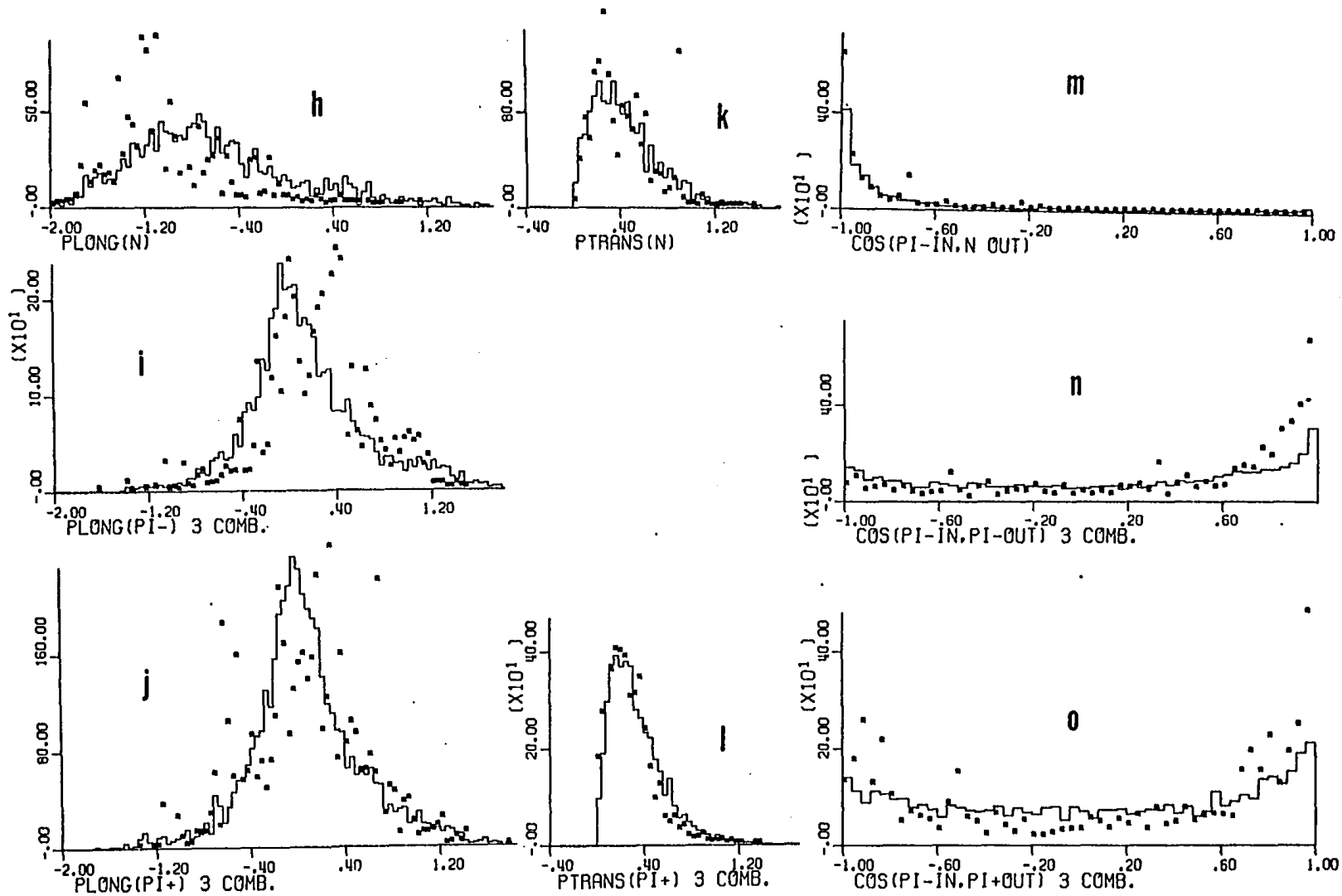

FIG. 12 PART 1 NEUTRON, 6 PI (11.9 GEV/C)

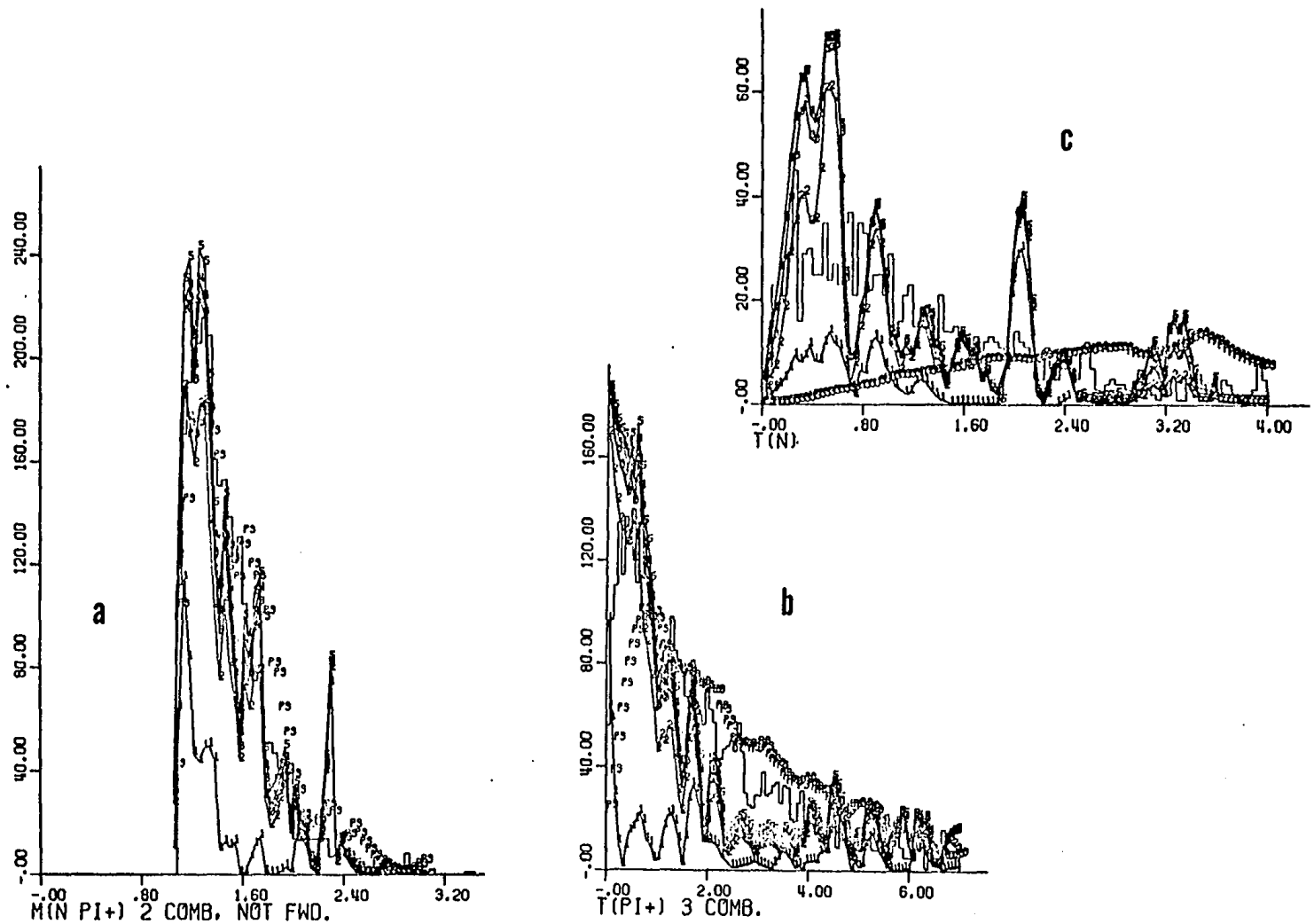

FIG. 12 PART 2 NEUTRON, 6 PI (11.9 GEV/C)

FIGURE 13

Variation of cross-sections with energy. Circles represent π-exchange cross-sections, while square symbols are used for Pomeron exchange. The number in each symbol is the multiplicity of the final state, K; 5-body proton and neutron states are distinguished by subscript p and n respectively. The ordinate is $\sigma^{(p)}_{3.9}$. The abscissa is

$$\left(\sigma^{(p)}_{11.9}\cdot\left(\frac{3.9}{11.9}\right)^{-K}\cdot\left(\frac{\text{phase-space volume at 3.9}}{\text{phase-space volume at 11.9}}\right)\right)\text{for } \pi\text{-exchange,}$$

$$\left(\sigma^{(p)}_{11.9}\cdot\left(\frac{3.9}{11.9}\right)^{1.8-K}\cdot\left(\frac{\text{phase-space volume at 3.9}}{\text{phase-space volume at 11.9}}\right)\right)\text{for Pomeron exchange.}$$

A dashed line with slope = 1 represents the prediction of Kittel et al. from 2-body experimental results.

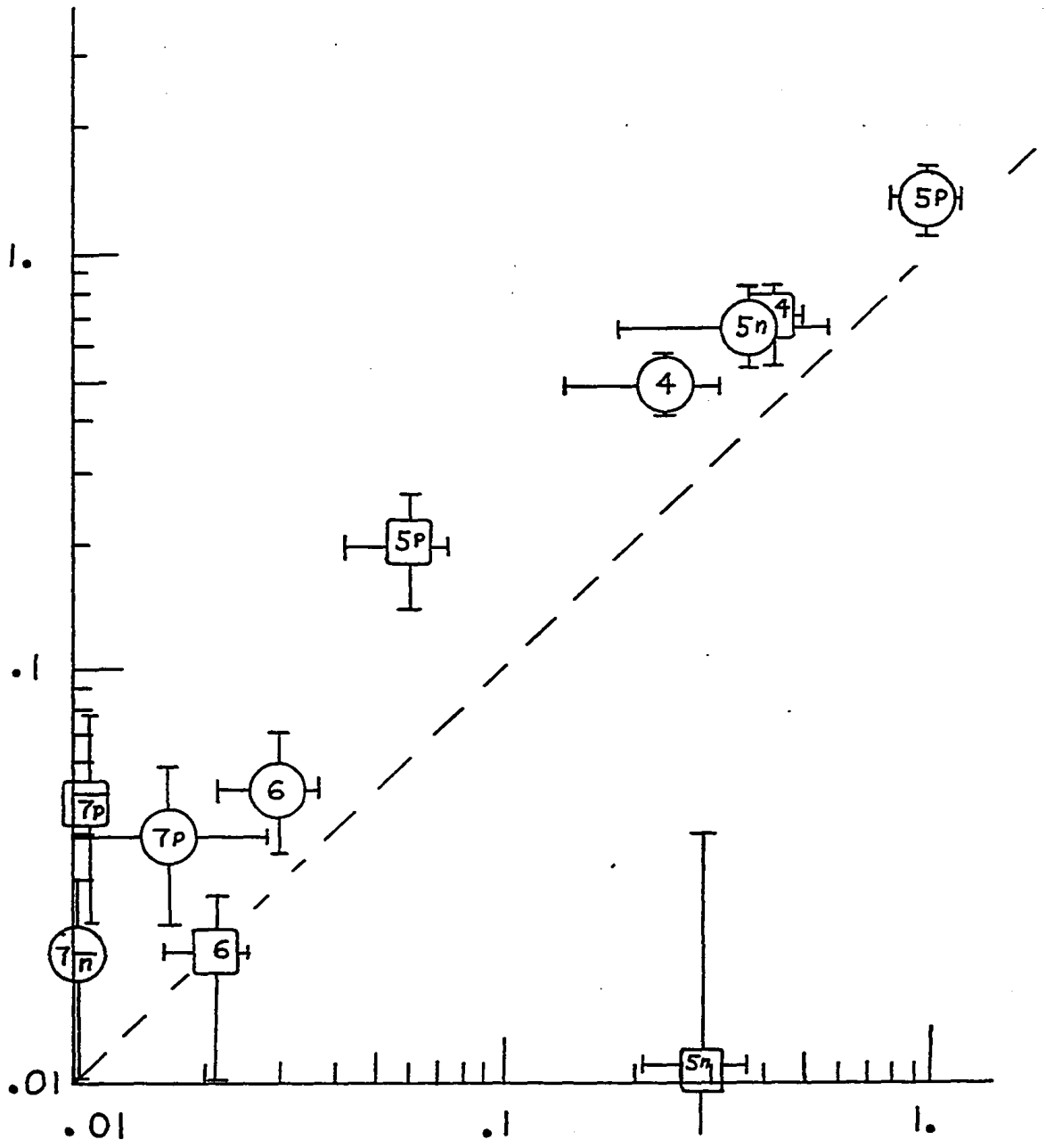

FIG. 13

FIGURE 14

(a) Pomeron exchange diagrams for nonresonant final states.

(b) Pomeron exchange diagrams for resonant final states.

(c) Classes of ratios employed in tests of factorization. N represents nucleon, either proton or neutron. l, m, n, k are multiplicity of pions at a vertex.

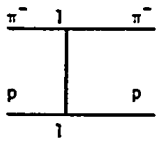

$\beta_{\pi,p} = \gamma_{\pi,\pi}\gamma_{p,p}$

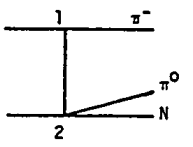

$\beta_{\pi,\pi p} = \gamma_{\pi,\pi}\gamma_{p,\pi p}$

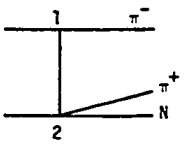

$\beta_{\pi,\pi N} = \gamma_{\pi,\pi}\gamma_{p,\pi N}$

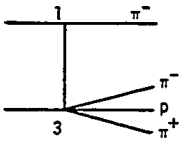

$\beta_{\pi,2\pi p} = \gamma_{\pi,\pi}\gamma_{p,2\pi p}$

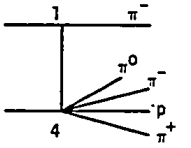

$\beta_{\pi,3\pi p} = \gamma_{\pi,\pi}\gamma_{p,3\pi p}$

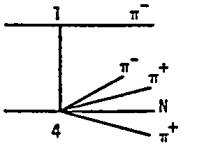

$\beta_{\pi,3\pi N} = \gamma_{\pi,\pi}\gamma_{p,3\pi N}$

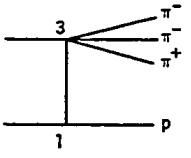

$\beta_{3\pi,p} = \gamma_{\pi,3\pi}\gamma_{p,p}$

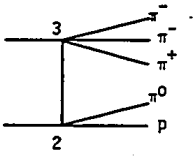

$\beta_{3\pi,\pi p} = \gamma_{\pi,3\pi}\gamma_{p,\pi p}$

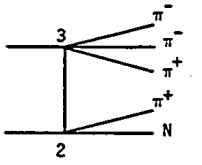

$\beta_{3\pi,\pi N} = \gamma_{\pi,3\pi}\gamma_{p,\pi N}$

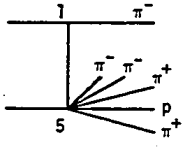

$\beta_{\pi,4\pi p} = \gamma_{\pi,\pi}\gamma_{p,4\pi p}$

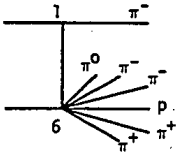

$\beta_{\pi,5\pi p} = \gamma_{\pi,\pi}\gamma_{p,5\pi p}$

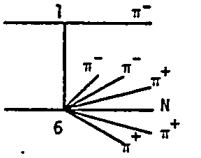

$\beta_{\pi,5\pi N} = \gamma_{\pi,\pi}\gamma_{p,5\pi N}$

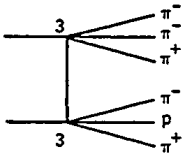

$\beta_{3\pi,2\pi p} = \gamma_{\pi,3\pi}\gamma_{p,3\pi p}$

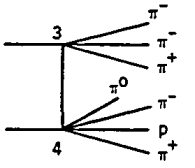

$\beta_{3\pi,3\pi p} = \gamma_{\pi,3\pi}\gamma_{p,3\pi p}$

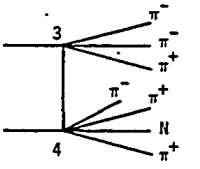

$\beta_{3\pi,3\pi N} = \gamma_{\pi,3\pi}\gamma_{p,3\pi N}$

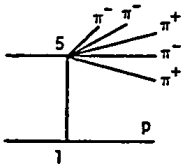

$\beta_{5\pi,p} = \gamma_{\pi,5\pi}\gamma_{p,p}$

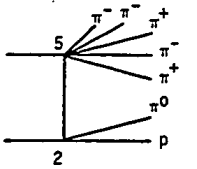

$\beta_{5\pi,\pi p} = \gamma_{\pi,5\pi}\gamma_{p,\pi p}$

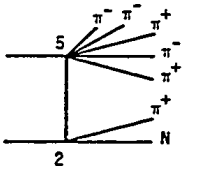

$\beta_{5\pi,\pi N} = \gamma_{\pi,5\pi}\gamma_{p,\pi N}$

Fig. 14 (a)

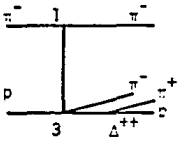

$\beta_{\pi,\pi\Delta^{++}} = \gamma_{\pi,\pi^-}\gamma_{p,\pi\Delta^{++}}$

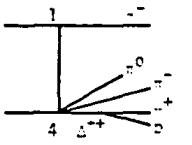

$\beta_{\pi,2\pi\Delta^{++}} = \gamma_{\pi,\pi^-}\gamma_{p,2\pi\Delta^{++}}$

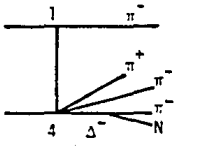

$\beta_{\pi,2\pi\Delta^{-}} = \gamma_{\pi\pi}\gamma_{p,2\pi\Delta^{-}}$

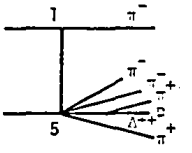

$\beta_{\pi,3\pi\Delta^{++}} = \gamma_{\pi\pi}\gamma_{p,3\pi\Delta^{++}}$

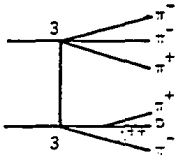

$\beta_{3\pi,\pi\Delta^{++}} = \gamma_{\pi,3\pi}\gamma_{p,\pi\Delta^{++}}$

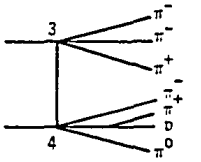

$\beta_{3\pi,2\pi\Delta^{++}} = \gamma_{\pi,3\pi}\gamma_{p,2\pi\Delta^{++}}$

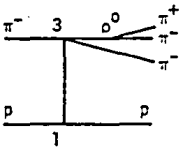

$\beta_{\rho\pi,p} = \gamma_{\pi,\rho\pi}\gamma_{pp}$

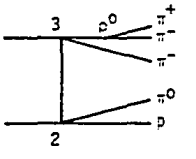

$\beta_{\rho\pi,\pi p} = \gamma_{\pi,\rho\pi}\gamma_{p,\pi p}$

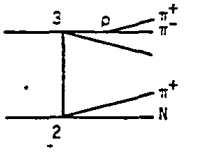

$\beta_{\rho\pi,\pi N} = \gamma_{\pi,\rho\pi}\gamma_{p,\pi N}$

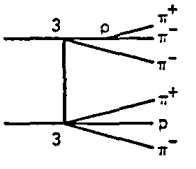

$\beta_{\rho\pi,2\pi p} = \gamma_{\pi,\rho\pi}\gamma_{p,2\pi p}$

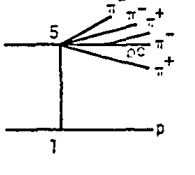

$\beta_{\rho 3\pi,p} = \gamma_{\pi,5\pi}\gamma_{p,p}$

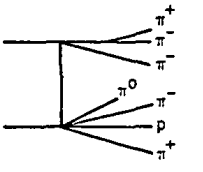

$\beta_{\rho\pi,3\pi p} = \gamma_{\pi,\rho\pi}\gamma_{p,3\pi p}$

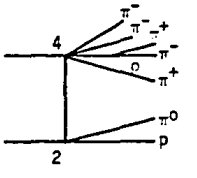

$\beta_{\rho,3\pi,\pi p} = \gamma_{\pi,\rho 3\pi}\gamma_{p,\pi p}$

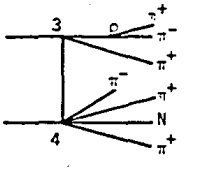

$\beta_{\rho\pi,3\pi N} = \gamma_{\pi,\rho\pi}\gamma_{p,3\pi N}$

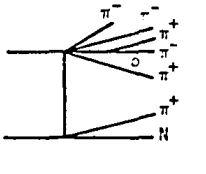

$\beta_{\rho 3\pi,\pi N} = \gamma_{\pi,\rho 3\pi}\gamma_{p,\pi N}$

Fig. 14 (b)

FIGURE 14(c)

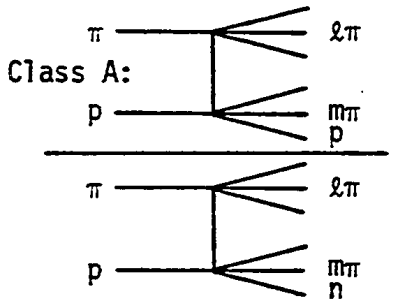

$$= \frac{\gamma_{\pi,\ell\pi}\gamma_{p,m\pi p}}{\gamma_{\pi,\ell\pi}\gamma_{p,m\pi n}} = \frac{\gamma_{p,m\pi p}}{\gamma_{p,m\pi n}}$$

$1 \leq \ell$ (odd)
$0 \leq m$

(= 1/2 for pure I = 1/2 state) at proton vertex

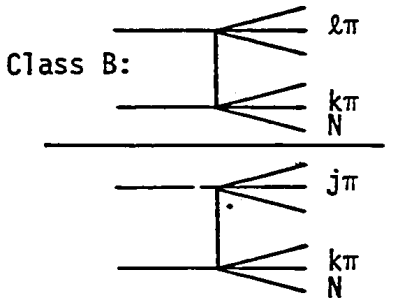

$$= \frac{\gamma_{\pi,\ell\pi}\gamma_{p,k\pi N}}{\gamma_{\pi,j\pi}\gamma_{p,k\pi N}} = \frac{\gamma_{\pi,\ell\pi}}{\gamma_{\pi,j\pi}}$$

$1 \leq \ell$ (odd)
$1 \leq j$ (odd)
$0 \leq k$

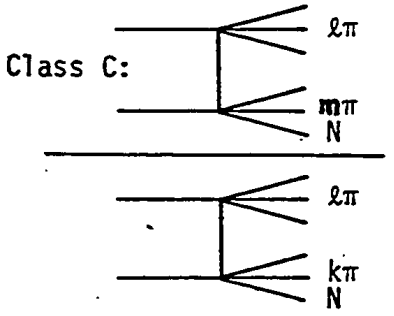

$$= \frac{\gamma_{\pi,\ell\pi}\gamma_{p,m\pi N}}{\gamma_{\pi,\ell\pi}\gamma_{p,k\pi N}} = \frac{\gamma_{p,m\pi N}}{\gamma_{p,k\pi N}}$$

$1 \leq \ell$ (odd)
$0 \leq m$
$0 \leq k$

FIGURE 15. RESULTS OF FACTORIZATION TESTS

σ_1 (abscissae) and σ_2 (ordinates) are partial cross-sections for Pomeron exchange appearing in numerator and denominator, respectively, of ratios given in Figure 14(c) and Equations 4.11-4.17. Results at 3.9 GeV/c are plotted separately from results at 11.9 GeV/c. Numbers to right of data points correspond to labels on the ratios in Equations 4.11 to 4.17. Each plot has points clustered at the origin corresponding to ratios whose numerator and denominator are both small. Error bars represent approximately one standard deviation. (a), (b), and (c) depict results for ratios of class A, B, and C, respectively. In (a), the dashed line with slope = 1/2 is the prediction for pure I = 1/2. In (c), there is a change of scale in order to include cross-sections for 2-body final states. These have not been determined in this experiment, and are not expected to represent pure Pomeron exchange.

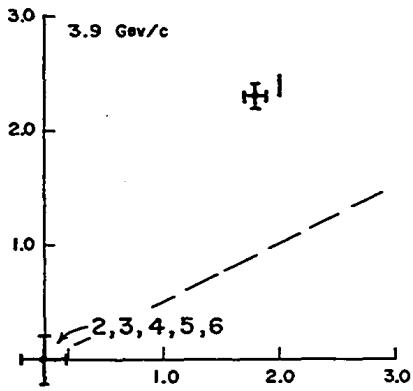

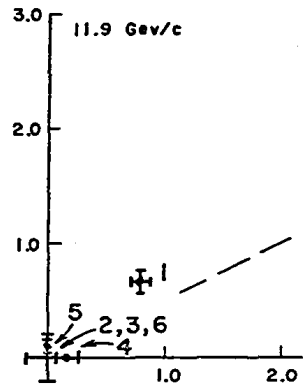

FIG. 15 (a)

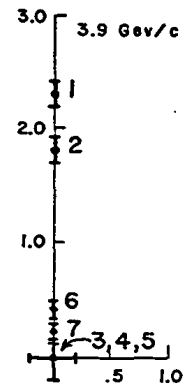

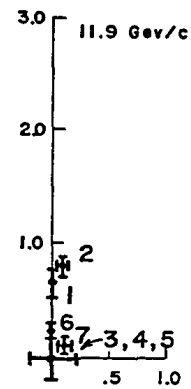

FIG. 15 (b)

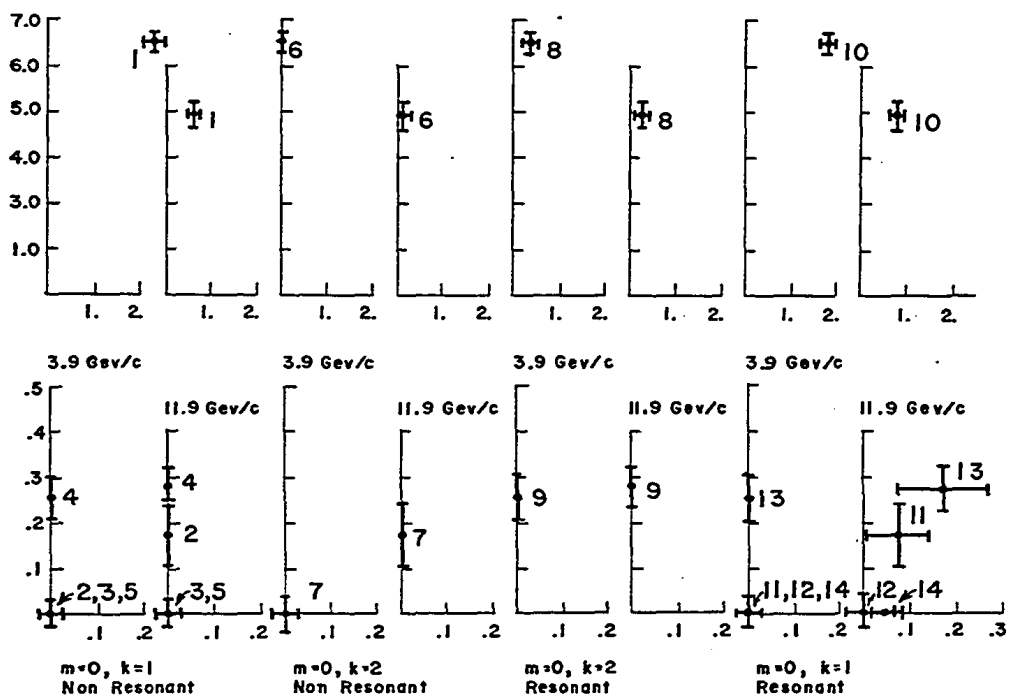

FIG. 15 (c)

APPENDIX A

MAXIMUM-LIKELIHOOD FITTING PROGRAM BUBBLES

The method used was first applied by J. Friedman of LRL.[5] Incorporation of peripheral effects was accomplished by P. Wohlmut et al., and a rather complete description of the overall procedure exists so it will not be repeated here.[2]

Briefly, for each event a frequency function is calculated which reflects the degree to which the model describes the event. This may be interpreted as a "probability" for the event. Probabilities for all events in a sample are multiplied together, yielding a likelihood function of variable parameters for the experiment. The parameters, which represent fractions of the events which are produced by a given process, are varied by numerical differentiation in such a way as to maximize the likelihood function. When a maximum has been determined, the values of the parameters represent a "best fit" of the assumed model to the data.

Several features have been added to the program, chiefly by P. Wohlmut and the author, to make it suitable for a larger class of applications.

A description of each process is furnished to the program in terms of two-track vertices. The order of specification of these vertices determines the order in which the normalization integral[6] is numerically integrated. The quadrature itself takes full advantage of the recursion relation for phase-space. This technique is quite general; a push-down store keeps account of integration steps so that the same program can compute integrals of any order.

Since this method of computing phase-space integrals with arbitrary weighting factors at all two-particle vertices is quite general and may have application outside the realm of this dissertation, it seems worthwhile to digress for a bit and describe it in some detail. R. Hagedorn† has shown that the invariant phase-space integral for an n-particle final state may be written as an n-2 fold integral in which each integral is an R_2 function.

$$R_2(a,b,c) = \frac{\pi}{2a^2}\sqrt{[a^2 - (b + c)^2][a^2 - (b - c)^2]} \qquad \text{EQN. A.1}$$

for a system of energy a breaking up into subsystems of mass b and c.

Employing the recurrence formula developed by Hagedorn and applying a weighting function ρ (J) at each vertex, one may write, for n particles,

$$R_n(E; m_1, m_2, \ldots, m_n) = \int_{L_\ell(n-1)}^{L_u(n-1)} dm_{n-1}^{*2}\rho(n-1)R_2(m_{n-1}^*; m_{n-1}, m_n)$$

$$\ldots \int_{L_\ell(n-2)}^{L_u(n-2)} dm_{n-2}^{*2}\rho(n-2)R_2(m_{n-2}^*; m_{n-1}^*, m_{n-2})$$

$$\ldots \int_{L_\ell(2)}^{L_u(2)} dm_2^{*2}\rho(2)R_2(m_2^*; m_3^*, m_2)\rho(1)R_2(E; m_2^*, m_1) \qquad \text{EQN. A.2}$$

The corresponding diagram with "bubbles" depicting variable masses is

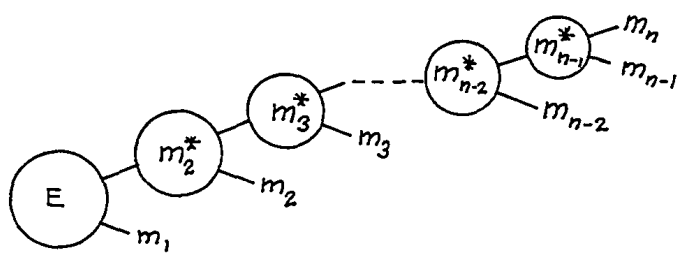

†R. Hagedorn, Relativistic Kinematics, Benjamin Press (1963).

where

E = total CM energy,

$m_1, \ldots, m_n$ represent fixed masses

$m_2^*, \ldots, m_{n-1}^*$ represent variable masses which break into downstream masses. Note that each m^* bubble corresponds to one integration.

The distinction between fixed (particle) and variable (resonant or phase-space distributed) masses is not a restriction. For example, m_1 may be replaced by $m_1^* \rightarrow m_1' + m_2'$ fixed masses, and then the corresponding $\rho(1)R_2(m_1^*; m_1', m_2')$ must be included in the integral. In this case, the order of integration is not fixed: The outermost integral may be either over dm_1^{*2} or dm_{n-1}^{*2}. However, the innermost integral always includes R_2 (E; disintegration product 1, disintegration product 2).

Writing the integral in this fashion allows one to determine the lower and upper integration limits, L (j) and L (j) by rote. The rules are:

1. Lower limit is always L = (M out(1) + M out(2))^2, where M out(1) and (2) are either fixed or variable masses outgoing from the corresponding bubble in the diagram.
2. Upper limit for outermost integral is $L_u(o) = E - \sum_{L=1}^{n} m_i + L_\ell(o)$. Upper limit for an inner integral is found by taking upper limit of next outer integral, adding lower limit for the inner integral, and subtracting bubble energy (m^*) for next outer integral.

An ℓ-point Gaussian quadrature can now be built around the integral. Starting at the outermost integral, a push-down store (last in = first out)

is used to keep track of the Gaussian quadrature point for each integrand as its "inner" integral is evaluated by looping over the "inner" integrand. The programming effort is modest. Compute time increases as ℓ^n and may be prohibitive for very high multiplicities, where a Monte Carlo integration would be more practical.

Multibody events have several identical particles, and there is usually no priori way to decide which π^+, for example, is to be associated with Δ^{++} or which $\pi^+\pi^-$ pair form a ρ^0. Hence, one must compute the frequency function using each of the identical particles in each place where it is allowed in the Feynman diagram. These "probabilities" are then added and averaged. Several difficulties attend this procedure. One is the tedious task of writing down each of the possible combinations; this is now done by the program, again in a general manner. The user must only list the track numbers to be attached at each two-point vertex in the diagram.

With 6- and 7-body events there are generally a large number of ways to permute the identical particles. The averaging process dilutes the derivatives so much that the program may have trouble converging on a solution. This difficulty is ameliorated by ordering all identical particles by the longitudinal component of cm momentum. Very forward pions are attached only at the meson vertex, and backward pions only at the baryon vertex. This saves time computing frequency functions for unlikely combinations, speeds convergence, and gives very nearly the same results (for cases where all permutations may be readily written out) as when all combinations are used.

The program exists as a FORTRAN IV deck of approximately 5000 source statements which has been used on the IBM 7040, the IBM 360, and the CDC 6400.

APPENDIX B

THE H-MESON QUESTION

In the plot of $M(\pi^+\pi^-\pi^0)$, Figure B1(a) at 3.9 GeV/c, a small noticeable enhancement appears over a smooth background at .995 mev. This is a region where several effects have been observed: the η', the H^0 meson, the δ,[B1] and more recently an enhancement at 953 mev.[B2] As with most other experiments in which similar effects have been observed, our enhancement is of order 2 to 3σ above a large background. It is also a region where, on the Dalitz plot, the ρ bands overlap.[B1] In this experiment, the ρ occurs where the slope of phase-space is steepest (Figure 2, Part 1(g)). It is not reasonable even to assume a constant background for ρ production in this region. Due to these complexities, it is difficult to say what precisely the enhancement is: We shall be content with showing several things which it is not.

The strongest arguments advanced against the $H^0(990)$ enhancement have been that it shows up only when a ρ-selection is made and that it can usually be explained as a consequence of misidentifying $\eta' \rightarrow \pi\pi\gamma$ events.[B3] Figure B1(a) shows the $\pi^+\pi^-\pi^0$ mass with a clear ω signal, a $2\text{-}\sigma$ peak at the η mass, and a $2.5\text{-}\sigma$ bump at 990 mev. Such an enhancement would be ignored if it were not observed in other experiments also.

From the uncut plot we conclude there are approximately 110 events in the bump which gives a cross-section of $.08 \pm .03$ mb[B4] which should be taken as an upper limit.

This cannot be the ϕ (1019) decay because the branching ratio $\phi \rightarrow K^+K^-/\phi \rightarrow \pi^+\pi^-\pi^0$ in π^-p data at 3.9 GeV/c is 47/13.[B5] No evidence is seen for $\phi \rightarrow K^+K^-$ in other π^-p experiments at similar energies.[B6]

The δ (962) is ruled out because it has a charged state and this is not seen in our data.

In Figure B2 is shown a scatter plot of m^2 (missing) versus $m^2(\pi^+\pi^-$, missing four-vector). On this plot evidence for $\eta' \to \eta\pi\pi$ would show up as an enhancement at m^2 (missing) $\cong$ .31 and $m^2(2\pi + mm) \cong .92$. Little or no enhancement is seen at the crossing of these bands (circled on the plot), and surely not enough to account for the bump observed in $m(\pi^+\pi^-\pi^o)$.

The η' is observed to decay into $\pi\pi\gamma$ 22-30 percent, into $\pi^+\pi^-\eta$ 66 percent of the time. In Figure B1(b) is shown the $m(5\pi)$ from the reaction $\pi^-p \to p\pi^+\pi^+\pi^-\pi^-\pi^-\pi^o$. Very little enhancement is seen at the η' mass, and the cross-section for $\pi^-p \to \eta'\pi^-p \to 5\pi$ is smaller than 3μb. This predicts that the partial cross-section for $\pi^-p \to \eta'\pi^-p \to \pi^+\pi^-\gamma$ is less than about 9μb, which is too small to explain the observed 80μb signal which is observed.

It would be interesting to see whether this enhancement is associated with Δ^o production. No strong correlation is seen when events in the 990 region are plotted (not shown).

Throughout the many models which were tested during the evolvement of the models described in this dissertation, it was constantly kept in mind to look for a process which gave a narrow bump at 990 mev. Although diffraction dissociation gives an enhancement at about 1.1, it is much broader than the 50 mev or so for the H-bump.

Cuts on the leading π^- also have failed to turn up any strong correlations. The bump appears to be slightly more strongly correlated with ρ^- or ρ^o than with ρ^+ (not shown).

We have considered the possibility that the enhancement is due to events with a missing γ but which fit missing π^0. Events were selected which fit $\pi^- p \to p\pi^+\pi^-\pi^-\pi^0$ but in which the calculated missing-mass-squared (from unfitted track data) is less than .01. This sample should be biased against missing π^0 and should enhance any signal due to missing γ. Figure B1(d) shows the mass of ($\pi^+\pi^-$ MM) for this sample. A clear ω signal remains, which indicates that our resolution is not good enough to discriminate between π^0 and γ. The region at 1.0 shows no increase in signal, which argues against the misidentified γ hypothesis.

Although these events show a strong ρ signal (Figure B1(c)), there is negative evidence that these ρ's are produced by a $\rho\gamma$ decay of a particle in this mass region. In Figure B1(e), (f), (g), the mass ($\pi^+\pi^-$) is presented for three mass regions in Figure B1(d), M($\pi^+\pi^-$ MM). Since no ρ signal is evident in any of these regions, we conclude that any meson (such as η' or possibly δ) which decays via this mode is below our threshold of detection.

REFERENCES

B1. A. H. Rosenfeld et al., UCRL-8030 (1970), Data on Particles and Resonant States.

B2. M. Aguilor-Benitez et al., Phys. Rev. Letters 25 (1971) 1635.

B3. C. Baltay, A. Rosenfeld, "Meson Spectroscopy," Benjamin Pub. (1968) 137.

B4. A. D. Johnson, M.S. Thesis, University of Hawaii (1968) UH-511-17-68 (unpublished).

B5. G. Goldhaber et al., UCRL-19229 (1969) (see also 1969 Lund Conference Notes, p. 301);
B. Chandhar and E. Marquit, Phys. Rev. D2 (1970) 2110.

B6. O. I. Dahl et al., UCRL-16978.

FIGURE B-1. EVIDENCE ON h-MESON

a. Mass of $\pi^+\pi^-\pi^0$ from $\pi^- p \rightarrow p\pi^+\pi^-\pi^-\pi^0$ at 3.9 GeV/c. A prominent ω appears in this uncut plot along with a small η^0 and an enhancement at 990 mev called the h^0.

b. Mass of $\pi^+\pi^+\pi^-\pi^-\pi^0$ from $\pi^- p \rightarrow p\pi^+\pi^+\pi^-\pi^-\pi^-\pi^0$ at 3.9 GeV/c. Production of η^1 in this channel is very small.

c-g. Events fitting $p\pi^+\pi^-\pi^-\pi^0$ hypothesis but with missing-mass (from unfitted track data) < .01 are selected.

c. $M(\pi^+\pi^-)$ has a prominent ρ signal.

d. $M(\pi^+\pi^-$ + missing 4-vector) is not enhanced in region of h^0 as it should be if the h^0 signal is due to misidentified $p\pi^+\pi^-\pi^-\gamma$ events.

e-g. Narrow (50 mev) bands below, at, and above h^0 region show no tendency toward enhancement in ρ region, so h-enhancement is not interpretable as $\rho\gamma$.

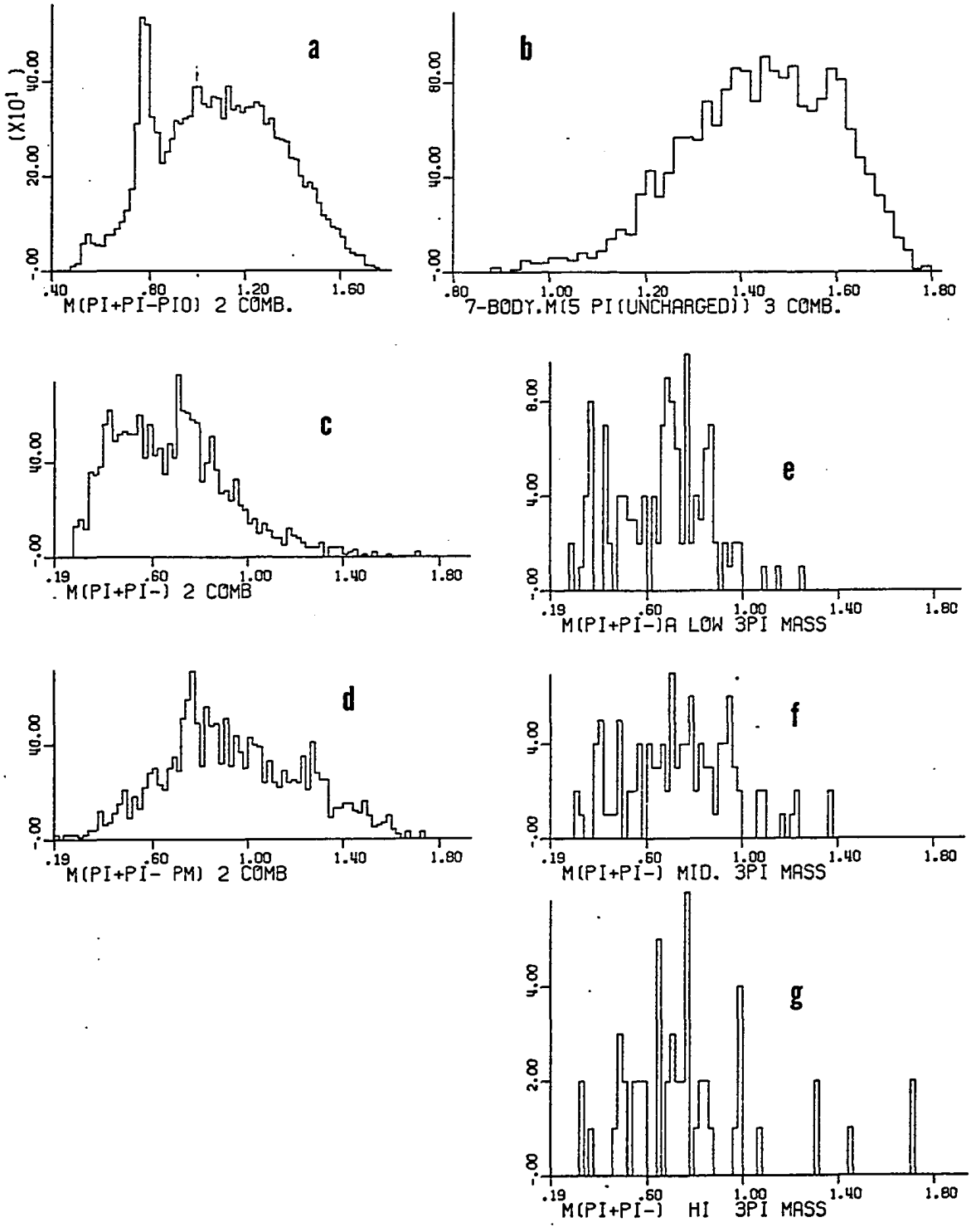
a
(X10¹)
40.00
20.00
.00
.40
.80
1.20
1.60
M(PI+PI-PIO) 2 COMB.
b
80.00
40.00
.00
.80
1.00
1.20
1.40
1.60
1.80
7-BODY.M(5 PI(UNCHARGED)) 3 COMB.
c
40.00
.00
.19
.60
1.00
1.40
1.80
M(PI+PI-) 2 COMB
e
8.00
4.00
.00
M(PI+PI-)A LOW 3PI MASS
d
M(PI+PI- PM) 2 COMB
f
M(PI+PI-) MID. 3PI MASS
g
2.00
M(PI+PI-) HI 3PI MASS

FIG. B-1

FIGURE B-2

Scatter plot showing small η' production. Missing mass squared versus (missing 4-vector + $\pi^+ + \pi^-$)^2. Significant $\eta' \to \eta\pi\pi$ should give an enhancement in the circled region.

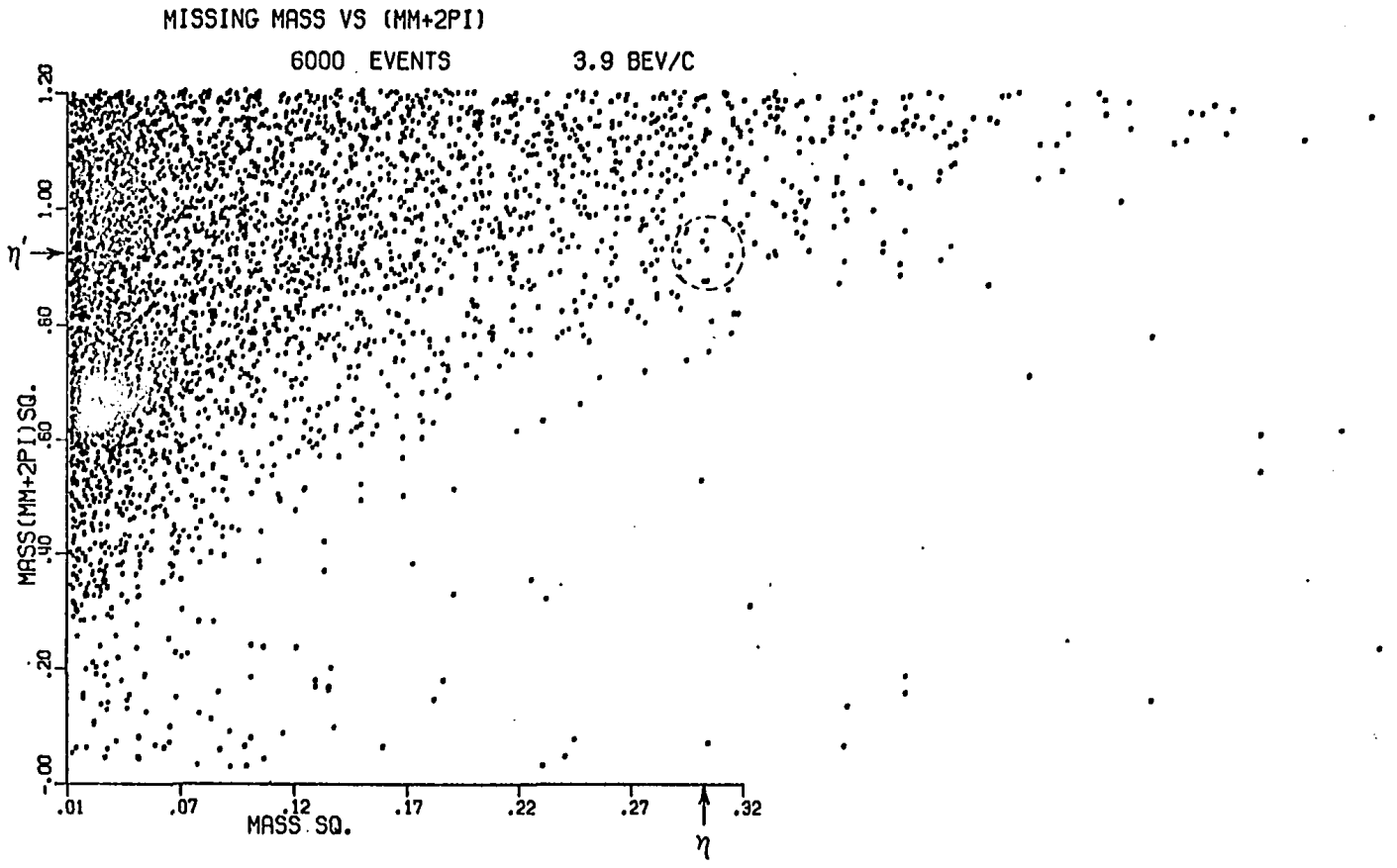
MISSING MASS VS (MM+2PI)
6000 EVENTS
3.9 BEV/C
MASS(MM+2PI)SQ.
1.20
1.00
.80
.60
.40
.20
.00
η'
.01
.07
.12
.17
.22
.27
.32
MASS SQ.
η

Fig. B-2

APPENDIX C

INVESTIGATION OF ρ-ω INTERFERENCE QUESTION

Evidence for interference of ρ with ω has been reported by several experimenters.† Some experiments show a dip in ρ^0 mass at precisely the mass of the ω (destructive interference) while others show constructive interference at ω mass.

We have looked for evidence of interference in both 4- and 5-body final states from $\pi^- p$ at 3.9 GeV/c. The tests for momentum-transfer-squared applied by CERN have been used. Results are shown in Figures C1 and C2. The strongest signal, which is about 2σ, occurs in the 4-body $\pi^+\pi^-$ for events with $t_p > .2$ GeV^2 and $\pi^+\pi^-$ paired so that $D12 = t\pi_1^- - t\pi^+\pi_2^-$ is larger (Figure C1). A hint of interference is present in the uncut $m(\pi^+\pi^-)$ in the form of a shoulder (Figure C1(a)).

In the 5-body data, a 2σ dip is to be seen in $m(\pi^+\pi^-)$ at the mass of the ω (Figure C2(a)). More curious still, there is a dip in the $m(\pi^-\pi^0)$ at precisely the same mass. This effect is slightly enhanced when the $m(\pi^-\pi^0)$ and $m(\pi^+\pi^-)$ histograms are added; the background is then very smooth, and there is a 3σ valley at the ω mass (Figure C2(c)). A slightly greater effect is seen, in $M(\pi^+\pi^-)$, when the combination giving greater $t(\pi^+\pi^-)$ is taken (Figure C2(c), (d)). Attempts to further enhance the effect have failed.

One would suppose that, since the omega mass is slightly displaced from the rho, one might enhance the asymmetry induced by interference by subtracting events in one side of the ρ from those on the other side.

---

†G. Goldhaber, UCRL 19850 (July 1970) has an extensive bibliography.

So far this has produced no useful results. There are at least two difficulties; the background is not homogeneous since phase space is dropping sharply with increasing $M(\pi^+\pi^-)$, and the number of ρ events above background is small to start with. Just about all one can say is that a smooth curve drawn under what appears to be the ρ bump very nearly intersects the valley in $m(\omega)$, so if the effect is real, it amounts to an almost maximal interference.

The idea that the valley in $M(\pi^+\pi^-)$ at $M(\omega)$ may be reflected in other mass combinations has been considered. There is a small but persistent bump at 990 mev in $m(\pi^+\pi^-\pi^0)$ which has been called the H meson. We have looked at the $\pi^+\pi^-\pi^0$ spectrum for events inside and outside the ρ-ω interference region and do not see any conclusive evidence for or against correlation.

The ρ-ω interference question remains an enigma. There is not enough evidence in this experiment to strengthen or weaken the case made by other observers. Nevertheless, the existence of narrow valleys at precisely the mass of the ω in several independent distributions is tantalizing. It is regretable that no way has been found to reduce the large background under the ρ enhancement.

FIGURE C-1

$M(\pi^+\pi^-)$ for $\pi^-p \to p\pi^+\pi^-\pi^-$ at 3.9 GeV/c. Selections are described in the text (Appendix C).

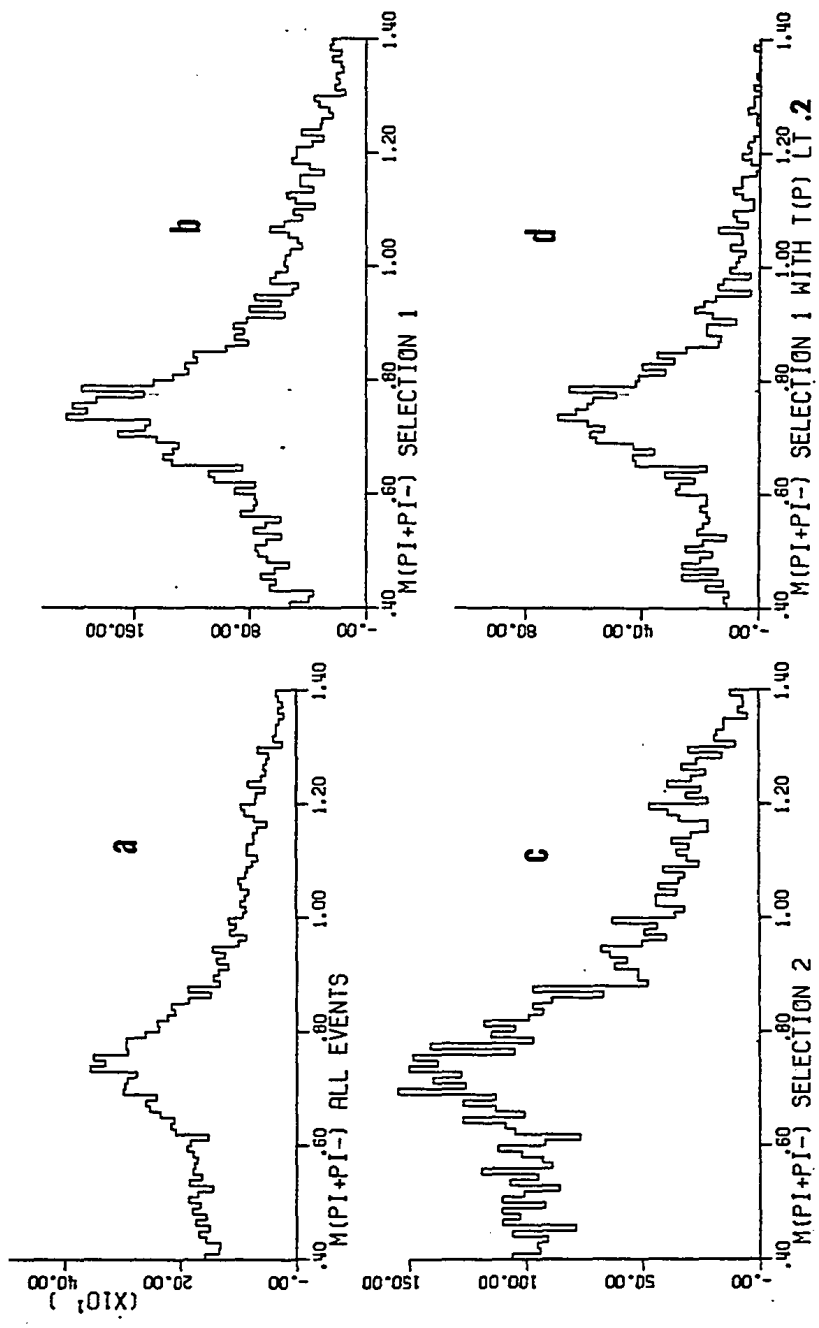
a
b
c
d
M(PI+PI-) ALL EVENTS
M(PI+PI-) SELECTION 1
M(PI+PI-) SELECTION 2
M(PI+PI-) SELECTION 1 WITH T(P) LT .2
(X10¹)
.40
.60
.80
1.00
1.20
1.40

FIG. C-1

FIGURE C-2

$M(\pi\pi)$ for $\pi^- p \rightarrow p\pi^+\pi^-\pi^-\pi^0$ at 3.9 GeV/c.

a. $M(\pi^+\pi^-)$

b. $M(\pi^0\pi^-)$

c. $M(\pi^+\pi^-)$, $M(\pi^+\pi^0)$, $M(\pi^-\pi^0)$ combined. All show small valley at $M(\omega)$.

d. $\pi^+\pi^-$ combination chosen which has smaller $t(\pi^+\pi^-)$.

e. $\pi^+\pi^-$ combination chosen which has larger $t(\pi^+\pi^-)$.

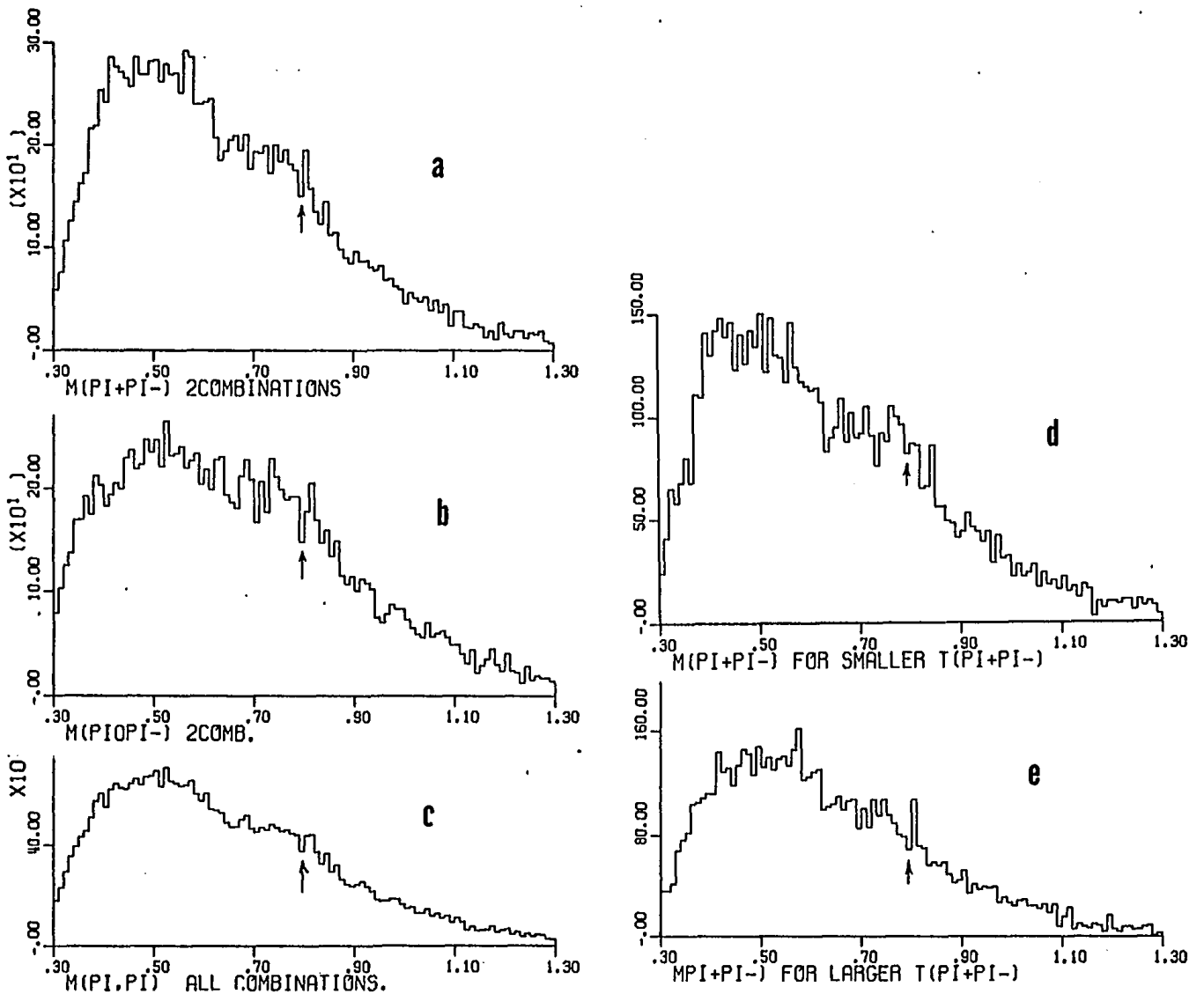
a
M(PI+PI-) 2COMBINATIONS
b
M(PIOPI-) 2COMB.
c
M(PI.PI) ALL COMBINATIONS.
d
M(PI+PI-) FOR SMALLER T(PI+PI-)
e
MPI+PI-) FOR LARGER T(PI+PI-)

FIG.C— 2

APPENDIX D

SEARCH FOR AN I = 2ρπ RESONANCE AND POSSIBLE LINK WITH SPLITTING OF THE A_2†

It has been proposed by Arnold and Uretsky[D1] that the A_2 splitting may be adequately explained by coherent interference between an A_2 meson of mass around 1300 mev and a width of 90 mev, and another state of the same spin and parity, and at the same mass, but having different width and I-spin. In analogy with the ρ-ω interference effect,[D2] the proposed new resonance manifests itself via electromagnetic transitions and can explain the A_2 splitting by having the same mass as the A_2, but a width less than 30 mev, and even G-parity. These authors postulate an object of $I^GJ^P = 2^+2^+$.

Tuan and Wu have shown[D3] that the non-chiral SU(2) × SU(2) group is an optimal group to explain hadronic mass degeneracies of different isospin multiplets. To preserve crossing symmetry, however, the members of the SU(2) × SU(2) group must have the same G-parity. Applying this analysis to the A_2 problem, Tuan[D4] has determined that SU(2) × SU(2) predicts three mass degenerate resonances in the A_2 region of $I^G = 0^-$, 1^-, 2^-. The 0^- and 2^- members are coupled to $q\bar{q}q\bar{q}$ configurations with $q\bar{q}$ pairs in S and D wave states respectively.

While the $I^GJ^P = 0^-2^+$ state cannot be isolated in the current experiment, we have search for the I = 2 even parity object of Arnold and Uretsky and the odd parity object of Tuan in the following reactions:

---

†This search was made in cooperation with P. G. Wohlmut at the suggestion of S. F. Tuan.

$$\pi^- + p \rightarrow p + \pi^+ + \pi^- + \pi^- \quad \ldots (1) \qquad \text{EQN. D.1}$$

$$\rightarrow p + \pi^+ + \pi^- + \pi^- + \pi^0 \quad \ldots (2)$$

$$\rightarrow p + \pi^+ + \pi^+ + \pi^- + \pi^- + \pi^- \quad \ldots (3)$$

$$\rightarrow p + \pi^+ + \pi^+ + \pi^- + \pi^- + \pi^- + \pi^0 \quad \ldots (4)$$

Reactions (1)-(4) have been studied at 3.9 GeV/c, and (1)-(2) at 11.8 GeV/c.

If one chooses the $I^G = 2^+$ alternative, demanding electromagnetic transition mixing in analogy to the ρ-ω mixing, we would expect the predominent decay mode to lie in either the $\pi^{\pm}\pi^{\pm}$ or the $\pi^{\pm}\pi^{\pm}\pi^0\pi^0$ channels. Thus a signal should appear in the $\pi^-\pi^-$ mass plot at 3.9 GeV/c in Figure 1a, or the corresponding plot, Figure 1b, at 11.8 GeV/c. If the four pion channel dominates, this signal should show up in Figure 2. No detectable signal is noted in either case. Furthermore, we would also expect the $f^0(1260)$ to show splitting in a manner analogous to the A_2 if the two pion mode exists, but no such effect is observed.

If the exotic interfering state is $I^G = 2^-$, we expect to isolate the signal in either the $\pi^-\pi^-\pi^0$ or the $\pi^+\pi^+\pi^0$ channels. Figures D4 and D5 show the corresponding mass plots at the two energies. No significant enhancement is noted. One might expect an enhanced signal in the pure I, I_z = 2, 2 diagram:

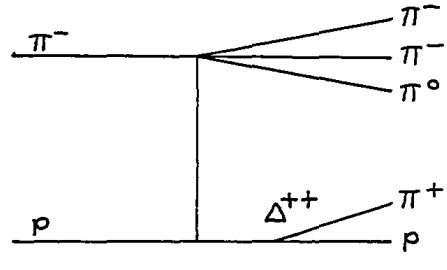

The above is shown in Figure D6, again with no obvious positive result. The general downward (low mass) peaking of Figure D4c is a result of the production of preferentially forward pions at 11.8 GeV/c. A further cut into the ρ^- or ρ^+ band is shown by asterisks in Figures D4 and D5.

Although there is no exotic I = 2 signal in evidence, the same data at 3.9 GeV/c show the splitting of the A_2 in a fashion completely consistent with the spectrometer experiments.[D5] This is demonstrated in Figure D3. The splitting may be explained by an underlying resonance in this channel only of width 30 mev, mass 1300 and $J^P = 2^+$. In addition, the cross-section in this peak is approximately 160 microbarns,[D8] of which 40 can be the interfering resonance. Unfortunately, at 11.8 GeV/c a similar analysis cannot be made due to the poorer resolution in the appropriate mass region.

In conclusion, we find the upper limit on the cross-section for an I = 2 resonant state in the 3π system to be 3 microbarns, which is in agreement with Katz et al,[D6] but contrary to the findings of Vanderhagen et al.[D7] If such a state were to exist and explain the extent of the A_2 splitting in our data, it would have to have a width of 30 mev, and be produced in the $\rho^0\pi^-$ channel with a cross-section of 40 microbarns. We note that Vanderhagen reports a width of 150 mev, which cannot explain the A_2 splitting.

TABLE D1

PRODUCTION UPPER LIMITS ON CROSS-SECTION FOR I = 2 RESONANCE

Reaction	Beam Mom. GeV/c	Cross-Section microbarns
$\pi^- + p \rightarrow p + \pi^+ + \pi^o + X^{--} \rightarrow \pi^-\pi^-$	3.9	< 3
	11.8	< 1
$p + A_2^-$	3.9	120
$p + X^-$	3.9	< 40
$p + \pi^+ + X^{--} \rightarrow \pi^-\pi^-\pi^o$	3.9	< 3
	11.8	< 2
$p + \pi^+ + \pi^+ + X^{--} \rightarrow \pi^-\pi^-\pi^o$	3.9	< 1
$p + \pi^- + \pi^- + \pi^- + X^{++} \rightarrow \pi^+\pi^+\pi^o$	3.9	< 1

REFERENCES

D1. R. C. Arnold and J. L. Uretsky, Phys. Rev. Lett. 23, 444 (1969).

B2. D. G. Coyne, UCRL-19450, talk at APS Winter Meeting at UCLA, December 1969.

D3. S. F. Tuan and T. T. Wu, Phys. Rev. Lett. 18, 349 (1967).

D4. S. F. Tuan, Phys. Rev. Letters 23, 1198 (1969).

D5. M. N. Focacci et al., Phys. Rev. Lett. 17,890 (1966).

D6. W. M. Katz et al., UR-875-294, "Search for π^- Resonances Produced in 7 GeV/c π^-d Interactions," University of Rochester.

D7. R. Vanderhagen et al., Phys. Lett. 24B, 493 (1967).

D8. P. G. Wohlmut, M.S. Thesis UH-511-18-68 (unpublished).

FIGURE D-1

a. $\pi^-\pi^-$ mass distribution for reaction (2) at 3.9 GeV/c.

b. $\pi^-\pi^-$ mass distribution for reaction (1) at 11.9 GeV/c. The shaded area corresponds to a cut including only events in the Δ^{++} region.

FIGURE D-2

Missing mass distribution at 3.9 GeV/c.

FIGURE D-3

Mass distribution for $\pi^- p \rightarrow p + A_2$ at 3.9 GeV/c. A background corresponding to Lorentz invariant phase space has been subtracted. The solid curve represents a coherent sum of two Breit-Wigner Amplitudes with mass 1300 and widths 90 mev and 30 mev. A relative phase of 180° is used for the curve in D-3(a) and 210° for the curve in D-3(b).

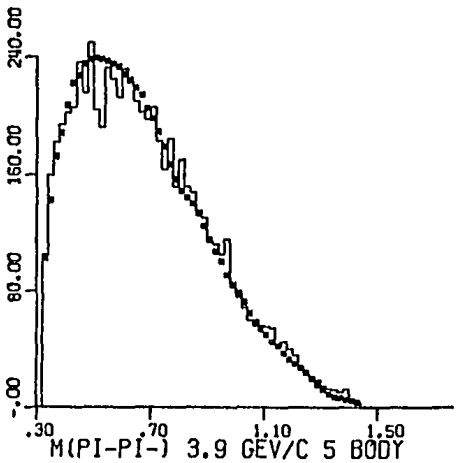

FIG. D1(A)

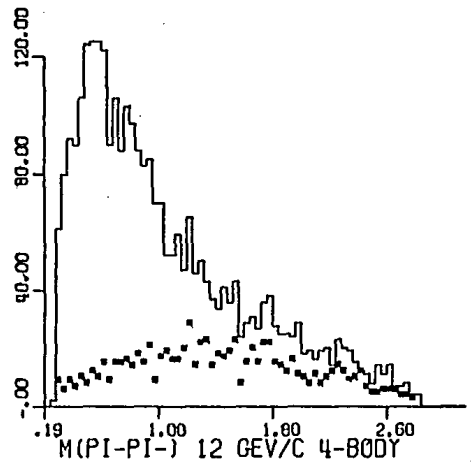

FIG. D1(B)

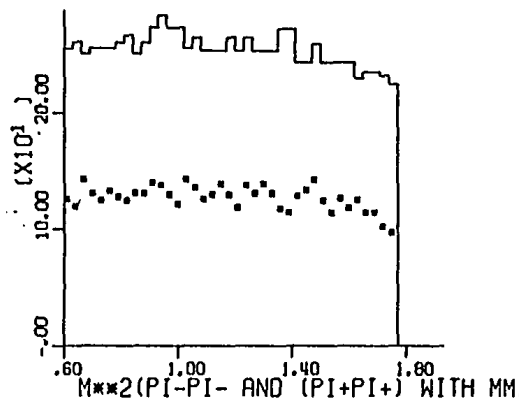

FIG. D2

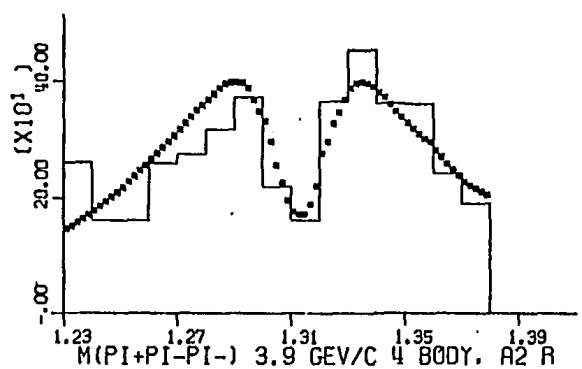

FIG D3(A)

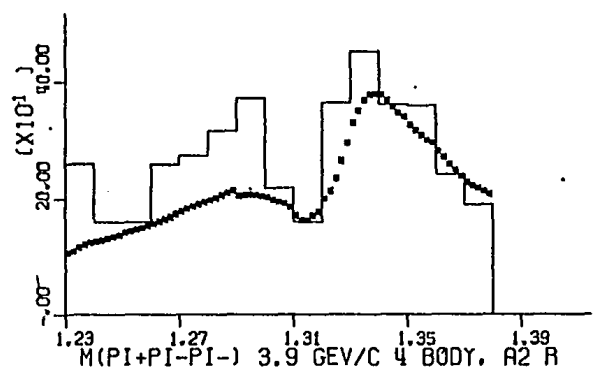

FIG D3(B)

FIGURE D-4

a. Mass distribution for $\pi^-\pi^-\pi^0$ for reaction (2) at 3.9 GeV/c. Shaded portion represents events in the ρ^- region.

b. Same distribution for reaction (4) at 3.9 GeV/c.

c. Same distribution for reaction (2) at 11.9 GeV/c. Shaded region represents events in the ρ^- band and produced with Δ^{++}.

FIGURE D-5

Mass distribution of $\pi^+\pi^+\pi^0$ for reaction (4) at 3.9 GeV/c.

FIGURE D-6

Mass distribution of $\pi^-\pi^-\pi^0$ for reaction (2) at 3.9 GeV/c. Events purified by subtracting a background: events in a narrow Δ^{++} band are weighted +1, events in adjacent regions receive a weight of -1, other regions are excluded.

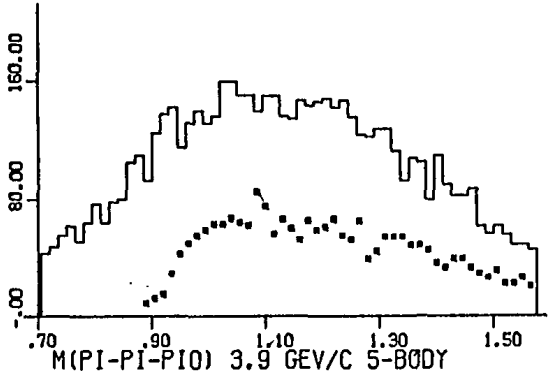

FIG. D4(A)

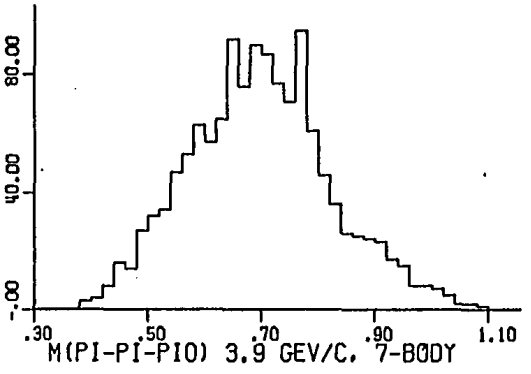

FIG. D4(B)

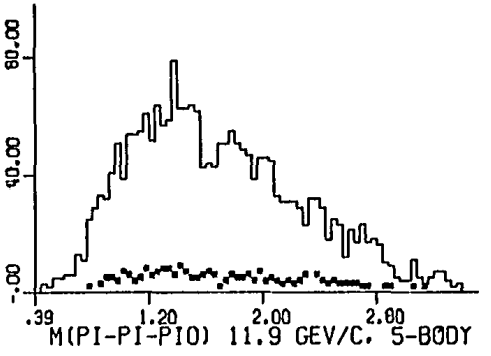

FIG. D4(C)

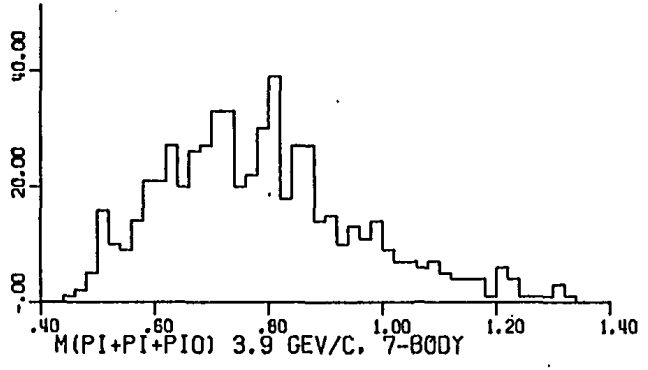

FIG. D5

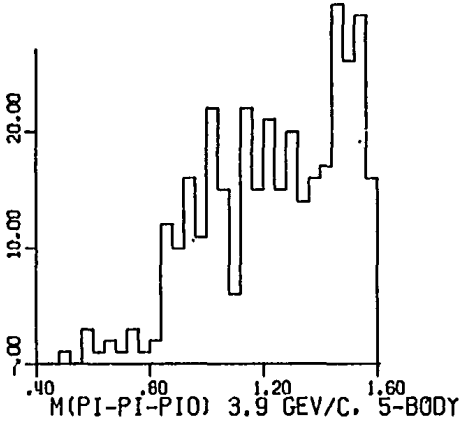

FIG. D6